Ewa Kądzielawa-Major

Exchange Interactions, Electronic States, and Pairing of Electrons in Correlated and Hybridized Systems

Oddziaływania wymiany, stany elektronowe i parowanie elektronów w skorelowanych układach z hybrydyzacją

Rozprawa doktorska wykonana
na Wydziale Fizyki, Astronomii i Informatyki Stosowanej
Uniwersytetu Jagiellońskiego w Krakowie

Promotor: prof. dr hab. Józef Spałek

Promotor pomocniczy: dr inż. Maciej Fidrysiak

Zakład Teorii Materii Skondensowanej i Nanofizyki
Instytut Fizyki im. Mariana Smoluchowskiego
Uniwersytet Jagielloński
Kraków, 2018

Oświadczenie

Ja niżej podpisana Ewa Kądzielawa-Major (nr indeksu: 1029627) doktorantka Wydziału Fizyki, Astronomii i Informatyki Stosowanej Uniwersytetu Jagiellońskiego oświadczam, że przedłożona przeze mnie rozprawa doktorska pt. „Exchange Interactions, Electronic States, and Pairing of Electrons in Correlated and Hybridized Systems" jest oryginalna i przedstwia wyniki badań wykonanych przeze mnie osobiście, pod kierunkiem prof. dr. hab. Józefa Spałka. Pracę napisałam samodzielnie.

Oświadczam, że moja rozprawa doktorska została opracowana zgodnie z Ustawą o prawie autorskim i prawach pokrewnych z dnia 4 lutego 1994 r. (Dziennik Ustaw 1994 nr 24 poz. 83 wraz z późniejszymi zmianami).

Jestem świadoma, że niezgodność niniejszego oświadczenia z prawdą ujawniona w dowolnym czasie, niezależnie od skutków prawnych wynikających z ww. ustawy, może spowodować unieważnienie stopnia nabytego na podstawie tej rozprawy.

Kraków, dnia ....
podpis doktorantki

Contents

Abstract

The general topics contained in the Thesis title are discussed on examples. Namely, we consider in detail the two particular aspects of modeling the heavy-fermion (f-electron) systems, i.e.,

1. Spin-triplet superconductivity of UGe_2, in conjunction with the unconventional ferromagnetic transitions observed in this system, and

2. Antiferromagnetic kinetic exchange interactions, both among the f and conduction c states, the so-called Kondo-type interactions, as well as the kinetic superexchange f-f interaction, both of which are derived within a single theoretical approach (canonical perturbation expansion, CPE).

It should be emphasized that both subjects are modeled with the help of the Anderson lattice models (cf. Chapter 2): The first topic is discussed on the basis of the orbitally degenerate Anderson lattice model, whereas the second comprises CPE approach with and without the orbital degeneracy.

The spin-triplet superconductivity, with inclusion of the orbital degeneracy, supplements the earlier studies of ferromagnetism in UGe_2 (cf. Chapter 3) by a detailed discussion of superconductivity within a single model and approach, in this case *the statistically consistent Gutzwiller approximation* (SGA, cf. Chapter 2). Our results agree semi-quantitatively with the principal observed properties of UGe_2 in the absence of external applied magnetic field, both the magnetic and superconducting properties. In particular, we propose that the onset of bulk superconductivity (the so-called A_1 phase) takes place in the limit, which can be regarded as *the Hund-metal limit*. In this limit both the Hund's-rule exchange and the direct intraatomic intraorbital Coulomb-interaction contributions are of comparable amplitude. Also, the proposed here pairing mechanism, based solely on real-space correlations, can be regarded as complementary to that involving specific type of the spin fluctuations.

What concerns the second part of the Thesis (cf. Chapter 4), the kinetic-exchange interaction in the strong-correlation limit, we estimate within the non-degenerate Anderson lattice model the magnitude of kinetic exchange interactions, as well as show that the interaction of Dzyaloshinskii-Moriya type may appear out of purely electronic correlations. We also sketch the situation for the orbital degeneracy and discuss results in the two cases, i.e., when f-occupancy per site $n^f \leqslant 1$ and $1 < n^f \leqslant 2$.

At the end (cf. Chapter 5), apart from summary of presented results, we point out other pertinent questions related to the topics discussed in the present Thesis.

The Thesis contains also a number of Appendices, where some of the computational details are provided and few extensions are briefly discussed.

Streszczenie

Ogólne tematy zawarte w tytule rozprawy zostały omówione na konkretnych przykładach. W szczególności rozważono dwa aspekty opisu układów ciężkofermionowych (układów z elektronami typu f), a mianowicie:

1. Trypletowe nadprzewodnictwo współistniejące z ferromagnetyzmem w konkretnym związku uranu, UGe_2, w tym sekwencję przejść fazowych nadprzewodzących i magnetycznych dla tego związku;

2. Antyferromagnetyczne oddziaływanie kinetycznej wymiany zarówno dla atomowych elektronów (f), jak i dla elektronów przewodnictwa (c), czyli tzw. oddziaływanie typu Kondo, oddziaływanie kinetycznej nadwymiany (ang. *superexchange*) pomiędzy elektronami f. Oba te oddziaływania otrzymujemy z wyjściowego modelu za pomocą kanonicznego rozwinięcia perturbacyjnego (ang. *canonical perturbation expansion*, CPE).

W obu powyższych zagadnieniach do opisu teoretycznego użyto modelu sieci Andersona (por. rozdział 2): w przypadku opisu UGe_2 był to model orbitalnie zdegenerowany, natomiast drugi temat przedyskutowano zarówno dla modelu niezdegenerowanego, jak i zawierającego orbitalną degenerację.

Uwzględnienie orbitalnej degeneracji stanowi uzupełnienie wcześniejszych badań dotyczących UGe_2, dzięki możliwości jednoczesnego opisu zarówno magnetyzmu, jak i nadprzewodnictwa. Model rozwiązano za pomocą *statystycznie konsystentnego przybliżenia Gutzwillera* (ang. *statistically consistent Gutzwiller approximation*, SGA, por. rozdział 2). Nasze wyniki (por. rozdział 3) zgadzają się jakościowo z wynikami eksperymentalnymi w zerowym zewnętrznym polu magnetycznym, a część wyników, np. magnetyzacja, odtworzona jest ilościowo. W szczególności zaproponowano, że stan nadprzewodzący ma początek w sytuacji, którą można nazwać *granicą metalu Hunda*. W tej granicy wkład do energii całkowitej pochodzący od wymiany Hunda oraz wewnątrzatomowego, wewnątrzorbitalowego oddziaływania Coulomba mają porównywalną wielkość. Zaproponowano także mechanizm parowania oparty na korelacjach w przestrzeni rzeczywistej, komplementarny do parowania bazującego na kwantowych fluktuacjach spinowych (paramagnony).

Druga cześć pracy (por. rozdział 4) dotyczy kanonicznego rozwinięcia perturbacyjnego (CPE) dla modelu sieci Andersona. Dla przypadku nieuwzględniającego degeneracji orbitalnej otrzymano model Andersona-Kondo poprzez wyrzutowanie lokalnych podwójnych obsadzeń f-elektronów. Model ten zawiera oddziaływania wymiany oraz oddziaływanie typu Działoszyńskiego-Moriyi, to drugie pochodzące od korelacji czysto elektronowych. Opisano też kanoniczne rozwinięcie perturbacyjne w sytuacji z

orbitalną degeneracją do najniższego (drugiego) rzędu i omówiono wyniki dla dwóch przypadków: gdy średnia liczba obsadzeń f-elektronów $n^f \leqslant 1$ oraz $1 < n^f \leqslant 2$.

Na koniec (w rozdziale 5) podsumowano otrzymane wyniki, a następnie przedyskutowano możliwe rozszerzenia tematów zawartych w tej pracy.

Rozprawa zawiera także serię dodatków (por. rozdziały A-D), w których umieszczono szczegółowe rachunki, a także omówiono pokrótce kilka rozszerzeń wyników dyskutowanych w jej głównej części.

List of abbreviations

c-electrons	conduction electrons
f-electrons	localized ($5f$) electrons
$\bar{\sigma}$	spin direction opposite to σ
FM2	ferromagnetic phase with large magnetic moment
FM1	ferromagnetic phase with lower magnetic moment
PM	paramagnetic phase
SC	superconductivity
A_2	superconducting phase with two unequal gap parameters
A_1	superconducting phase with one non-zero gap parameters
A	superconducting phase with two equal gap parameters
HF-BCS	Hartree-Fock+Bardeen-Cooper-Schrieffer approximation
SGA	statistically consistent Gutzwiller approximation
$\hat{\mathcal{H}}$	Hamiltonian
$\mu_0 H$	magnetic field
h	reduced magnetic field, $h = 1/2 g \mu_B \mu_0 H$
CPE	Canonical perturbation expansion

Acknowledgments/Podziękowania

W tym miejscu chciałabym serdecznie podziękować wszystkim, którzy wspierali mnie przy powstawaniu tej rozprawy.

Przede wszystkim chcę wyrazić wdzięczność prof. Józefowi Spałkowi za zaproponowanie tematyki pracy, wieloletnią opiekę, dyskusje naukowe oraz wyrozumiałość w podejmowaniu prób zakończenia doktoratu zaburzanego przez życie rodzinne. Jednocześnie dziękuję za krytyczne przeczytanie niniejszej pracy i wiele cennych uwag.

Osobne podziękowania należą się dr. Maciejowi Fidrysiakowi za wszelką pomoc, inspirujące dyskusje, a przede wszystkim za miłą atmosferę współpracy i sugestie odnośnie tej rozprawy.

Pragnę również podziękować dr Danucie Goc-Jagło za okazane wsparcie, a także byłym i obecnym członkom Zakładu Teorii Materii Skondensowanej i Nanofizyki: dr. Marcinowi Abramowi, dr. Jasiowi Kaczmarczykowi, dr. hab. Andrzejowi Kapanowskiemu, dr. Andrzejowi Kądzielawie, Piotrkowi Kuterbie, dr. Grzesiowi Rutowi, dr. hab. Adamowi Rycerzowi, Dominikowi Suszalskiemu, dr. Marcinowi Wysokińskiemu. Dziękuję, że mogłam być częścią tego zespołu.

Przyjaciółkom: Faustynie, Julce, Kasi, dziękuję za słowa otuchy.

Szczególnie jestem wdzięczna moim Rodzicom za pomoc w codziennych sprawach i w opiece nad dziećmi.

Na końcu chcę podziękować Jankowi za cierpliwość, nieustanne wsparcie i wiarę we mnie, a także Jerzykowi i Tadziowi za Wasze uśmiechy oraz za to, że nauczyliście mnie wykorzystywać czas w stu procentach.

Finansowanie Praca była początkowo realizowana w ramach programu TEAM/2010-6/7 finansowanego przez Fundację na rzecz Nauki Polskiej (FNP), a następnie w ramach projektu MAESTRO, No. DEC-2012/04/A/ST3/00342 z Narodowego Centrum Nauki (NCN).

Obliczenia Część obliczeń przedstawionych w niniejszej pracy została wykonana na klastrze EDABI zakupionym w ramach grantu MAESTRO i oprogramowanym przez członków naszego zespołu.

1. Introduction: A brief overview of relevant phenomena

In this Chapter we discuss the most important concepts and phenomena, which can help to put the main topics of the present Thesis in a wider scope.

1.1. Magnetism

Before we discuss the history of the superconductivity and point out steps, which have led to the discovery of heavy fermion systems, let us recall a few issues related to the topic of magnetism. Understanding of these features is necessary in the subsequent analysis of coexistence of magnetism and superconductivity in the heavy fermion system UGe_2.

In general, a material can exhibit various phenomena influenced by the magnetic field, i.e.,

- ferromagnetism – magnetic moments of unpaired electrons in a material spontaneously line up parallel to one another in the ground state, as a result a material has non-zero macroscopic magnetization. In itinerant ferromagnets, only a majority part of itinerant electrons are lined up in the parallel fashion;
- antiferromagnetism – total magnetization is zero, however there are sublattices periodically arranged with non-zero magnetizations, antiparallel with respect to each other. Again, in the case of itinerant antiferromagnetism the moments of sublattices are aligned only partially;
- ferrimagnetism – similar to antiferromagnetism in a material there are sublattices with non-zero magnetizations, but the total magnetization is also non-zero;
- paramagnetism – unpaired electrons in a material are free to align their magnetic moments in any direction, the total magnetization is zero at each lattice site;
- diamagnetism – tendency of a material to oppose applied magnetic field; in such a material there are no unpaired electron spins, which could overcome the orbital effect, as in paramagnetic or ferromagnetic case; the dominant component of magnetic moment comes from the orbital degrees of freedom (Landau diamagnetism).

The principal other characteristics are:

- Curie temperature – the temperature, above which a material loses spontaneous magnetization; it designates the temperature boundary between ferromagnetic and paramagnetic phases;

- metamagnetism – it refers to a discontinuous increase in the magnetization of a system, e.g., under application of an external magnetic field.

In this Thesis only ferromagnetic and paramagnetic phases of itinerant and correlated electrons are analyzed also coexisting with the spin-triplet-paired states, as we discuss next. Additionally, the selected material, UGe_2, exhibits spontaneous metamagnetic transitions as a function of pressure. Hence, it cannot be regarded as typical ferromagnet, exhibiting also transition to the unconventional superconducting state, as we discuss next.

1.2. Spin-triplet superconductivity (superfluidity) and its coexistence with magnetism

The history of superconductivity began over 100 years ago. Since the first observation of the phenomenon in mercury by H. Kamerlingh Onnes in 1911 [1], the topic raises a constant interest. It turned out, that upon lowering temperature below certain critical temperature $T_S = 4.17$ K, the electrical resistivity jumps to practically unobservable value. From this circumstance stems the name the superconductivity. However, it cannot be understood as a simple idealization of the classical conductivity, as is exemplified by a whole bunch of new observed phenomena, as e.g. expelling of the magnetic field. The effect was discovered by W. Meissner and R. Ochsenfeld in 1933 [2, 3]. Superconductors show large diamagnetism, it means that magnetic field cannot penetrate superconductor, except a thin surface layer. The magnetic field is expelled from the interior cooled below the critical temperature in type-I superconductors. The feature is not like diamagnetism in normal materials, where it arises from induced magnetic moment inside the material and is oriented in the opposite direction to it. In the case of superconductivity it is due to the appearance of the supercurrents – electric currents flowing without loses in the surface area of the material, totally compensating the applied magnetic field. At least, this is true for type-I superconductors. A different situation arises in type-II superconductors, as had been discovered by J. N. Ryabinin and L. V. Shubnikov [4]. Namely, above certain strength of the magnetic field (the lower critical field H_{c1}) it is energetically favorable for them to allow for a penetration of magnetic flux quanta associated with vortices. Above the upper critical filed H_{c2} superconducting state is destroyed.

The flux penetration for type-I superconductors was first theoretically rationalized by F. and H. Londons [5], who introduced the important notion of penetration depth – bulk region near the surface, in which the field compensating supercurrents are confined to.

In 1950 V. L. Ginzburg and L. D. Landau proposed a macroscopic theory [6] that described superconductivity in terms of the postulated global (macroscopic) wave function – an order parameter, which is non-zero in the superconducting phase. This phenomenological theory provided an explanation of many of superconducting features, e.g., a distinction between type-I and type-II superconductors. It also explained the phenomenon of magnetic flux quantization both in the type-I superconductors with a hollow and in type-II superconductors with vortices.

The microscopic theory explaining the superconductivity was introduced in 1957 by J. Bardeen, L. N. Cooper, and J. R. Schrieffer [7], widely known as BCS theory. Appearance of the phonon mediated attractive interaction between electrons, which can overcome the Coulomb repulsion among them, causes that electrons tend to form pairs, known as *the Cooper pairs*. The BCS theory provides a proper description for both type-I and type-II conventional superconductors. Also, a macroscopic Ginzburg-Landau theory can be derived from it [8].

In parallel, the discovery of superfluidity observed for the first time in liquid ^{4}He eighty years ago [9, 10] proves that a similar phenomenon can be observed for neutral particles (atoms in this case). In the case of superfluidity the liquid cooled below the critical temperature $T_{\mathrm{S}} = 2.17$ K starts to flow without energy loss – the viscosity acquires a zero value. Both superconductivity and superfluidity are macroscopic quantum phenomena and they share a lot of similarities as we have lossless matter flow, quantization of vortex flux, etc. In effect, superconductivity sometimes is referred to a superfluidity of electron liquid. However, there are also important differences, e.g. a superfluidity owes its properties to neutral helium atoms, whereas a superconductivity is attributed to electrically charged electron pairs, which still behave approximately as bosons.

Atoms of ^{4}He are boson particles, thus can undergo the Bose-Einstein condensation. In contrast, the first unconventional superfluid was observed in ^{3}He [11], which is composed of fermions. There is an effective attractive interaction between helium ^{3}He atoms (or more precise between two fermionic quasi-particles), what results in the spin-triplet, p-wave channel pairing. They form pairs, which can be regarded approximately as bosons and thus can condensate. Due to the spin-triplet pairing, a number of order parameters can appear, and that situation allows for occurrence of several superfluid phases. Two different phase transitions were observed owing to two different superfluid phases: A and B phase. Later on, $A_1 \rightarrow A$ phase transition in superfluid ^{3}He was observed in an applied magnetic field [12].

As said above, the systems, for which superconductivity cannot be explained by the BCS theory are known as unconventional superconductors. Within the BCS theory, superconductivity cannot appear in systems with a strong Coulomb interaction, because it competes with phonon-mediated attractive force and the pairing is destabilized. Therefore, for description of unconventional superconductivity a different pairing mechanism is required. A concrete mechanism is discussed later, let us focus first on the selected experimental findings.

Superconductivity in heavy-fermion systems: The first observation was carried out by F. Steglich *et al.* in 1979 in the compound $CeCu_2Si_2$ [13]. Heavy fermion systems owe their name to large effective mass, 100-1000 times greater than the mass of free electron. The heavy fermion systems comprise intermetallic compounds with rare-earth $4f$ (e.g., Ce) or actinide $5f$ (e.g., U) elements and exhibits variety of phenomena, among which is the superconductivity coexisitng with different forms of magnetism (antiferromagnetism, ferromagnetism, paramagnetism or metamagnetism). The high-temperature (high-T_c) superconductivity was discovered in 1986 by J. G. Bednorz, K. A. Müller [14]. They observed for the first time what is termed now the high-T_c superconductivity, which cannot be explained within the BCS theory. The superconducting state in those materials evolves not from conducting state, but from antiferromagnetic Mott insulator state and sets in by doping.

A novel superconductivity and coexisting with ferromagnetism in heavy fermion systems was observed for the first time in UGe_2 by S. S. Saxena *et al.* in 2000 [15] and was followed in next few years by series of discoveries of the same phenomenon in related compounds (URhGe, UCoGe, UIr) [16, 17, 18]. For an extensive review of this field see [19, 20]. The experimental results have stimulated an interest in developing the theory, which could explain coexistence of ferromagnetism and superconductivity at the same time. It has been argued that $5f$ electrons from uranium atoms play this double role, furthermore superconductivity has to be of spin-triplet type [21]. Spin-triplet superfluidity has been known to appear in condensed ^{3}He [22] and is attributed to pairing due to quantum spin fluctuations (paramagnons) [23, 24].

It should be mentioned that there exist other compounds, in which ferromagnetism coexisting with superconductivity was observed. However, later on it turned out that such a coexistence is not so obvious. In 1980 the superconductivity in weak itinerant ferromagnet Y_4Co_3 (or Y_9Co_7) was reported [25] and examined theoretically [26]. Although, evidence for the existence of superconductivity is transparent, the coexisting ferromagnetism in this compound is sensitive to Co atoms ordering in a sample [27, 20] and no ferromagnetism occurs in the better-quality samples [28]. Another example is $ZrZn_2$ – d-electron compound, in which superconductivity in the ferromagnetically ordered phase has been claimed [29]. However, it was later shown, that the superconductivity in this compound is limited to a layer at surface of a sample modified by spark erosion [30].

About the spin-triplet pairing, such a phase appears most likely in layered perovskite oxide Sr_2RuO_4 [31, 32], but without coexisting ferromagnetism. From theoretical side, the spin-triplet superconductivity in this case has been analyzed in detail in the weak-coupling limit [33, 34, 35].

The next interesting material is UPt_3, in which two superconducting phase transitions at $T_S = 0.55$ K and 0.45 K occur [36]. Such a behavior means that multicomponent order parameter is needed to describe properly the behavior of the compound, a characteristic feature of spin-triplet superconductor, in this case coexisting with antiferromagnetism, which appears at Néel temperature $T_N = 5$ K. However, no detailed testing of theoretical concept was undertaken in this case.

Apart from the topic of the superconductivity coexisting with ferromagnetism,

one should also mention much larger class of materials, in which superconductivity coexists or competes with antiferromagnetism [19]:

- competition of antiferromagntism and superconductivity: Ce systems such as the series CeM_2X_2, e.g., $CeCu_2Si_2$, $CeCu_2Ge_2$; the series $Ce_nM_mIn_{3n+2m}$, e.g., $CeCoIn_5$; other, e.g., $CeNiGe_3$ and UPt_3;
- superconductivity coexisting with antiferromagnetism: UPd_2Al_3, UNi_2Al_3, $CePt_3Si$,URu_2Si_2.

1.3. Magnetic and superconducting properties of UGe_2 and related systems

We focus now on the properties of UGe_2, which is of main interest to us. The compound crystallizes into orthorhombic centrosymmetric structure, as presented in Figure 1.1. The ferromagnetic ordering is aligned along a-axis.

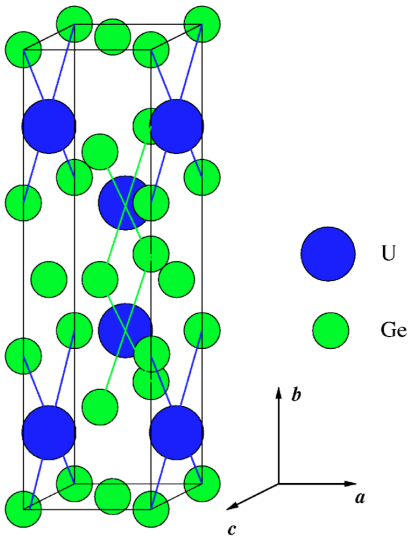

Figure 1.1.: Crystal structure of UGe_2: base-centered orthorhombic $Cmmm$ structure. Two primitive cells are shown. Figure taken from [37].

In UGe_2 the majority (over 90%) of the magnetic moment is carried by uranium $5f$ electrons [20]. Moreover, ferromagnetism has an itinerant nature. It means that on the contrary to the localized type, the magnetism comes from a disproportion of spin-up and spin-down itinerant electrons (quasi-particles), which contribute to the spin-splitting of the Fermi-surface.

Let us recall once more, that in the year 2000 S. Saxena *et al.* have found [15] that UGe_2 becomes superconducting while remaining relatively strongly ferromagnetic, what differs it from the discovered later UCoGe [17] and URhGe [16], which are weak ferromagnets. Later on it turned out that UGe_2 exhibits two distinct ferromagnetic phases: FM2 and FM1 separated by the first-order phase transition at zero temperature [38]. Figure 1.2 (taken from [38]) contains the phase diagram of UGe_2: (a) on temperature-pressure plane, the Curie temperature T_C decreases with applied hydrostatic pressure and vanishes altogether at critical pressure $p_c \simeq 1.6$ GPa in a discontinuous manner; FM2 and FM1 phases are separated by temperature T_x. In Figure 1.2(b) the magnetization is drawn as a function of applied pressure: There are two phase transitions FM2→FM1 and FM1→PM. Figure 1.2(c) contains phase diagram on applied magnetic field-temperature plane. Superconductivity (SC) coexist with ferromagnetism (FM) in a relatively wide range of applied pressure $1 \div 1.6$ GPa (cf. Figure 1.2(a)); both phases disappear simultaneously at critical pressure $p_c \simeq 1.6$ GPa, which provides an evidence, that both

ferromagnetism and superconductivity may be induced by the same mechanism and involving f-electrons. This are the principal features of UGe_2, which interest here.

In Figure 1.3 pressure-temperature phase diagram of UGe_2 is shown indicating types of the magnetic phase transitions [39]. The tricritcal point (TCP) separates regimes of the paramagnetic-ferromagnetic phase transition: At low pressure phase transition is continuous, whereas near critical pressure p_c the transition changes its type to the first order. Additionally, the critical ending point (CEP) is highlighted in Figure 1.3. It separates the first order phase transition between two distinct ferromagnetic phases, FM2 and FM1, from the crossover regime, where the phases are indistinguishable and therefore, there is no phase transition between them. The superconductivity dome is not marked on this plot.

Figure 1.4, taken from [40], contains calculated evolution of the tricritical point (TCP) in applied magnetic field into the quantum critical ending point (QCEP). It agrees with the wing shaped p-H-T phase diagram obtained in experiment [41].

Equally interesting is the behavior of UGe_2 in applied magnetic field. In Figure 1.5 the upper critical field normalized to the superconducting transition temperature H_{c2}/T_c is presented as a function of normalized temperature, for applied magnetic fields parallel to a, b and c direction in the crystal and for three different pressure ranges: from top to bottom: below p_x (FM2 phase), above p_x (FM1 phase), close to the critical pressure suppressing ferromagnetism in FM1 phase. A peculiar property is the unusual reentrant behavior of the upper critical field (reverse "S" shape of H_{c2} curve) for field parallel to the easy magnetic a axis in Figure 1.5 middle plot.

Superconductivity coexisting with ferromagnetism was also reported for UCoGe [17] and URhGe [16]. Both of them have the same orthorhombic crystal structure and are much weaker itinerant ferromagnets, then UGe_2.

Apart from the discovery of superconductivity coexisting with ferromagnetism in URhGe [16], further studies [43] have shown a metamagnetic transition within the ferromagnetic state and revealed that the compound has two magnetic field ranges for superconductivity: low- and high-field superconducting pockets. In the case of UCoGe, superconductivity survives in the paramagnetic phase [44] (cf. Figure 1.6). The situation differs from the case of UGe_2. Nevertheless, superconductivity in UCoGe has different symmetries in the FM and PM phases, denoted as S_1 and S_2 in Figure 1.6.

In this Thesis we will concentrate solely on the situation for UGe_2, as the other related systems (URhGe, UCoGe, and UIr) can be regarded as much weaker itinerant ferromagnets and therefore, a substantial, if not essential, contribution due to spin fluctuations to the pairing may take place. In other words, in order to incorporate those compounds into our description, one should most probably generalize our description to incorporate in it *renormalized spin fluctuations*. No such an effort has been attempted in the literature so far.

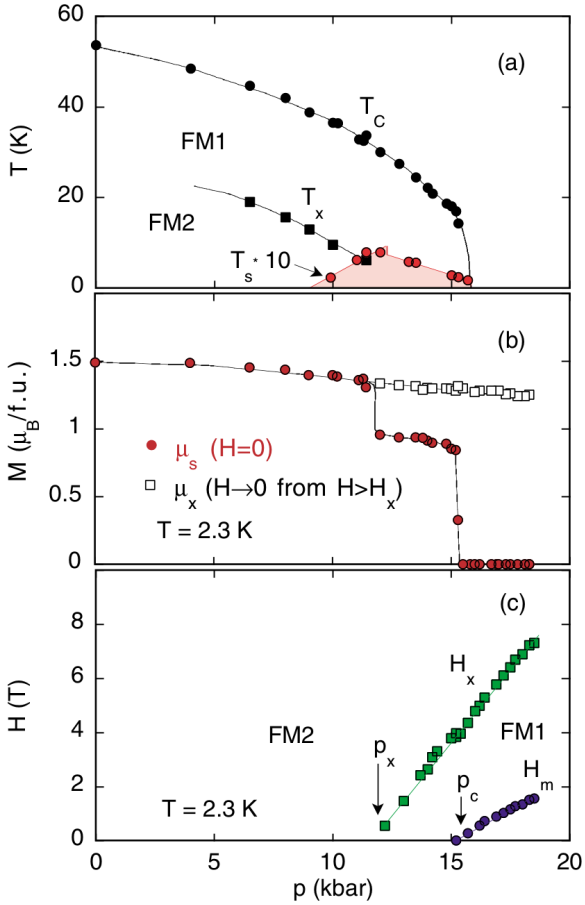

Figure 1.2.: UGe_2 phase diagram. Distinct ferromagnetic phases: FM2, FM1 and their critical temperatures and magnetic moment are shown as functions of exerted pressure (cf. (a) and (b), respectively), as well as the critical applied magnetic fields (c). The superconducting phase is shown as a dome. The magnetic transitions are of the first order; the metastable phase (open squares) is also marked in (b). Figure taken from [38].

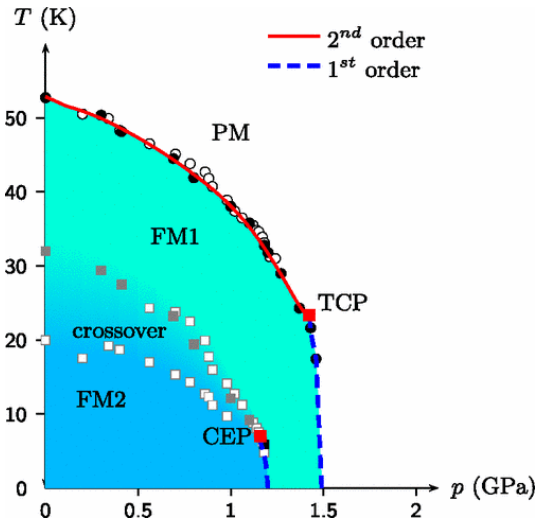

Figure 1.3.: Magnetic phase diagram on temperature-pressure plane with characteristic points: CEP (critical ending point) and TCP (tricritical point). Figure taken from [39].

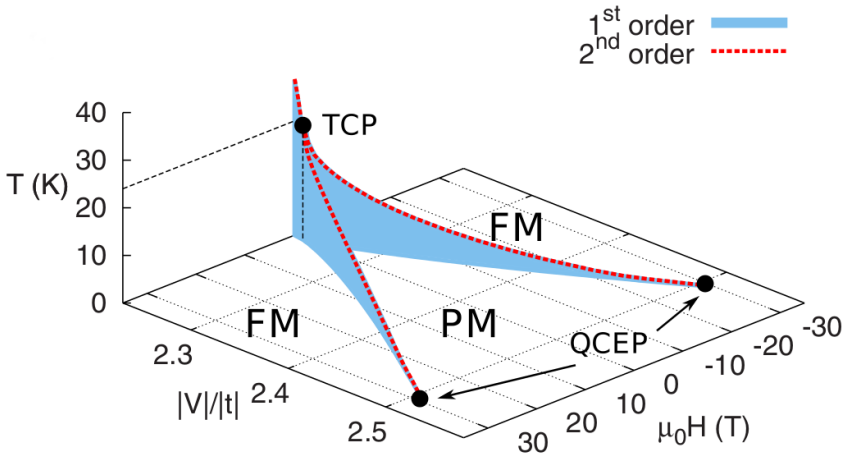

Figure 1.4.: Wing structure of the phase transition planes derived in the non-degenerate Anderson lattice model in SGA approximation. Figure taken from [40].

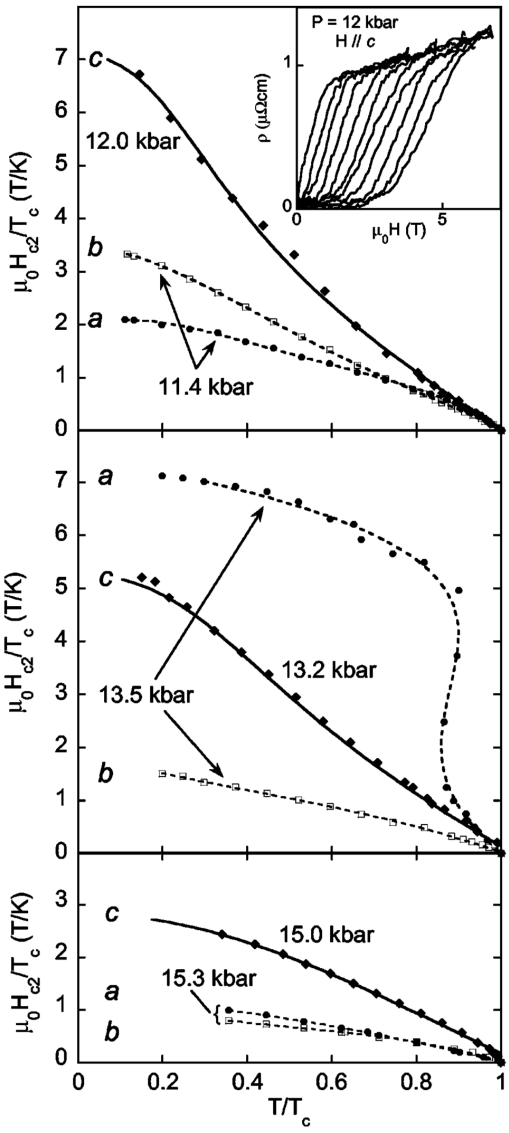

Figure 1.5.: Upper critical field H_{c2} normalized to the superconducting transition temperature T_c versus reduced temperature, for applied magnetic fields parallel to a, b and c axes. Top panel for pressures slightly below p_x (FM2 phase), middle panel for pressures above p_x (FM1 phase), bottom close to the critical pressure suppressing ferromagnetism. Inset: the electrical resistivity dependence of applied field parallel to c axis, for $p = 12$ kbar and at different temperatures from 0.1 to 0.6 K in steps of 0.05 K. Figure taken from [42].

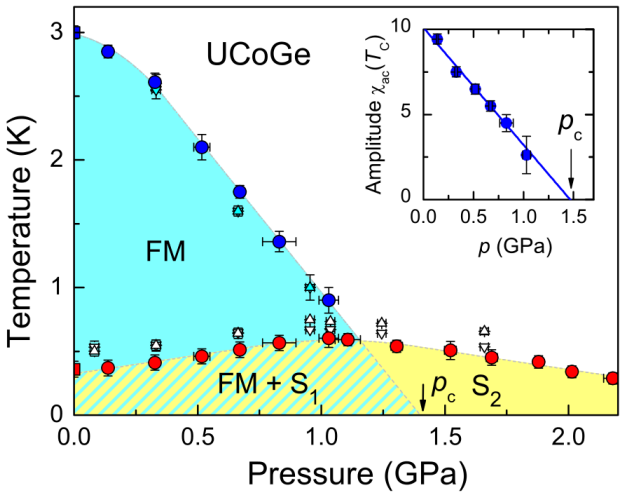

Figure 1.6.: Phase diagram for UCoGe. The superconductivity (yellow area S_1, S_2) in this compound exists also in the paramagnetic phase. Inset: Amplitude of the ac susceptibility $\chi_{ac}(T)$ at the Curie temperature T_C. From the linear p-dependence critical pressure value $p_c = 1.46$ GPa is extrapolated. Figure taken from [44].

1.4. f-electron correlations and dual behavior

Conventionally, electrons in solids can be classified as either localized on their parent atoms or as itinerant (band electrons). However, in the case of strongly correlated systems, especially in heavy fermion systems containing $4f$ (Ce-based compounds) or $5f$ (U-based compounds), such a sharp distinction is oversimplified, since those electrons exhibit both features, if not simultaneously [45], then depending on the situation, e.g., heavy fermions at low temperature are itinerant and heavy, whereas at high temperature localized (the effective mass $m^* \to \infty$, effective magnetic moment approaches that of Ce^{3+}, or U^{3+} or U^{4+} atomic configurations).

The BCS theory does not provide a proper description for correlated electrons, because strong repulsive Coulomb interaction overcomes any phonon-mediated attractive potential. Since superconductivity may require a pairing mechanism, few suggestions for correlated electrons appear. One idea is that the specific quantum ferromagnetic spin fluctuations may drive the superconductivity. It has been tested for UCoGe [46, 47, 48], because the compound has a low magnetic moments ($m \sim 0.039\ \mu_B$/U), so that fluctuations play a significant, if not crucial, role in the weakly-ferromagnetic and paramagnetic regimes. On the contrary, the idea of real-space pairing has been raised [49, 50] for strongly correlated electrons. In the system like UGe_2, where superconductivity coexists with strong ferromagnetism ($m \sim 1.5\mu_B$/U in FM2 phase and $m \sim 1\mu_B$/U in FM1 phase, moments per formula unit, i.e., per U atom), local correlations might play a significant if not crucial role. However, the theory of unconventional superconductivity is still not fully understood, it remains a challenge for theoretical physicists. Here we formulate and test the latter mechanism on example of heavy-fermion system UGe_2.

1.5. Aim and scope of the Thesis

Having in mind presented background we formulate now the goals of this Thesis.

The first subject is to construct a fairly complete phase diagram of UGe_2 at zero temperature and test the concept of real space pairing in the spin-triplet case.

Namely, we continue the studies of magnetism in UGe_2 [51, 40, 52], and both magnetism and superconductivity [53], which involve the orbital degeneracy of f- and c-orbitals, as modeled by the orbitally degenerate Anderson lattice model. The method we are using is the *statistically consistent Gutzwiller approximation* (SGA) [54, 55], which was successfully applied to t-J model and its extensions to describe properties of the high-temperature superconductivity [56, 57, 58], as well as to orbitally non-degenerate Anderson and Anderson-Kondo models to describe features of heavy-fermion systems [51, 40, 52, 59, 60]. Explicitly, superconductivity in the Anderson lattice model was studied in our group in the non-degenerate case within the *Diagrammatic Expansion for Gutzwiller Wave Function* (DE-GWF) [61], with the singlet f-f and f-c pairings, as well as in the non-degenerate Anderson-Kondo lattice model [59, 60] in SGA approximation.

Here we address specifically the situation which is applicable to UGe_2 and there-

fore, we limit ourselves to considering the magnetic moments of f and c character, as well as the appearing superconducting phases: A, A_1 and A_2, each under the proper conditions.

We also combine the superconducting and ferromagnetic phases into a single framework, here discussed as a function of hybridization, mimicking the external pressure dependence. The principal result is that our model describes for the first time and in a *semiquantitative* manner a fairly complete phase diagram for UGe_2. In particular, we select the set of microscopic parameters, for which the ferromagnetic Curie temperature T_C is at least by two order of magnitude higher than the corresponding superconducting ordering temperature T_{SC}, which is of the order of 1 K or a bit smaller (~ 0.5 K). This is a quite nontrivial feature of our formulation, as both properties are obtained within a single scheme for the correlated and hybridized f-c states.

In the second part of Thesis (Chapter 4) we focus on the canonical perturbation expansion (CPE) for both the orbitally non-degenerate and degenerate Anderson lattice models, which is a development of earlier studies for the non-degenerate case [62, 63], where the modified version of Schrieffer-Wolff transformation [64] from Anderson to Anderson-Kondo lattice model has been proposed in the first nontrivial (second) order.

Technical details are presented in the Appendices:

Appendix A Energies of the single-site f-electron Hamiltonian

Appendix B Details of calculations of renormalization factors in SGA approximation

Appendix C Short discussion about the Stoner criterion for ferromagnetism in the orbitally degenerate Anderson model in Hartree-Fock-BCS approximation

Appendix D Numerical details, i.e., Tables with exemplary raw data, calculated band structures, discussion why we have to integrate over the Brillouin zone, instead of much faster summation, and calculations leading to determination of the ground state.

At the end we supply two articles, in which parts of the results presented in Thesis were published, i.e.,

Paper 1 E. Kądzielawa-Major, M. Fidrysiak, P. Kubiczek, and J. Spałek. *Spin-triplet paired phases inside ferromagnet induced by Hund's rule coupling and electronic correlations: Application to* UGe_2. arXiv:1712.08028.

Paper 2 E. Kądzielawa-Major and J. Spałek. *Anderson-Kondo lattice Hamiltonian from the Anderson-lattice model: A modified Schrieffer-Wolff transformation and the effective exchange interactions.* Acta Phys. Pol. A, **126**, 100 (2014).

2. Model and formalism: Real-space pairing in the Anderson lattice model

2.1. Introduction

It is well established that many aspects of the heavy-fermion physics are captured by the Anderson lattice model (or periodic Anderson model), given by the Hamiltonian

$$\hat{\mathcal{H}} = \sum_{ij\sigma} t_{ij}\hat{c}^{\dagger}_{i\sigma}\hat{c}_{j\sigma} + \epsilon^{f}\sum_{i\sigma}\hat{n}^{f}_{i\sigma} + U\sum_{i}\hat{n}^{f}_{i\uparrow}\hat{n}^{f}_{i\downarrow} + \sum_{ij\sigma}\left(V_{ij}\hat{f}^{\dagger}_{i\sigma}\hat{c}_{j\sigma} + V^{*}_{ij}\hat{c}^{\dagger}_{i\sigma}\hat{f}_{j\sigma}\right), \quad (2.1)$$

involving the band electrons (c) and a localized level (f). Standard notation is introduced, where i, j label lattice-site positions, $\sigma = \{\uparrow, \downarrow\}$ is the spin index. Annihilation (creation) operators $\hat{f}_{i\sigma}$, $\hat{c}_{i\sigma}$ ($\hat{f}^{\dagger}_{i\sigma}$, $\hat{c}^{\dagger}_{i\sigma}$) on i-th site, with spin σ, correspond to the f- and c-electrons, respectively. The band carriers (c) are mobile and their dynamics is accounted for by the first (kinetic) term on the right-hand-side of Eq. (2.1). The second part describes localized f-electrons and their strong on-site interaction U. Finally, these two fermionic species are coupled by the hybridization V_{ij} that stems from wave function overlapping in the crystal environment. This picture is actually quite accurate for some heavy-fermion materials, e.g. cerium-based system $CeIn_3$, where the $4f_{5/2}$ multiplet is split into the Γ_7 doublet and Γ_8 quadruplet, out of which the doublet turns out to have lower energy [65, 66].

The above Anderson lattice model (2.1) can be further studied by means of canonical transformation, which effectively eliminates the energetically costly double occupied f-states, to provide the effective magnetic Kondo interaction between localized electrons and conduction bands. The procedure of obtaining the resulting Hamiltonian is exactly described in Chapter 4 and the paper [63]. The resulting Hamiltonian, i.e., Anderson-Kondo Hamiltonian, contains among others f-c Kondo interaction $\sim J^{(\mathrm{K})}_{im}\left(\hat{\mathbf{S}}^{f}_{i}\cdot\hat{\mathbf{S}}^{c}_{m} - \hat{\nu}^{f}_{i}\hat{n}^{c}_{m}/4\right)$, where $J^{(\mathrm{K})}_{im}$ is the antiferromagnetic Kondo exchange integral, $\hat{\mathbf{S}}^{f}_{i}$, $\hat{\mathbf{S}}^{c}_{m}$ are spin operators for f- and c-electron, respectively, and $\hat{\nu}^{f}_{i}$, $\hat{n}^{c}_{m}$ are number of particles operators. The Anderson-Kondo lattice model can be used for description of cerium-based compounds [59, 60]. The effective Kondo interaction induces competition between two limiting cases (i) antiferromagnetic-type (or, more generally, spin-density-wave-type ordering) and (ii) Fermi liquid hosting heavy quasiparticles (the so-called heavy-fermion regime). The latter phase emerges due to screening of the localized f-states by conduction electrons. The transition between those two states is governed by the phase diagram due Doniach [67] that describes

well several families of f-electron materials.

For modeling uranium compounds underscreened Anderson lattice with two f-orbitals and one c-band was proposed and discussed in the context of URu_2Si_2 [68, 69].

In this Thesis, we focus primarily on the uranium-based compound UGe_2. The experiments on this compound [70, 71] point to the nominal U^{3+} or U^{4+} uranium oxidation state (resulting in $5f^3$ or $5f^2$ electronic configurations, respectively). In this situation, the minimal Anderson-lattice-model description turns out to be insufficient. At least two f-orbitals should be included to account for the degeneracy inherent to this material. Another important difference between U and Ce compounds is that the $5f$ electrons are typically less correlated than their $4f$ counterparts. This places UGe_2 in the regime of intermediate- to (possibly) strong correlations. An important question that will be addressed here is whether the multi-orbital structure of this material plays the role in stabilization of the magnetic order and superconductivity emerging on the border between distinct ferromagnetic phases.

Motivated by the case of UGe_2, in this chapter we thus introduce the orbitally degenerate Anderson lattice model (doubly degenerate both f-orbitals and c-band) and compare it with its non-degenerate correspondant. Then, the mechanism leading to the emergence of local spin-triplet pairing in this model is described. In the last part of this chapter we present the method, *statistically consistent Gutzwiller approach* (SGA), which is used in the Thesis to obtain results discussed in detail in Chapter 3.

The non-degenerate Anderson lattice model was analyzed in our group in [51, 40, 52] in the context of magnetic properties of UGe_2. Since it was not sufficient to account for spin-triplet superconductivity, because of absence of the specific pairing mechanism in the model, the idea of incorporating the orbital degeneracy into the model was introduced and analyzed [53]. The orbital degeneracy allows for inclusion of the Hund's coupling, which plays a significant role in the pairing mechanism and considered in this Thesis.

The *statistically consistent Gutzwiller approach*, described in Section 2.5 was originally introduced in [54, 55] and successfully incorporated in the case of degenerate Hubbard model [56, 57] or Anderson-Kondo lattice model [59, 60] to describe properties of selected narrow-band systems.

2.2. Orbitally degenerate Anderson lattice model

The non-degenerate Anderson lattice model, containing two types of electrons representing localized (here $5f$) orbitals and conduction (c) bands is not sufficient to describe interorbital interactions between different f-states in real materials, as well as it cannot lead to interorbital spin-triplet superconductivity. Therefore, we consider double degeneracy of both c- and f-states, so that each of them is characterized by an additional orbital index $l = 1, 2$. The initial Hamiltonian (orbitally degenerate

Anderson lattice model) in the site (real-space) language is given

$$\hat{\mathcal{H}} = \hat{\mathcal{H}}^c + \hat{\mathcal{H}}^{cf} + \hat{\mathcal{H}}^f, \tag{2.2}$$

where the first term $\hat{\mathcal{H}}^c$ is the kinetic (band) terms describing the conduction electrons, the second $\hat{\mathcal{H}}^{cf}$ accounts for mixing between c- and f-electrons, and the last $\hat{\mathcal{H}}^f$ is the Hamiltonian of localized f-electron levels. This three terms are defined as

$$\hat{\mathcal{H}}^c = \sum_{ijl\sigma} t_{ijl} \hat{c}^\dagger_{il\sigma} \hat{c}_{jl\sigma}, \tag{2.3}$$

$$\hat{\mathcal{H}}^{cf} = \sum_{ijl\sigma} \left(V_{ij} \hat{f}^\dagger_{il\sigma} \hat{c}_{jl\sigma} + V^*_{ij} \hat{c}^\dagger_{il\sigma} \hat{f}_{jl\sigma} \right), \tag{2.4}$$

$$\begin{aligned} \hat{\mathcal{H}}^f &= \epsilon^f \sum_{il\sigma} \hat{n}^f_{il\sigma} + U \sum_{il} \hat{n}^f_{il\uparrow} \hat{n}^f_{il\downarrow} + U' \sum_i \left(\hat{n}^f_{i1\uparrow} \hat{n}^f_{i2\downarrow} + \hat{n}^f_{i2\uparrow} \hat{n}^f_{i1\downarrow} \right) \\ &\quad + (U' - J) \sum_{i\sigma} \hat{n}^f_{i1\sigma} \hat{n}^f_{i2\sigma} - J \sum_i \left(\hat{f}^\dagger_{i1\uparrow} \hat{f}_{i1\downarrow} \hat{f}^\dagger_{i2\downarrow} \hat{f}_{i2\uparrow} + \hat{f}^\dagger_{i2\uparrow} \hat{f}_{i2\downarrow} \hat{f}^\dagger_{i1\downarrow} \hat{f}_{i1\uparrow} \right) \end{aligned} \tag{2.5}$$

$$= \epsilon^f \sum_{il\sigma} \hat{n}^f_{il\sigma} + U \sum_{il} \hat{n}^f_{il\uparrow} \hat{n}^f_{il\downarrow} + U' \sum_i \hat{n}^f_{i1} \hat{n}^f_{i2} - 2J \sum_i \left(\hat{\mathbf{S}}^f_{i1} \cdot \hat{\mathbf{S}}^f_{i2} + \frac{1}{4} \hat{n}^f_{i1} \hat{n}^f_{i2} \right). \tag{2.6}$$

Standard notation is introduced, where i, j label lattice-site positions, $l = 1, 2$ is the orbital index for both the starting atomic f and delocalized c orbitals, $\sigma = \{\uparrow, \downarrow\}$ is the spin index. Annihilation (creation) operators $\hat{f}_{il\sigma}$, $\hat{c}_{il\sigma}$ ($\hat{f}^\dagger_{il\sigma}$, $\hat{c}^\dagger_{il\sigma}$) on i-th site on l-th orbital, with spin σ, correspond to the f- and c-electrons, respectively. Those two species can be mixed via the hybridization term $\hat{\mathcal{H}}^{cf}$ (2.4), with V_{ij}, being the magnitude of hybridization between i and j sites and for the same orbital l. The term $\hat{\mathcal{H}}^c$ (2.3) contains only the hopping term for itinerant c-electrons. The hopping integral t_{ijl} describes c-electrons jumping from i-th site to j-th on the same orbital l. Additionally, $t_{iil} = 0$ is chosen to establish reference level of atomic states f with respect to that for the conduction electrons.

The complex part of model is $\hat{\mathcal{H}}^f$ (2.6), where $\hat{n}^f_{il\sigma} \equiv \hat{f}^\dagger_{il\sigma} \hat{f}_{il\sigma}$ is the f-electrons number operator and $\hat{\mathbf{S}}^f_{il}$ is f-electron spin operator $\left(\hat{S}^{f+}_{il}, \hat{S}^{f-}_{il}, \hat{S}^{fz}_{il} \right)$ and $\hat{S}^{f+}_{il} \equiv \hat{f}^\dagger_{il\uparrow} \hat{f}_{il\downarrow}$, $\hat{S}^{f-}_{il} \equiv \hat{f}^\dagger_{il\downarrow} \hat{f}_{il\uparrow}$, $\hat{S}^{fz}_{il} \equiv \frac{1}{2} \left(\hat{n}^f_{il\uparrow} - \hat{n}^f_{il\downarrow} \right)$. The Hamiltonian $\hat{\mathcal{H}}^f$ (2.6) encompasses the following terms:

- ϵ^f – single-particle part of the energy of f-electron with respect to the conduction-band reference point, since it has been chosen that for c-electrons: $t_{iil} = 0$,
- U – the intraatomic intraorbital repulsive Coulomb interaction (the Hubbard term), the largest energy scale in the system,
- U' – the intraatomic interorbital Coulomb interaction between f-electrons,
- J – intraatomic interorbital ferromagnetic exchange, *the Hund's coupling*, which

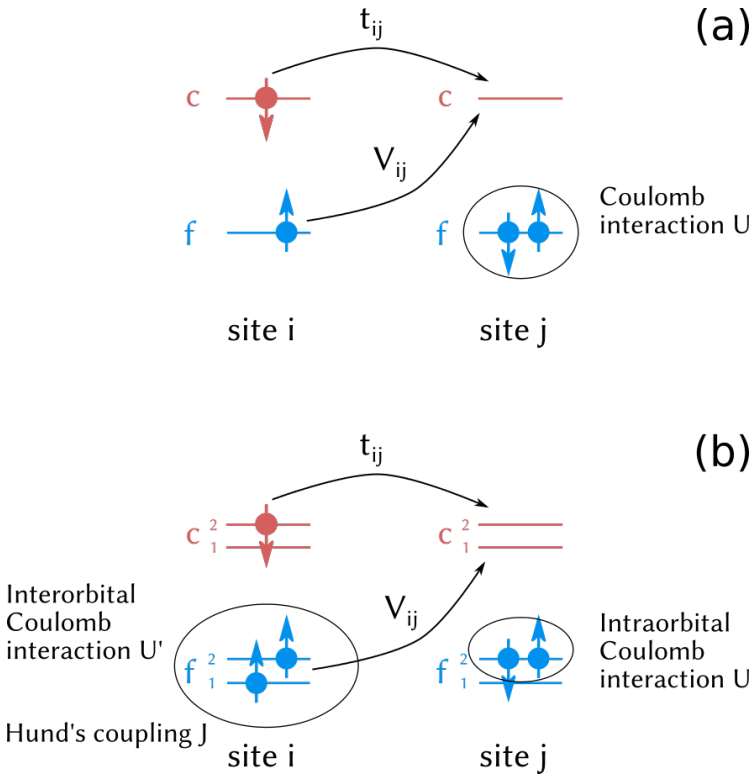

Figure 2.1.: Schematic representation of different interaction terms in the Anderson lattice models. (a) Non-degenerate, (b) orbitally degenerate case. The inclusion of the degeneracy into the model allows for the occurrence of new types of interactions: interorbital Coulomb interaction U' and most importantly the Hund's coupling J.

expresses explicitly, together with the term $\sim U'$, the difference from an orbitally non-degenerate case.

The direct ferromagnetic exchange J favors formation of interorbital spin-triplet configurations, which is commonly referred to as the Hund's rule. From full rotational invariance of the orbital basis we assume that $U' = U - 2J$.

A remark is in order at this point. Full rotational symmetry would require that the so-called pair-hopping term $\sim J' \hat{f}^\dagger_{i1\uparrow} \hat{f}^\dagger_{i1\downarrow} \hat{f}_{i2\downarrow} \hat{f}_{i2\uparrow}$ is also included in the f-electron Hamiltonian (2.5). However, already at the level of mean-field decoupling of this contribution $\sim J' \langle \hat{f}^\dagger_{i1\uparrow} \hat{f}^\dagger_{i1\downarrow} \rangle \langle \hat{f}_{i2\downarrow} \hat{f}_{i2\uparrow} \rangle$, it becomes apparent that is supports interorbital spin-singlet pairing. The latter is not a feasible option for UGe_2 for several reasons: (i) The substantial on-site repulsion U would inhibit intra-orbital s-wave pairing (this happens, e.g. for the case high-T_c cuprates, described reasonably well by the one-band Hubbard model with substantial local interactions), (ii) in UGe_2, superconductivity coexists with large-moment ferromagnetic order (moments vary in the range $\sim 1 - 1.5\,\mu_B$/U), and (iii) the upper-critical field H_{c2} is known to exceed its Pauli limiting for certain pressures [70]. Thus, we discard the pair-hopping

term in the further discussion. A more formal analysis of this aspect, along with the discussion of the energy-level structure of the local Hamiltonian $\hat{\mathcal{H}}^f$, is presented in Appendix A.

2.3. Real-space representation of pairing operators

To identify the dominant pairing channels, we need to rewrite the local interaction term $\hat{\mathcal{H}}^f$ in terms of the spin-triplet- and the spin-singlet-pairing operators $\hat{A}^\dagger_{im}$ and $\hat{B}^\dagger_i$, respectively [72]. The latter are defined as

$$\hat{A}^\dagger_{im} = \begin{cases} \hat{f}^\dagger_{i1\uparrow}\hat{f}^\dagger_{i2\uparrow} & m = 1, \\ \frac{1}{\sqrt{2}}\left(\hat{f}^\dagger_{i1\uparrow}\hat{f}^\dagger_{i2\downarrow} + \hat{f}^\dagger_{i1\downarrow}\hat{f}^\dagger_{i2\uparrow}\right) & m = 0, \\ \hat{f}^\dagger_{i1\downarrow}\hat{f}^\dagger_{i2\downarrow} & m = -1, \end{cases} \tag{2.7}$$

$$\hat{B}^\dagger_i = \frac{1}{\sqrt{2}}\left(\hat{f}^\dagger_{i1\uparrow}\hat{f}^\dagger_{i2\downarrow} - \hat{f}^\dagger_{i1\downarrow}\hat{f}^\dagger_{i2\uparrow}\right), \tag{2.8}$$

where the three triplet components correspond to z-axis spin projection $m = 1, 0, -1$. The above pairing operators can be expressed in terms of the spin-spin and density-density interactions as follows:

$$\sum_m \hat{A}^\dagger_{im}\hat{A}_{im} \equiv \hat{\mathbf{S}}^f_{i1}\cdot\hat{\mathbf{S}}^f_{i2} + \frac{3}{4}\hat{n}^f_{i1}\hat{n}^f_{i2}, \tag{2.9}$$

$$\hat{B}^\dagger_i\hat{B}_i \equiv -\left(\hat{\mathbf{S}}^f_{i1}\cdot\hat{\mathbf{S}}^f_{i2} - \frac{1}{4}\hat{n}^f_{i1}\hat{n}^f_{i2}\right). \tag{2.10}$$

With the help of this representation, one can rewrite the f-electron part of the orbitally degenerate Anderson model $\hat{\mathcal{H}}^f$ (2.6) using spin-triplet- and spin-singlet-pairing operators (2.7)-(2.8)

$$\hat{\mathcal{H}}^f = \epsilon^f\sum_{il\sigma}\hat{n}^f_{il\sigma} + U\sum_{il}\hat{n}^f_{il\uparrow}\hat{n}^f_{il\downarrow} + (U'+J)\sum_i\hat{B}^\dagger_i\hat{B}_i + (U'-J)\sum_{im}\hat{A}^\dagger_{im}\hat{A}_{im}. \tag{2.11}$$

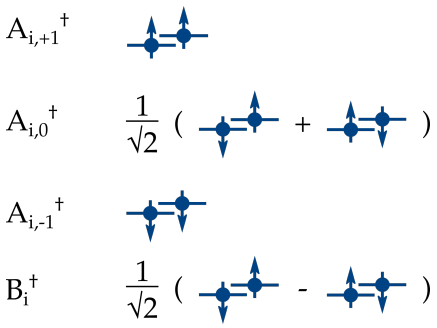

Figure 2.2.: Schematic picture of real-space pairing related to (2.7) and (2.8),

We can see that the exchange interaction turns into the local (real-space) spin-triplet pairing and vice versa. If $J > U'$ or, equivalently, $J > U/3$, the last term in (2.11) $(U' - J)\,\hat{A}^{\dagger}_{im}\hat{A}_{im}$ provides an attractive interaction between f-electrons located on different orbitals of the same atom in the spin-triplet channel. In analogy to the BCS theory, the system prefers paired states characterized by non-zero anomalous averages $\langle A_{im}\rangle \neq 0$. Spin-singlet pairing is not favorable, because it leads to electronic configurations with larger energy $U' + J = U - J > 0$.

The above analysis is clearly simplistic as it bases on the Hartree-Fock decoupling of the interaction. However, the proper inclusion of the correlation effects is not expected to affect the symmetry of the order parameter, though substantial quantitative changes are anticipated. This is explicitly demonstrated in the following chapters within the Gutzwiller wave function ansatz for the ground state. Hereafter we thus assume that the Hund's rule exchange is large enough to overcome the interorbital repulsion and to provide overall attractive pairing in the spin-triplet channel. A direct consequence of such a local attractive coupling is that the spatial part of the Cooper pair should have s-wave symmetry. It should be emphasized that the considered s-wave triplet pairing is unconventional in the sense that it is not admissible in the one-band situation as a direct consequence of Fermi statistics. Here, the overall antisymmetry of the Cooper-pair wave function is due to formation of the orbital singlet by the paired electrons.

2.4. The magnetic field

To incorporate the magnetic field, we add the Zeeman term to the Hamiltonian (2.2)

$$\hat{\mathcal{H}}^{\mathrm{Z}} = -g\mu_B\mu_0\mathbf{H}\cdot\hat{\mathbf{S}}, \tag{2.12}$$

where g is the Landé factor, μ_B is the Bohr magneton and $\mu_0\mathbf{H}$ is magnetic field, whose components are measured in Tesla (T) units. We assume that values of the Landé factor are the same for both f- and c-electrons: $g = 2$, which is the value for free electrons. Note that the value of f electron Landé factor g in UGe_2 is not known precisely, however other choices of g for the non-degenerate Anderson lattice model and its influence on results was examined in Ref. [52]. The best agreement of calculations with experimental data [41] provides $g = 2$. Choice of other values of Landé factor leads to a shift of metamagnetic transition (critical ending point - CEP, cf. Figure 1.3). In our calculations, we take magnetic field oriented in z-direction $\mu_0\mathbf{H} = (0, 0, \mu_0 H)$, so that

$$\hat{\mathcal{H}}^{\mathrm{Z}} = -\frac{1}{2}g\mu_B\mu_0 H\sum_{il\sigma}\sigma\left(\hat{n}^{c}_{il\sigma} + \hat{n}^{f}_{il\sigma}\right) = -h\sum_{il\sigma}\sigma\left(\hat{n}^{c}_{il\sigma} + \hat{n}^{f}_{il\sigma}\right), \tag{2.13}$$

where $\sigma = +1$ for spin up, and $\sigma = -1$ for spin down. To simplify the notation, introduce the reduced magnetic field $h = \frac{1}{2}g\mu_B\mu_0 H$, measured in the units of $|t|$ – the nearest-neighbor hopping of c-electrons.

Note that at this point, we are unable to include the orbital magnetic field effects

by means of Peierls substitution [73]. This is due to the necessity of considering exceedingly large unit cells for low experimentally accessed fields, that are related to the emergence of the Hofstadter butterfly spectrum [74]. To illustrate this point we estimate the size of the unit cell for $\mu_0 H = 10$ T. The area of the magnetic cell S corresponds to the slab of the lattice encompassing one flux quantum, explicitly

$$S = \frac{\Phi_0}{\mu_0 H} \simeq 2 \cdot 10^{-16} \text{ m}^2, \tag{2.14}$$

where $\Phi_0 \simeq 2.07 \cdot 10^{-15}$ Wb is the magnetic flux quantum. Therefore, in our calculations we should take cell over 100×100, which is too expensive numerically.

By explicitly studying physics of the degenerate Anderson lattice model in the following chapters, we will show that the field-induced metamagnetic and superconducting transitions close to the first-order instability points are driven to large extent by the Zeeman magnetic fields and thus the Pauli limit, considered here turns out to be a good approximation. This changes as one moves to more itinerant (large-hybridization regime), where this approximation brakes down.

2.5. Statistically consistent Gutzwiller approximation (SGA)

For weakly correlated electron systems, where the interaction energy is non-zero, but much smaller than the other energy scales (for example, kinetic energy), the standard Hartree-Fock-BCS approximation provides satisfactory results. Nevertheless, many of realistic compounds are considered to be moderately/intermediately or strongly correlated. In intermediate region correlations have significant impact on other energy scales.

2.5.1. Short description of the method

Here we discuss main idea of the *statistically consistent Gutzwiller approximation* (SGA). The method can be constructed in following steps

1. Define the correlated wave function $|\Psi_{\text{G}}\rangle$ using correlator – an operator, which takes into account local correlations, and its action on the wave function of uncorrelated electrons. The correlator depends on a variational parameter and acts on the each lattice site by reducing the possibility of doubly occupied sites and orbitals.

2. Calculate the ground state energy E_{G} in the correlated state $E_{\text{G}} = \langle\Psi_{\text{G}}|\hat{\mathcal{H}}|\Psi_{\text{G}}\rangle / \langle\Psi_{\text{G}}|\Psi_{\text{G}}\rangle$.

3. Obtain the effective Hamiltonian $\hat{\mathcal{H}}_{\text{eff}}$, i.e., Eq. (2.30), depending on the variational parameters, which contains renormalized parameters, e.g., hybridization, f-level, pairing amplitude. Construction of the effective Hamiltonian bases

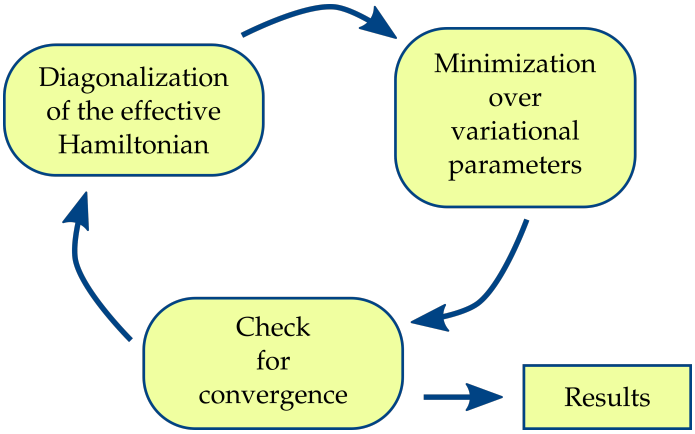

Figure 2.3.: The minimization procedure, in which the ground state of the system is acquired: Steps 4, 5, and 6 from the description of the method.

on the introduction of constraints for each mean-field average $\langle\hat{O}\rangle_0$ that appears in the calculated ground state energy E_G, i.e., $\hat{\mathcal{H}}_\mathrm{eff} = E_\mathrm{G} - \mu N_e + \sum_{\hat{O}} \lambda_{\hat{O}} \left(\hat{O} - \langle\hat{O}\rangle_0\right)$, cf. Eq. (2.29).

4. Diagonalize the effective Hamiltonian $\hat{\mathcal{H}}_\mathrm{eff}$.

5. Minimize the energy functional $\mathcal{F} = -\frac{1}{\beta} \ln \mathrm{Tr} \exp\left(-\beta\hat{\mathcal{H}}_\mathrm{eff}\right)$, where $\beta = 1/k_\mathrm{B}T$ and k_B is the Boltzmann constant, over variational parameters.

6. Check for convergence. If convergence is not achieved, go back to the point 4. Minimization procedure after obtaining the effective Hamiltonian is depicted in Figure 2.3.

Within SGA method the initial model (2.2) is mapped into the effective Hamiltonian (2.30), which describes quasiparticles: eigenvalues of the effective Hamiltonian are interpreted as quasiparticle excitation energies [75].

The effective Hamiltonian and its eigenvalues are obtained analytically, the 5th and 6th steps are done numerically.

2.5.2. Formal description of the method

Now, we introduce the formal method of solving the orbitally degenerate Anderson model (2.2), the so-called statistically consistent Gutzwiller approximation (SGA) [54, 55]. We define the Gutzwiller wave function $|\Psi_\mathrm{G}\rangle$ via $|\Psi_0\rangle$ – the product state (Slater determinant)

$$|\Psi_\mathrm{G}\rangle = \hat{\mathcal{P}}_\mathrm{G}|\Psi_0\rangle = \prod_{il} \hat{\mathcal{P}}_{il}|\Psi_0\rangle, \tag{2.15}$$

where $\hat{\mathcal{P}}_{il}$ acts on i-th site and l-th orbital and reduces the possibility of doubly occupations. $\hat{\mathcal{P}}_{\mathrm{G}}$ denotes the Gutzwiller correlator [76, 77] and in general:

$$\hat{\mathcal{P}}_{il} = \lambda_{il\emptyset}\left(1-\hat{n}^f_{il\uparrow}\right)\left(1-\hat{n}^f_{il\downarrow}\right) + \sum_{\sigma}\lambda_{il\sigma}\hat{n}^f_{il\sigma}\left(1-\hat{n}^f_{il\bar{\sigma}}\right) + \lambda_{ild}\hat{n}^f_{il\uparrow}\hat{n}^f_{il\downarrow}, \tag{2.16}$$

where $\hat{n}^f_{il\sigma}$ is the f-electron number operator as before, $\lambda_{il\alpha}$ are Language multipliers and d means double occupancy ($\uparrow\downarrow$). Note that in the system, there are two electron species: f and c. Only the first kind is correlated and c-electrons stay uncorrelated, since the Coulomb interaction of conducting electrons is omitted. In our considerations it is assumed that factors $\lambda_{il\alpha}$, where $\alpha \in \{\emptyset, \uparrow, \downarrow, d\}$, do not depend on site number or orbital (isotropic system with equivalent orbitals $l = 1, 2$), therefore in notation indexes i and l are skipped: $\lambda_{il\alpha} \to \lambda_\alpha$.

To solve our system we need to find the ground state energy E_{G} calculated in correlated state $|\Psi_{\mathrm{G}}\rangle$

$$E_{\mathrm{G}} = \frac{\langle\Psi_{\mathrm{G}}|\hat{\mathcal{H}}|\Psi_{\mathrm{G}}\rangle}{\langle\Psi_{\mathrm{G}}|\Psi_{\mathrm{G}}\rangle} = \frac{\langle\Psi_0|\hat{\mathcal{P}}_{\mathrm{G}}\hat{\mathcal{H}}\hat{\mathcal{P}}_{\mathrm{G}}|\Psi_0\rangle}{\langle\Psi_{\mathrm{G}}|\Psi_{\mathrm{G}}\rangle}. \tag{2.17}$$

Thus, one has to obtain the action of correlator $\hat{\mathcal{P}}_{\mathrm{G}}$ on f-electron operators occurring in initial Hamiltonian (2.2), i.e.: $\hat{f}^\dagger_{il\sigma}$, $\hat{n}^f_{il\sigma}$, $\hat{n}^f_{il\uparrow}\hat{n}^f_{il\downarrow}$, $\hat{n}^f_{i1}\hat{n}^f_{i2}$, $\hat{\mathbf{S}}^f_{i1}\cdot\hat{\mathbf{S}}^f_{i2}$.

To explicitly illustrate the effect of the correlator $\hat{\mathcal{P}}_{\mathrm{G}}$ on the quasiparticle properties, we show, step by step, how $\hat{\mathcal{P}}_{il}$ (2.16) acts on f-electron creation operator $\hat{f}^\dagger_{il\sigma}$. Impact of the correlator on remaining operators are discussed carefully in Appendix B. Using definition (2.16), one can write down

$$\hat{\mathcal{P}}_{il}\hat{f}^\dagger_{il\sigma}\hat{\mathcal{P}}_{il} = \lambda_\emptyset\lambda_\sigma\hat{f}^\dagger_{il\sigma} + \left(\lambda_d\lambda_{\bar{\sigma}} - \lambda_\emptyset\lambda_\sigma\right)\hat{f}^\dagger_{il\sigma}\hat{n}^f_{il\bar{\sigma}}. \tag{2.18}$$

Let us denote

$$\hat{n}^{f\ \mathrm{HF}}_{il\sigma} = \hat{n}^f_{il\sigma} - n^f_{l\sigma}, \tag{2.19}$$

$$n^f_{l\sigma} = \langle\Psi_0|\hat{n}^f_{il\sigma}|\Psi_0\rangle = \langle\hat{n}^f_{il\sigma}\rangle_0. \tag{2.20}$$

Generally, mean value of a operator $\hat{O}$ calculated in the uncorrelated state is denoted as $\langle\hat{O}\rangle_0 = \langle\Psi_0|\hat{O}|\Psi_0\rangle$. Note that $\langle\hat{n}^{f\ \mathrm{HF}}_{il\sigma}\rangle_0 = 0$. From (2.18) we obtain

$$\hat{\mathcal{P}}_{il}\hat{f}^\dagger_{il\sigma}\hat{\mathcal{P}}_{il} = q_\sigma\hat{f}^\dagger_{il\sigma} + \left(\lambda_d\lambda_{\bar{\sigma}} - \lambda_\emptyset\lambda_\sigma\right)\hat{n}^{f\ \mathrm{HF}}_{il\bar{\sigma}}\hat{f}^\dagger_{il\sigma}, \tag{2.21}$$

where factor q_σ is defined as

$$q_\sigma = \lambda_\emptyset\lambda_\sigma + \left(\lambda_d\lambda_{\bar{\sigma}} - \lambda_\emptyset\lambda_\sigma\right)n^f_{l\bar{\sigma}}. \tag{2.22}$$

In the initial Hamiltonian (2.2) the only part containing single f-electron creation or annihilation operator is the hybridization term (2.4). The mean value evaluated

in correlated state $|\Psi_{\mathrm{G}}\rangle$ is denoted as $\langle\hat{O}\rangle_{\mathrm{G}} = \langle\Psi_{\mathrm{G}}|\hat{O}|\Psi_{\mathrm{G}}\rangle$. Therefore,

$$\langle\hat{f}^{\dagger}_{il\sigma}\hat{c}_{jl\sigma}\rangle_{\mathrm{G}} = \langle\hat{\mathcal{P}}_{il}\hat{f}^{\dagger}_{il\sigma}\hat{c}_{jl\sigma}\hat{\mathcal{P}}_{il}\rangle_0 \simeq q_{\sigma}\langle\hat{f}^{\dagger}_{il\sigma}\hat{c}_{jl\sigma}\rangle_0. \tag{2.23}$$

Factor q_σ defined in Eq. (2.22) is the f-c hybridization renormalization. The last expression in Eq. (2.23) is fulfilled exactly only in the limit $d \to \infty$, i.e., in the limit of infinite lattice coordination number, where we include correlation effects coming from other sites. Such an expansion is known as *Diagrammatic Expansion for Gutzwiller Wave Function* (DE-GWF), where correlations from other sites are taken into account with introduced real-space cutoff [78, 79, 80, 61].

In similar way actions of the Gutzwiller correlator on remaining operators are obtained. Detailed calculations are presented in Appendix B. We would like to mention only a few important assumptions. Firstly, in our calculations orbitals are equivalent, therefore $n^f_{1\sigma} = n^f_{2\sigma}$. Secondly, since we aim to describe spin-triplet superconductivity, it is chosen that only equal spin components of pairing operator (2.7) are non-zero, it is $\langle\hat{f}^{\dagger}_{i1\sigma}\hat{f}^{\dagger}_{i2\sigma}\rangle_0 \neq 0$ and $\langle\hat{f}^{\dagger}_{i1\sigma}\hat{f}^{\dagger}_{i1\bar{\sigma}}\rangle_0 = 0$, thus $\langle\hat{\mathbf{S}}^{+}_{i1}\hat{\mathbf{S}}^{-}_{i2}\rangle_0 = \langle\hat{\mathbf{S}}^{-}_{i1}\hat{\mathbf{S}}^{+}_{i2}\rangle_0 = 0$ and mean values of the singlet-pairing operator (2.8) and $m = 0$ component of spin-triplet pairing operator (2.7) vanish: $\langle B^{\dagger}_i\rangle_0 = 0$, $\langle A^{\dagger}_{i0}\rangle_0 = 0$. This can be well justified for the case of UGe_2 as it exhibits substantial uniaxial-type magnetic anisotropy [81], which disfavors opposite-spin pairing. As intraorbital Coulomb interaction is quite large, intraorbital spin-singlet pairing is also omitted $\langle\hat{f}^{\dagger}_{il\uparrow}\hat{f}^{\dagger}_{il\downarrow}\rangle_0 = 0$. The latter is also discussed in Appendix A in the context of inclusion of the pair-hopping term.

The ground state energy calculated in the correlated state with the Zeeman term (2.13) included is obtained

$$\begin{aligned} E_{\mathrm{G}} = &\sum_{ijl\sigma}\left(t_{ij} - h\sigma\delta_{ij}\right)\langle\hat{c}^{\dagger}_{il\sigma}\hat{c}_{jl\sigma}\rangle_0 + \sum_{ijl\sigma}\left(q_{\sigma}V_{ij}\langle\hat{f}^{\dagger}_{il\sigma}\hat{c}_{jl\sigma}\rangle_0 + C.c.\right) \\ &+ \Lambda\sum_{l\sigma}\left(\epsilon^f - h\sigma\right)n^f_{l\sigma} + \Lambda U\sum_{l} d^2 + \Lambda U'\left(n^f_{1\uparrow}n^f_{2\downarrow} + n^f_{1\downarrow}n^f_{2\uparrow}\right) \\ &+ \Lambda\left(U' - J\right)\sum_{\sigma} n^f_{1\sigma}n^f_{2\sigma} + \left(g_{1\sigma}U' + g_{2\sigma}\left(U' - J\right)\right)\sum_{i\sigma}\langle\hat{f}^{\dagger}_{i1\sigma}\hat{f}^{\dagger}_{i2\sigma}\rangle_0\langle\hat{f}_{i2\sigma}\hat{f}_{i1\sigma}\rangle_0, \end{aligned} \tag{2.24}$$

where Λ is the total number of lattice sites, d^2 – intraorbital double occupancies and factors $g_{1\sigma}$, $g_{2\sigma}$ are given below:

$$d^2 = \langle\hat{n}^f_{il\uparrow}\hat{n}^f_{il\downarrow}\rangle_{\mathrm{G}} = \lambda^2_d n^f_{l\uparrow}n^f_{l\downarrow}, \tag{2.25}$$

$$g_{1\sigma} = 2\times(\lambda^2_d - \lambda^2_{\bar{\sigma}})\times(\lambda^2_{\sigma} + (\lambda^2_d - \lambda^2_{\sigma})n^f_{l\bar{\sigma}})\times n^f_{l\bar{\sigma}}, \tag{2.26}$$

$$g_{2\sigma} = (\lambda^2_d - \lambda^2_{\bar{\sigma}})^2\times\left(n^f_{l\bar{\sigma}}\right)^2 + \left(\lambda^2_{\sigma} + (\lambda^2_d - \lambda^2_{\sigma})n^f_{l\bar{\sigma}}\right)^2, \tag{2.27}$$

$$\mathcal{V}_{\sigma} = g_{1\sigma}U' + g_{2\sigma}\left(U' - J\right). \tag{2.28}$$

Indices $\alpha = 1, 2$ in the coefficients $g_{\alpha\sigma}$ do not stand for orbital index, but enumerate the factors. We would like to stress also that in article [82] the pairing potential $\mathcal{V}_\sigma$ is defined with opposite sign: $\mathcal{V}_{\sigma} = -\left(g_{1\sigma}U' + g_{2\sigma}\left(U' - J\right)\right)$ (here negative value of $\mathcal{V}_\sigma$ means that the coupling is attractive, i.e., it supports superconductivity). Next,

the effective Hamiltonian is obtained as

$$\hat{\mathcal{H}}_{\text{eff}} = E_{\text{G}} - \mu N_e + \sum_{\hat{O}} \lambda_{\hat{O}} \left(\hat{O} - \langle \hat{O} \rangle_0 \right), \tag{2.29}$$

where operators $\hat{O}$ are composed from two creation or annihilation operators with non-zero averages. Specifically, $\hat{O} \in \{\hat{c}^\dagger_{il\sigma}\hat{c}_{jl\sigma},\ \hat{f}^\dagger_{il\sigma}\hat{c}_{jl\sigma},\ \hat{c}^\dagger_{il\sigma}\hat{f}_{jl\sigma},\ \hat{n}^f_{il\sigma},\ \hat{n}^c_{il\sigma},\ \hat{f}^\dagger_{i1\sigma}\hat{f}^\dagger_{i2\sigma},\ \hat{f}_{i2\sigma}\hat{f}_{i1\sigma}\}$ and $\lambda_{\hat{O}} = \frac{\partial E_{\text{G}}}{\partial \langle \hat{O} \rangle_0}$. The coefficients $\lambda_{\hat{O}}$ of the last term of (2.29) play the role of Lagrange multipliers, ensuring that the expectation value obtained by solving the Bogoliubov-de-Gennes (BdG) equations and optimization of the free energy functional are the same. This is essential feature of the SGA method and the factor that distinguishes it from the simple Gutzwiller approximation. As was shown previously, this consistency needs to be respected in order to reproduce correctly the thermodynamics of the correlated compounds [83, 75]. In this way the effective Hamiltonian can be written as

$$\begin{aligned}
\hat{\mathcal{H}}_{\text{eff}} = &\sum_{ijl\sigma} \left(t_{ij} - (\mu + h\sigma)\,\delta_{ij} \right) \hat{c}^\dagger_{il\sigma}\hat{c}_{jl\sigma} + \sum_{ijl\sigma} \left(q_\sigma V_{ij} \hat{f}^\dagger_{il\sigma}\hat{c}_{jl\sigma} + H.c. \right) \\
&+ \sum_{il\sigma} \epsilon^f_\sigma \hat{n}^f_{il\sigma} + \mathcal{V}_\sigma \sum_{i\sigma} \left(\langle \hat{f}^\dagger_{i1\sigma}\hat{f}^\dagger_{i2\sigma} \rangle_0 \hat{f}_{i2\sigma}\hat{f}_{i1\sigma} + \langle \hat{f}_{i2\sigma}\hat{f}_{i1\sigma} \rangle_0 \hat{f}^\dagger_{i1\sigma}\hat{f}^\dagger_{i2\sigma} \right) \\
&+ \Lambda U \sum_l d^2 + \Lambda U' \left(n^f_{1\uparrow} n^f_{2\downarrow} + n^f_{1\downarrow} n^f_{2\uparrow} \right) + \Lambda \left(U' - J \right) \sum_\sigma n^f_{1\sigma} n^f_{2\sigma} + E_0,
\end{aligned} \tag{2.30}$$

where ϵ^f_σ is renormalized f-orbital energy given as follows

$$\begin{aligned}
\epsilon^f_\sigma = \frac{\partial E_{\text{G}}}{\partial n^f_{l\sigma}} - \mu = \epsilon^f - h\sigma + U\lambda_d^2 n^f_{il\bar{\sigma}} + (U' - J) n^f_{il'\sigma} + U' n^f_{il'\bar{\sigma}} \\
+ \left(\frac{\partial q_{\bar{\sigma}}}{\partial n^f_{il\sigma}} \times V \left(\langle \hat{f}^\dagger_{i1\bar{\sigma}}\hat{c}_{i1\bar{\sigma}} \rangle_0 + \langle \hat{f}^\dagger_{i2\bar{\sigma}}\hat{c}_{i2\bar{\sigma}} \rangle_0 \right) + C.c. \right) \\
+ \left(\frac{\partial g_{1\bar{\sigma}}}{\partial n^f_{il\sigma}} U' + \frac{\partial g_{2\bar{\sigma}}}{\partial n^f_{il\sigma}} (U' - J) \right) |\langle \hat{f}_{i2\bar{\sigma}}\hat{f}_{i1\bar{\sigma}} \rangle_0|^2 - \mu
\end{aligned} \tag{2.31}$$

and E_0 is a reminder proportional to unity. In Appendix B details of obtaining the effective Hamiltonian are presented, both with a comparison to Hartree-Fock-BCS method (cf. Table B.1).

Let us recall that our model was simplified to the case with non-zero equal-spin triplet gap parameters only $\langle \hat{f}_{i2\sigma}\hat{f}_{i1\sigma} \rangle_0 \neq 0$ and $\langle \hat{f}_{i2\uparrow}\hat{f}_{i1\downarrow} \rangle_0 = \langle \hat{f}_{i2\downarrow}\hat{f}_{i1\uparrow} \rangle_0 = 0$. We take on-site hybridization: $V_{ij} = \delta_{ij} V$ and assume real values of parameters: $V^* = V$, $\epsilon_{\mathbf{k}} = \epsilon^*_{\mathbf{k}}$, $\langle \hat{f}^\dagger_{i1\sigma}\hat{f}^\dagger_{i2\sigma} \rangle_0 = \langle \hat{f}_{i2\sigma}\hat{f}_{i1\sigma} \rangle_0$, and also $\epsilon_{\mathbf{k}} = \epsilon_{-\mathbf{k}}$. The effective Hamiltonian

(2.30) transformed to the momentum space reads:

$$\hat{\mathcal{H}}_{\text{eff}} = \sum_{\mathbf{k},\sigma} \Psi^{\dagger}_{\mathbf{k}\sigma} \begin{pmatrix} \epsilon_{\mathbf{k}} & 0 & q_\sigma V & 0 \\ 0 & -\epsilon_{\mathbf{k}} & 0 & -q_\sigma V \\ q_\sigma V & 0 & \epsilon^f_\sigma & \Delta^{ff}_{\sigma\sigma} \\ 0 & -q_\sigma V & \Delta^{ff}_{\sigma\sigma} & -\epsilon^f_\sigma \end{pmatrix} \Psi_{\mathbf{k}\sigma} + E'_0, \tag{2.32}$$

where spin-triplet superconducting gap parameter $\Delta^{ff}_{\sigma\sigma}$ is defined up to the phase factor:

$$\Delta^{ff}_{\sigma\sigma} = |\mathcal{V}_\sigma| \times \left| \langle \hat{f}_{i2\sigma} \hat{f}_{i1\sigma} \rangle_0 \right| \tag{2.33}$$

and $\Psi^{\dagger}_{\mathbf{k}\sigma} = \left(\hat{c}^{\dagger}_{\mathbf{k}1\sigma}, \hat{c}_{-\mathbf{k}2\sigma}, \hat{f}^{\dagger}_{\mathbf{k}1\sigma}, \hat{f}_{-\mathbf{k}2\sigma} \right)$ with transformation to momentum space defined as $\hat{f}_{il\sigma} = \frac{1}{\sqrt{\Lambda}} \sum_{\mathbf{k}} e^{-i\mathbf{k}\mathbf{R}_i} \hat{f}_{\mathbf{k}l\sigma}$, $\hat{c}_{il\sigma} = \frac{1}{\sqrt{\Lambda}} \sum_{\mathbf{k}} e^{-i\mathbf{k}\mathbf{R}_i} \hat{c}_{\mathbf{k}l\sigma}$. The conduction band energy in two-dimensional lattice reads

$$\epsilon_{\mathbf{k}} = 2t(\cos(k_x) + \cos(k_y)) + 4t' \cos(k_x)\cos(k_y) - \mu, \tag{2.34}$$

whereas the hopping integral of c-electron takes the form

$$t_{ij} = \begin{cases} t & \text{for } i,j \text{ – the nearest neighbors,} \\ t' & \text{for } i,j \text{ – the next nearest neighbors,} \\ 0 & \text{otherwise.} \end{cases} \tag{2.35}$$

The hybridization renormalization q_σ is given by (2.22) and the renormalized f-orbital energy ϵ^f_σ by (2.31). The remaining part of (2.32) is

$$\begin{aligned} E'_0 = E_0 &+ \sum_{\mathbf{k}l\sigma} \left(\epsilon_{\mathbf{k}} + \epsilon^f_\sigma \right) + 2\Lambda U d^2 + \Lambda U' \left(n^f_{1\uparrow} n^f_{2\downarrow} + n^f_{1\downarrow} n^f_{2\uparrow} \right) \\ &+ \Lambda \left(U' - J \right) \sum_\sigma n^f_{1\sigma} n^f_{2\sigma}. \end{aligned} \tag{2.36}$$

Interestingly, eigenvalues $\lambda = 1, ..., 4$ (quasiparticle bands) of matrix in (2.32) can be calculated analytically:

$$E^{(\lambda)}_{\mathbf{k}\sigma} = \pm \sqrt{q^2_\sigma V^2 + \frac{1}{2}\left(E^2 + \epsilon^2_{\mathbf{k}}\right) \pm \frac{1}{2} \sqrt{\left(E^2 - \epsilon^2_{\mathbf{k}}\right)^2 + 4q^2_\sigma V^2 \left(\left(\Delta^{ff}_{\sigma\sigma} \right)^2 + \left(\epsilon_{\mathbf{k}} + \epsilon^f_\sigma \right)^2 \right)}}, \tag{2.37}$$

where $E^2 = \left(\Delta^{ff}_{\sigma\sigma} \right)^2 + \left(\epsilon^f_\sigma \right)^2$. This facilitates the discussion of the quasiparticle spectra and the spectral weights for the considered model, as is done in Appendix D.3.

Finally, the values of the Lagrange multipliers λ_α are specified as follows:

$$\lambda_{\emptyset}^2 = 1 + x n_{l\uparrow}^f n_{l\downarrow}^f, \tag{2.38}$$

$$\lambda_{\sigma}^2 = 1 - x\left(1 - n_{l\sigma}^f\right) n_{l\bar{\sigma}}^f, \tag{2.39}$$

$$\lambda_{d}^2 = 1 + x\left(1 - n_{l\uparrow}^f\right)\left(1 - n_{l\downarrow}^f\right), \tag{2.40}$$

where x is a single variational parameter. This ensures that the SGA method corresponds to the formal limit of infinite lattice coordination number and provides a formal background for further diagrammatic expansion of our approach. From (2.40), (2.25):

$$x = \frac{d^2 - n_{l\uparrow}^f n_{l\downarrow}^f}{\left(1 - n_{l\uparrow}^f\right)\left(1 - n_{l\downarrow}^f\right) n_{l\uparrow}^f n_{l\downarrow}^f}. \tag{2.41}$$

Substituting (2.41) to (2.38)-(2.40):

$$\lambda_{\emptyset}^2 = \frac{1 - n_{l\uparrow}^f - n_{l\downarrow}^f + d^2}{\left(1 - n_{l\uparrow}^f\right)\left(1 - n_{l\downarrow}^f\right)}, \tag{2.42}$$

$$\lambda_{\sigma}^2 = \frac{n_{l\sigma}^f - d^2}{n_{l\sigma}^f\left(1 - n_{l\bar{\sigma}}^f\right)}, \tag{2.43}$$

$$\lambda_{d}^2 = \frac{d^2}{n_{l\uparrow}^f n_{l\downarrow}^f}. \tag{2.44}$$

We minimize the generalized Landau grand-potential functional with Lagrange multipliers assuring the correct statistical consistency:

$$\mathcal{F} = -\frac{1}{\beta}\ln \mathrm{Tr}\exp\left(-\beta\mathcal{H}_{\mathrm{eff}}\right), \tag{2.45}$$

where $\beta = 1/k_{\mathrm{B}}T$ and k_{B} is the Boltzmann constant. The minimization condition for determining solution of model (quantities and Lagrange multipliers):

$$\frac{\partial\mathcal{F}}{\partial x} = 0, \qquad \frac{\partial\mathcal{F}}{\partial\langle\hat{O}\rangle_0} = 0, \qquad \frac{\partial\mathcal{F}}{\partial\lambda_{\hat{O}}} = 0 \tag{2.46}$$

E_{G}, $\lambda_{\hat{O}}$ depend on x. μ is fixed by electron density. Minimization procedure is depicted in Figure 2.3.

2.6. A brief summary

In this Chapter the orbitally degenerate Anderson lattice model (four-orbital) was introduced. The model is suitable for description of hybridized systems with partially

filled f-shell, i.e., heavy fermion systems, and it allows to consider a delocalization of the initially atomic f-states.

Subsequently, we have discussed the main idea of SGA approximation, which is to include the effect of correlations using the Gutzwiller correlator $\hat{\mathcal{P}}_{\mathrm{G}}$, which acts on the product state. In this formalism the effective Hamiltonian (2.30) is obtained, which contains renormalized parameters.

In the next Chapter we present results for orbitally degenerate Anderson lattice model, that are obtained within the SGA method, described here.

3. Application to UGe_2

3.1. Introduction

In this chapter we solve the four-orbital degenerate Anderson lattice model, introduced in the previous section in Equation (2.2) as relevant to the case of UGe_2, and compare the results with available experimental data.

An important methodological remark should be made at this point. The majority of experiments on UGe_2 have been performed under applied hydrostatic pressure, which does not enter explicitly the parametrized Hamiltonian (2.2). To make the discussion quantitative, the experimental conditions need thus to be related to the model parameters. The approach that we adopt here relies on the observation that the crystal undergoes compression in response to pressure, thereby increasing the average overlap between orbitals in the crystal. This, in turn, can affect the effect of Kondo-screening of the f-levels which would lead to further (possibly substantial and non-linear) renormalization of the hybridization magnitude at the level of the effective Hamiltonian. The precise dependence of the hybridization on pressure cannot be precisely determined here without referring to full-scale first-principle calculation. We however, expect that it should be a *monotonically increasing* function of pressure. As the first approximation, we assume that only the hybridization acquires pressure dependence, which can be estimated by fitting to the positions of the magnetic and superconducting transition points. Working out the pressure-dependence of other model parameters would be a worthy extension of our present study, though it would likely lead to an *underdetermined* regression problem.

3.2. Discussion of results: Coexistent magnetic and superconducting phases

3.2.1. Phase diagram: The case of UGe_2

We have started with the orbitally degenerate Anderson lattice model with two f- and two c-orbitals (2.2) and obtained the effective Hamiltonian in the SGA approximation (2.30). Now a solution of the model and an analysis of results will be presented for the parameters $U/|t| = 3.5$, $J/|t| = 1.1$, $t'/|t| = 0.25$, $\epsilon^f/|t| = -4$, $k_BT = 0|t|$. These parameters have been chosen so that the values of the ordered magnetic moments in the respective ferromagnetic phases match the experiment, and the scale of the maximal superconducting transition temperature is of the order of 1 K. A more detailed justification of this choice is provided in Section 3.2.2. Since the first-principle calculations for UGe_2 provide evidence for the presence of cylindrically-

shaped Fermi surface [84, 37], we perform the calculations for a two-dimensional lattice.

Since the motivation of our research is a description of uranium compound UGe_2, total occupancy per site $n^{\mathrm{tot}} \equiv n^f + n^c$ (where n^f and n^c are the f- and c-electrons occupancies per site on both orbitals) must be greater than occupancy on $5f$ level for U^{3+} ion [19, 45, 85] ($n^{\mathrm{tot}} > 3$). We take $n^{\mathrm{tot}} = 3.25$, which is dictated by good agreement with experiment.

The main result of this Thesis is the phase diagram calculated for above parameters, presented in Figure 3.1 [82]. Exemplary expectation values and parameters, on the basis of which Figure 3.1 was drawn, are shown in Tables D.1 and D.2 in Appendix D.1. Recall that in our calculations intraatomic hybridization strength V mimics changes of pressure measured in experiments. Figure 3.1(a) shows magnetic moments per formula unit: total magnetization $m^{\mathrm{tot}} = m^f + m^c$ as well as partial $m^f = 2\left(n^f_{l\uparrow} - n^f_{l\downarrow}\right)$ and $m^c = 2\left(n^c_{l\uparrow} - n^c_{l\downarrow}\right)$ for f- and c-electrons, respectively. Three distinct magnetic phases are marked:

- ferromagnetic phase FM2 with large magnetic moment,
- ferromagnetic phase FM1 with low magnetic moment,
- paramagnetic phase PM with zero magnetic moment.

Both magnetic phase transitions (FM2 $\rightarrow$ FM1 and FM1 $\rightarrow$ PM) are of the first order, although the first of them (FM1$\rightarrow$FM2) is relatively close to second order. Jump in the total magnetization, indicating the type of FM2$\rightarrow$FM1 transition, is evident in Figure 3.1(d).

Differences in the electronic structure between the two ferromagnetic phases FM2 and FM1 are clearly visible in Figure 3.2, containing density of states. In the FM2 phase, f-electrons are placed well below the Fermi energy ϵ_F, close to localization and carry nearly saturated magnetic moments (for two f-orbitals and the gyromagnetic factor $g = 4$, its maximal value is $2\,\mu_B$/U). On the other hand, in the FM1 phase, the Fermi energy ϵ_F lies in the minority (spin-up) band, whereas the majority band is pushed down below the Fermi level. Such a behavior stabilizes the total magnetization, which is constant throughout entire FM1 phase. It also reflects the half-metallic character of the phase, since on Fermi energy level density of states for spin-up direction is zero. Available band-structure calculations [85] are consistent with the proposed half-metallic character of FM1 state.

Apart from the magnetic properties, Figure 3.1(b) contains also spin-up (purple) and spin-down (green) triplet superconducting gap parameters $\Delta^{ff}_{\sigma\sigma}$, defined in Equation (2.33), with three superconducting phases marked:

- A_2 with two different gap parameters: $\Delta^{ff}_{\downarrow\downarrow} > \Delta^{ff}_{\uparrow\uparrow} \neq 0$,
- A_1 with with one non-zero gap parameter: $\Delta^{ff}_{\uparrow\uparrow} = 0$ and $\Delta^{ff}_{\downarrow\downarrow} \neq 0$,
- A with two equal spin-triplet gap parameters $\Delta^{ff}_{\uparrow\uparrow} = \Delta^{ff}_{\downarrow\downarrow}$.

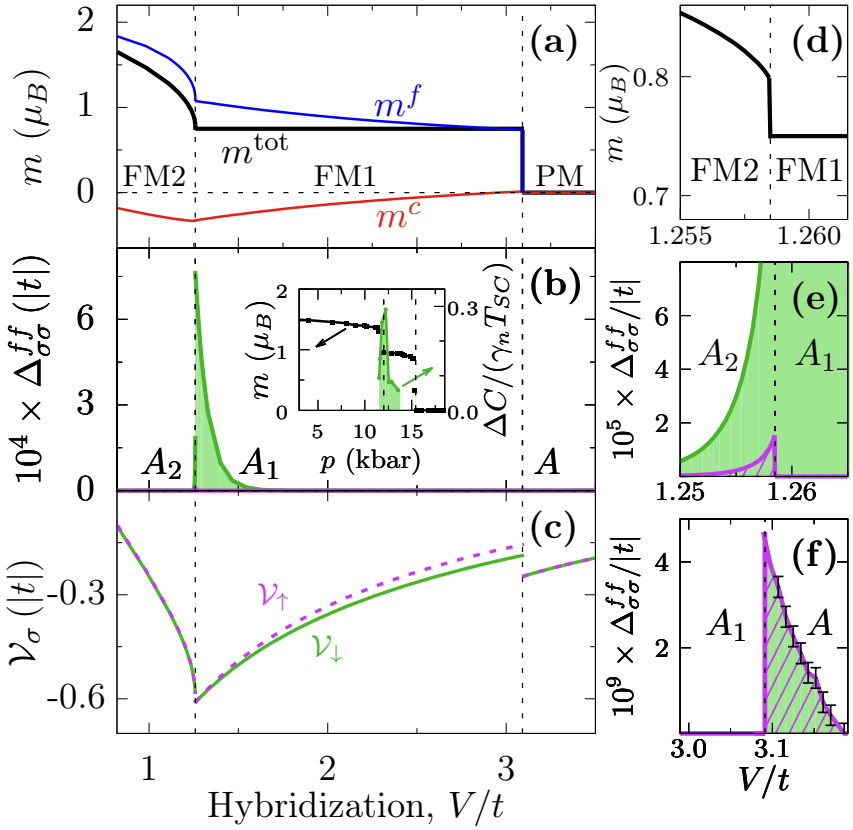

Figure 3.1.: The obtained phase diagram for zero temperature, the Hund's coupling $J/|t| = 1.1$, the Coulomb interaction $U/|t| = 3.5$, and $t'/|t| = 0.25$, $\epsilon^f/|t| = -4$. Exemplary numerical results are presented in Tables D.1 and D.2 in Appendix D.1. (a) The total magnetic moment per formula unit, and the partial f- and c-electron contributions are marked as m^{tot} (black line), m^f (blue line), and m^c (red line), respectively. Three different magnetic phases: FM2, FM1, and PM are marked in the figure and explained in the text. (b) Triplet f-f superconducting gap components: $\Delta^{ff}_{\uparrow\uparrow}$ – purple, $\Delta^{ff}_{\downarrow\downarrow}$ – green. The three superconducting phases: A_2, A_1, and A are marked. Experimental magnetization for UGe_2, adapted from [38], is shown on inset with the normalized specific-heat jump at superconducting transition T_{SC} [86]. (c) The effective spin-dependent pairing potential $\mathcal{V}_\sigma$. (d) Jump of total magnetic moment on FM2→FM1 metamagnetic phase transition boundary. (e)-(f) Superconducting gap components (colors are same as in (b)) near FM2→FM1 and FM1→PM, respectively. Since $\Delta^{ff}_{\sigma\sigma}$ in the A phase are extremely small, error bars are also marked. Figure taken from [82].

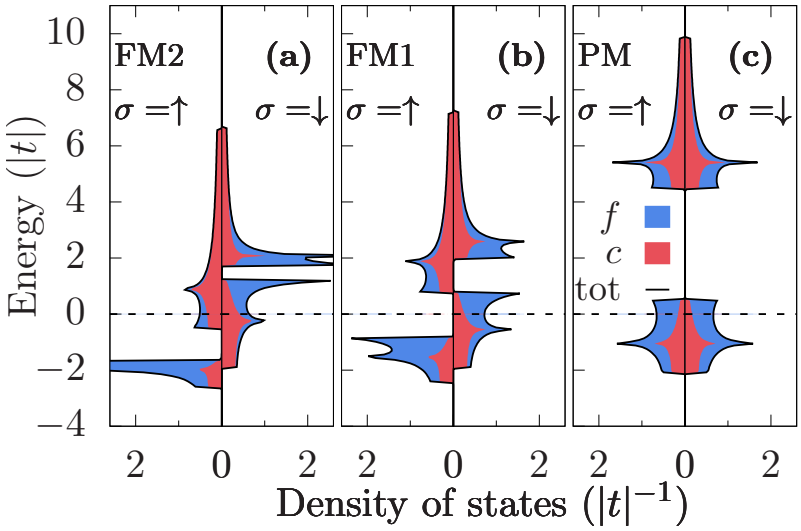

Figure 3.2.: Density of states in three magnetic phases: (a) FM2 $V/t = 1.1$, (b) FM1 $V/t = 1.625$, and (c) PM $V/t = 3.25$. f- and c-orbitals are marked by blue and red color, respectively. Dirac-delta functions were smeared out by adding a small imaginary part to the spectral function, which takes the Lorentzian form of the typical width $\epsilon = 10^{-3}|t|$. Superconducting gap is not visible because of its small magnitude. Figure taken from [82].

Names of phases correspond to those used for description of superfluidity in ^{3}He [22], since in both systems extraordinary properties are induced by the spin-triplet pairing.

Experimental results for UGe_2 are shown in inset of Figure 3.1(b): magnetization versus pressure [38] and normalized specific heat jump ($\Delta C/\gamma_n T_{SC}$) at the superconducting transition temperature T_{SC} [86]. The calculated phase diagram matches well the experiment with the same sequence of the FM2, FM1, and PM states. Also, in both cases, superconductivity has peak at FM2→FM1 phase boundary and exists on both sides of transition.

To further clarify the structure of calculated phase diagram, in Figure 3.3 we show schematic picture of all obtained phases. At zero temperature with increasing hybridization strength, system passes multiple phases: it starts from ferromagnetic phase FM2, goes to coexisting phase FM2+A_2, than FM1+A_1 and ends in PM+A phase with small and quickly vanishing superconducting gap parameters.

Effective spin-dependent coupling $\mathcal{V}_\sigma$ (2.28) as a function of hybridization is presented in Figure 3.1(c). Note that the superconducting pairing potential $\mathcal{V}_\sigma$ is the largest at transition FM2+A_2 → FM1+A_1. Close-ups on both superconducting phase transitions are presented in Figure 3.1(e) and 3.1(f). As the gap parameters are discontinuous, both $A_2 \to A_1$ and $A_1 \to A$ superconducting transitions are of the first order.

One can ask, why only one (spin-down) gap component $\Delta^{ff}_{\downarrow\downarrow}$ is non-zero. It happens

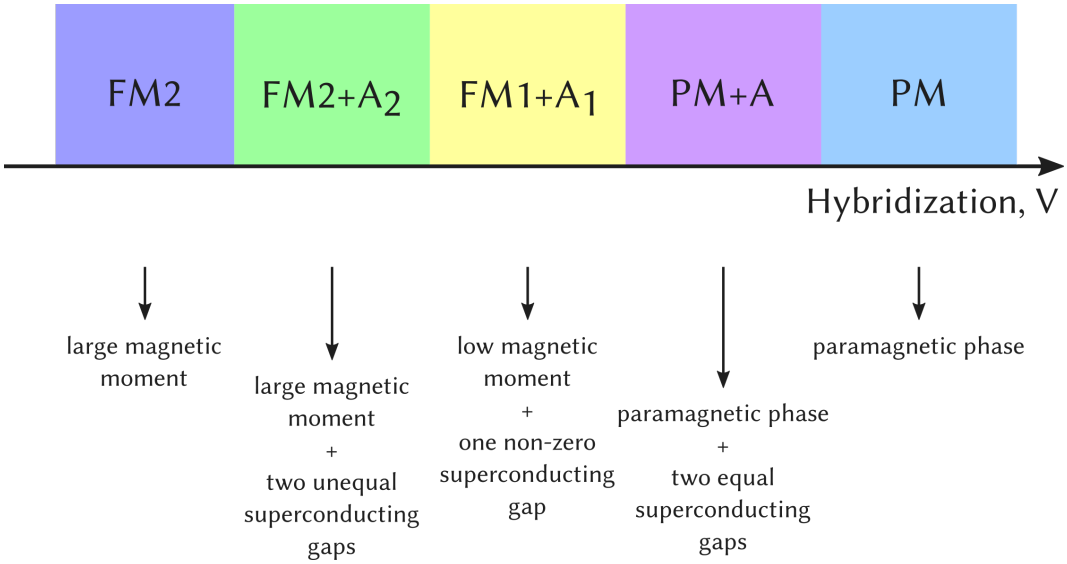

Figure 3.3.: Sequence of superconducting and magnetic phases with increasing f-c hybridization V at zero temperature in the absence of magnetic field.

due to half-metallic character of FM1 phase. Conductivity exists in the spin-down direction only and on Fermi energy level density of states for spin-up direction is zero (hybridization gap in density of states), as shown in Figure 3.2(b).

Figure 3.4(a) presents spin-dependent effective f-electron energy levels $\epsilon^f_\sigma + \mu = \frac{\partial E_G}{\partial n^f_{i\sigma}}$, determined in Equation (2.31), as a function of hybridization V/t. Correlations influence f-energy level in all phases, since bare f-level for both spin directions is $\epsilon^f = -4|t|$. Figure 3.4(b) shows the chemical potential μ.

We now turn to the discussion of the correlated quasiparticle properties. In Figure 3.5 we plot the following renormalization factors: (a) double occupancy d^2, Lagrange multiplier renormalizing double occupancy λ_d^2, along with spin-dependent f-c hybridization renormalization q_σ; (b) $g_{1\sigma}$ and (c) $g_{2\sigma}$ – spin-dependent pairing potential renormalizations. They modify the pairing potential from $\mathcal{V}_{\mathrm{HF}} = (U' - J)$ to $\mathcal{V}_\sigma$, allowing superconductivity to exist in broader parameter region (compare with Figure 3.10: correlation-driven superconductivity). The renormalization of the f-c hybridization is small, because factors q_σ for both spin directions are almost equal to one. In the limits $V/t \to 0$ and $V/t \to \infty$ they approach unity. The lowest value near FM2→FM1 phase transition is ~ 0.943 for both spins. Exemplary values of the factors q_σ are presented in the Table 3.1.

Occupancies for f- and c-orbital are plotted in Figure 3.6 for parameters the same as before. Just before phase transition in FM2 phase for hybridization $V/t = 1.25845$ f-orbital occupancy is almost 2: $n^f \simeq 1.9998$ and after in FM1 phase for $V/t = 1.25850$ exceeds 2: $n^f \simeq 2.0003$ and decreases with increasing hybridization strength. It is important to mention, that although in FM2 phase occupancy per site $n^f \sim 2$, f-electrons with a predominant spin-up direction are located on different

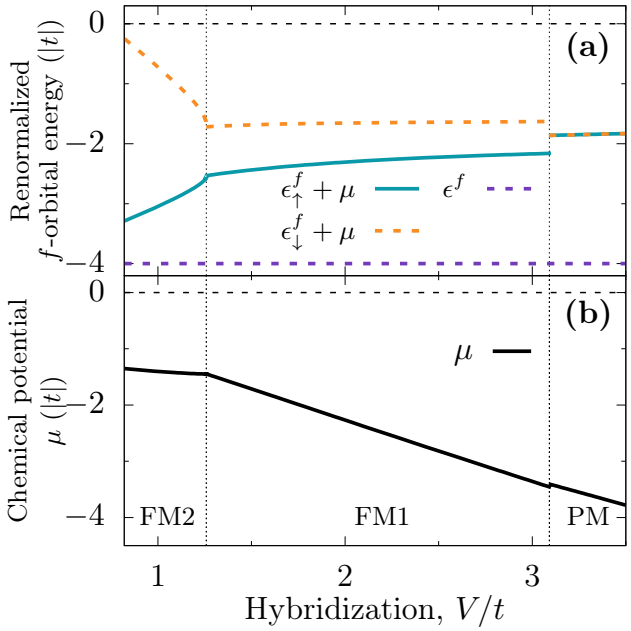

Figure 3.4.: (a) Renormalized f-electron energy levels $\epsilon^f_\sigma + \mu = \frac{\partial E_G}{\partial n^f_{l\sigma}}$ defined by Equation (2.31) for spin up and spin down. (b) Chemical potential μ, both as functions of hybridization V/t for parameters $U/|t| = 3.5$, $J/|t| = 1.1$, $k_\mathrm{B}T/|t| = 0$.

Table 3.1.: Exemplary values of the spin-dependent factor q_σ, which renormalizes the f-c hybridization, in various phases.

V/t	$q_\uparrow$	$q_\downarrow$	Phase
-1.1	0.9609	0.9607	FM2
-1.254	0.9434	0.9433	FM2+A_2
-1.2545	0.9432	0.9431	FM1+A_1
-2.95	0.9877	0.9867	FM1+A_1
-3.25	0.9861	0.9861	PM+A

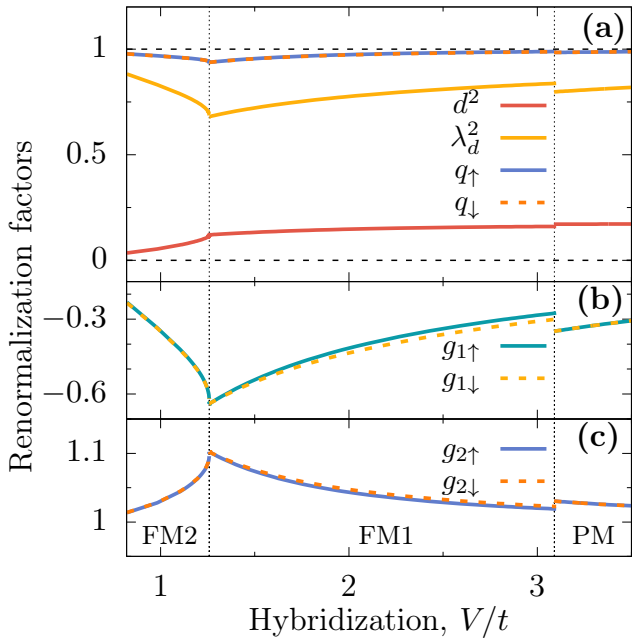

Figure 3.5.: Renormalization factors as functions of hybridization V/t: (a) d^2, λ_d^2, q_σ, (b) $g_{1\sigma}$, (c) $g_{2\sigma}$ defined by Equations (2.25), (2.40), (2.22), (2.26), and (2.27), respectively for parameters $U/|t| = 3.5$, $J/|t| = 1.1$, $k_\mathrm{B}T/|t| = 0$. Here $g_{1\sigma}$, $g_{2\sigma}$ renormalize the pairing potential $\mathcal{V}_\mathrm{HF} = (U' - J) \to \mathcal{V}_\sigma$.

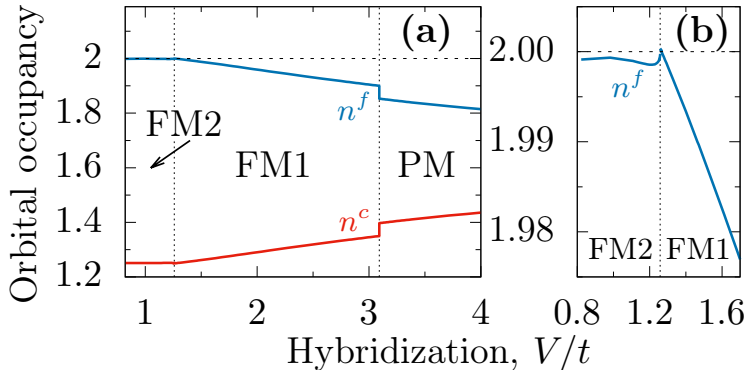

Figure 3.6.: (a) f- (blue) and c-orbital (red) occupancies as functions of f-c hybridization V/t. Note that $n^\mathrm{tot} = n^c + n^f = 3.25$. (b) Close-up of the FM2→FM1 phase transition region [82].

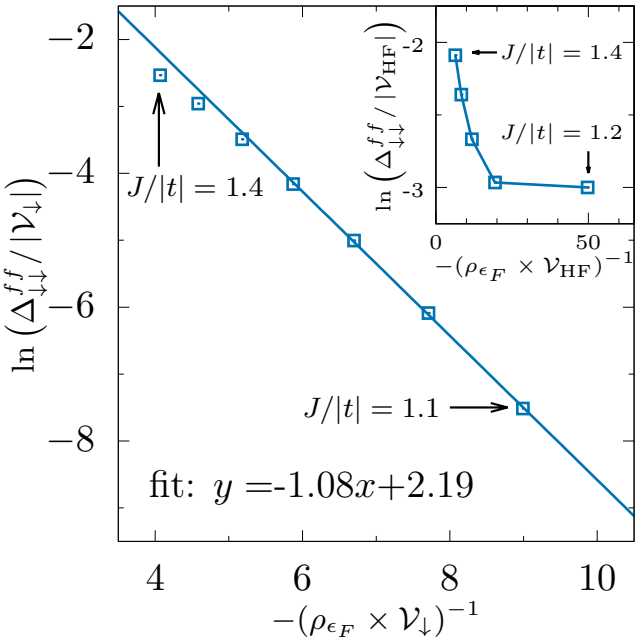

Figure 3.7.: BCS-type scaling for $U/|t| = 3.5$ and different Hund's coupling values J, for fixed hybridization $V/t = 1.32$. Inset: failure of scaling with the Hartree-Fock-BCS pairing potential $\mathcal{V}_{\rm HF} = U' - J$.

orbitals and intraorbital double occupancy $d^2 = \lambda_d^2 n_{l\uparrow}^f n_{l\downarrow}^f$ (Figure 3.5(a)) is small.

In Figure 3.7 scaling of the mean value of dominant spin-down pairing operator $\langle \hat{f}_{i2\downarrow}\hat{f}_{i1\downarrow}\rangle_0 = \Delta^{ff}_{\downarrow\downarrow}/|\mathcal{V}_\sigma|$ is presented for $U/|t| = 3.5$ and fixed hybridization strength $V/t = 1.32$ as a function of Hund's coupling J (the system is then in FM1 phase for all J values). Within the BCS theory, the superconducting gap $\Delta \propto \mathcal{V}\exp\left(-(\rho\mathcal{V})^{-1}\right)$, where ρ is the density of states on Fermi surface per orbital per spin and $\mathcal{V}$ is the pairing potential. The pairing potential in our model depends on Hund's coupling J. The gap $\Delta^{ff}_{\downarrow\downarrow}$ increases rapidly with increasing Hund's exchange. It is discussed in greater detail in the next Section explaining choice of model parameters, i.e., Figure 3.9. In Figure 3.7 the coefficient ~ -1.08 demonstrates a good linear scaling. The value is not far from -1 obtained in the BCS theory.

A scaling with HF-BCS values also has been checked (inset of Figure 3.7). Unrenormalized pairing coupling $\mathcal{V}_{\rm HF}$ for Hund's coupling lower than $U/3$ ($J > U/3 \simeq 1.17|t|$) becomes positive and superconducting state in HF-BCS approximation cannot exist in the system, because it has not the lowest energy. Therefore, in inset of Figure 3.7, the points corresponding to J lower than $3.5/3 \simeq 1.17$ are not marked. The inset shows that inclusion of the bare Hartree-Fock value of pairing potential leads to break-down of BCS scaling.

3.2.2. Choice of model parameters

In the previous Section the main results were presented for particular choice of model parameters. Here we would like to explain carefully, why such parameters were chosen, and compare results with those obtained for other sets of parameters.

As mentioned before, total occupancy per site $n^{\mathrm{tot}} = 3.25$ was dictated by occupancy of $5f$ electrons for U^{3+} ion (> 3) and comparison with experiment. In works [51, 40, 52] concerning the non-degenerate Anderson lattice model total occupancy $n^{\mathrm{tot}} = 1.6$ has given satisfactory results. Influence of different choices of n^{tot} value in case of degenerate model was studied in [53]. Choice of n^{tot} value establishes magnetization plateau in FM1 phase, i.e., for $n^{\mathrm{tot}} = 3.25$ the total magnetization is $m^{\mathrm{tot}} = \left(4 - n^{\mathrm{tot}}\right) \mu_B = 0.75\mu_B$.

In Figure 3.8 the phase diagram is presented for the set of parameters: intraorbital Coulomb interaction $U/|t| = 4.0$, Hund coupling $J/|t| = 1.6$, for temperature $T/|t| = 10^{-8}$, $\epsilon^f/|t| = -4$, $t'/|t| = 0.25$. It was calculated within the SGA approximation. The sequence of superconducting (A_2, A_1, A) and magnetic (FM2, FM1, PM) phases is the same as for Figure 3.1, however phase transitions take place for other hybridization values and not all of them are of the first order.

From above consideration, we can argue that for larger values of intraorbital Coulomb interaction U, the sequence of phase transitions remains the same, however FM2→FM1 phase transition becomes continuous. This is a distinct quantum tricritical behavior, controlled by the on-site repulsion as the tuning parameter. In the calculations for $U/|t| = 4$ in SGA approximation (Figure 3.8) we do not observe jumps in total magnetization or superconducting gap parameters near FM2→FM1 phase transition (or is too small to observe it). Taking Coulomb interaction $U/|t| = 3.5$ with small Hund's coupling J is enough to observe the first order transition between FM2 and FM1 phases. The transition FM1+A_1 →PM+A for larger U parameter values remains of the first order. Additionally, A_1 phase occurring in FM1 phase has gap parameter at least two orders of magnitude larger than for $U/|t| = 3.5$ and $J/|t| = 1.1$, while in the A phase it is at least six orders of magnitude larger.

Since experimentally superconductivity in UGe_2 in paramagnetic phase is not observed (it disappears at the FM1/PM border) [15, 38], we would like to comment appearance of superconducting A phase in the paramagnetic regime in our results (cf. Figures 3.1 and 3.8). First of all, $A_1 \rightarrow A$ phase transition is of the first order. Comparing Figures 3.1 and 3.8 obtained for intraorbital Coulomb interaction $U/|t| = 3.5$, Hund's exchange $J/|t| = 1.1$ and $U/|t| = 4$, $J/|t| = 1.6$, respectively, one can observe that smaller superconducting A gaps parameters are for smaller values of both parameters. It justifies the choice of U and J parameters. Also for $U/|t| = 3.5$ and $J/|t| = 1.1$ the superconducting A-phase gap parameters are of order $10^{-9}|t|$, which poses a question about measurability of the superconductivity in an experiment.

Figure 3.9 contains dominant spin-triplet gap component ($\Delta^{ff}_{\downarrow\downarrow}$) as a function of hybridization for different Hund's coupling J values near FM2→FM1 phase transition. For the hybridization $V/t = 1.32$ and the Hund's coupling $J/|t| = 1.4$, the dominant equal-spin-down gap parameter $\Delta^{ff}_{\downarrow\downarrow} \simeq 9 \times 10^{-2}\ |t|$ is at least two order

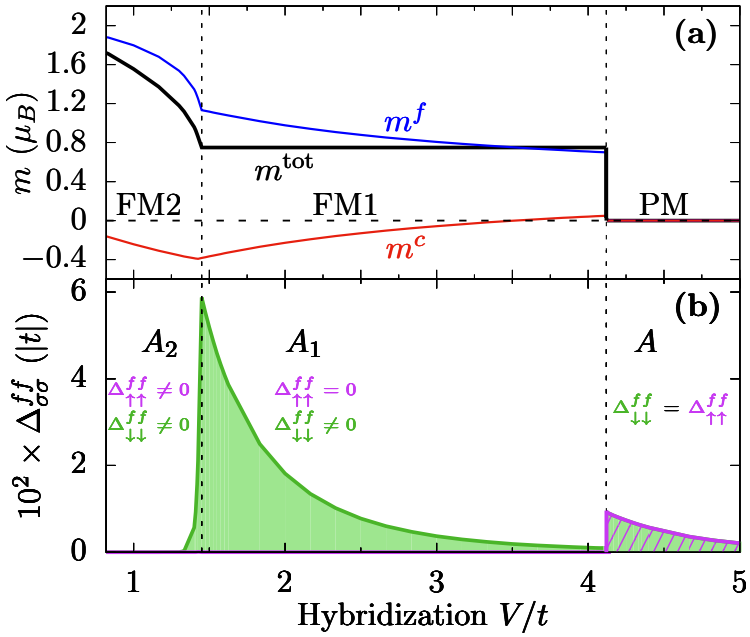

Figure 3.8.: Calculated phase diagram for temperature $T/|t| = 10^{-8}$, Hund coupling $J/|t| = 1.6$, and intraorbital Coulomb interaction $U/|t| = 4.0$ within the SGA approximation. (a) Magnetic moments: total m^{tot} per formula unit – black solid line, f-component m^f – blue and c-component m^c – red. Similarly as in Figure 3.1 there are marked three different magnetic phases: FM2, FM1, PM. Phases FM2 and FM1 are broader than for $U/|t| = 3.5$ and $J/|t| = 1.1$. (b) Triplet f-f superconducting gap components: $\Delta^{ff}_{\uparrow\uparrow}$ – purple, $\Delta^{ff}_{\downarrow\downarrow}$ – green. There are marked three regions of different superconducting phases: A_2, A_1, A. A_1 phase occurring in FM1 phase has gap parameter at least two orders of magnitude larger than for $U/|t| = 3.5$ and $J/|t| = 1.1$, while in A phase it is at least six orders of magnitude larger. Figure taken from [82].

of magnitude bigger than for the $J/|t| = 1.1$ (then $\Delta^{ff}_{\downarrow\downarrow} \simeq 3 \times 10^{-4}\ |t|$). Therefore, in our calculations superconductivity is investigated in the lower Hund's coupling J regime.

However, too small values of Hund's coupling J suppress superconductivity. The superconducting state occurs only if the effective pairing potential dependent on J is negative. In Hartree-Fock-BCS approximation this pairing potential is $\mathcal{V}_{\mathrm{HF}} = U' - J = U - 3J$, thus, to obtain superconducting state for $U/|t| = 3.5$, Hund's coupling must fulfill $J > 3.5/3 \simeq 1.17$. The chosen value $J/|t| = 1.1$ does not satisfy the condition. However, since the calculations are provided in SGA approximation, in which correlations influence on pairing is included, the pairing potential is renormalized to value $\mathcal{V}_\sigma$ defined in (2.28) and allows the superconductivity to exist in broader regime (cf. the discussion of effects of correlations in Section 3.2.3).

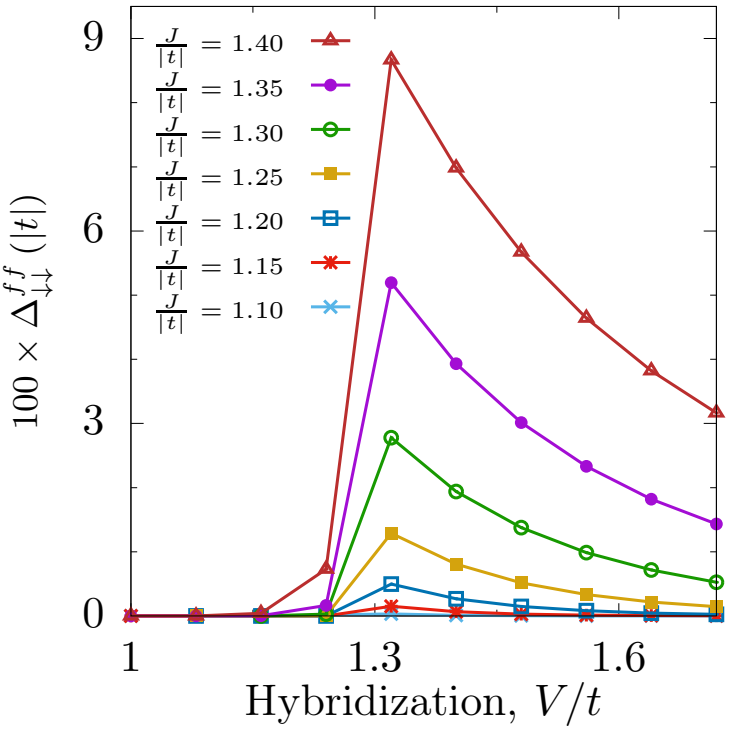

Figure 3.9.: Values of dominant spin-down gap parameter near FM2+A_2 →FM1+A_1 phase transition for $U/|t| = 3.5$ and different values of Hund's coupling J. We have chosen such a Hund's coupling value that the superconducting transition temperature $T_{\mathrm{SC}} \approx 0.92$ K for $|t| = 0.5$ eV and $V/t = 1.3$, which is close to that obtained from experiment in high-quality UGe_2 samples ($T_{\mathrm{SC}} = 0.8$ K). See temperature dependence, Figure 3.14. With increasing Hund's rule coupling J critical superconducting temperature T_{SC} increases.

3.2.3. Influence of correlations on superconductivity: Comparison with the Hartree-Fock-BCS solution

The most important effect of correlations is extension of the regime, where the spin-triplet pairing occurs. Due to the fact that correlation renormalizes the pairing potential from Hartree-Fock-BCS value $\mathcal{V}_{\mathrm{HF}} = U' - J$ to $\mathcal{V}_\sigma$, defined in Equation (2.28), superconductivity survives even for lower Hund's coupling values J than $U/3$. Pairing potentials $\mathcal{V}_{\mathrm{HF}}$ and renormalized $\mathcal{V}_\sigma$ for both spin directions are presented in Figure 3.10 as functions of Hund's coupling J for intraorbital Coulomb interaction $U/|t| = 3.5$ and fixed f-c hybridization $V/t = 1.32$. The plot is divided in three regions:

- non-SC: for small J values $\mathcal{V}_{\mathrm{HF}} > 0$ and $\mathcal{V}_\sigma > 0$, the pairing potentials in both approximations are positive, therefore the paired state is not favorable in the system;

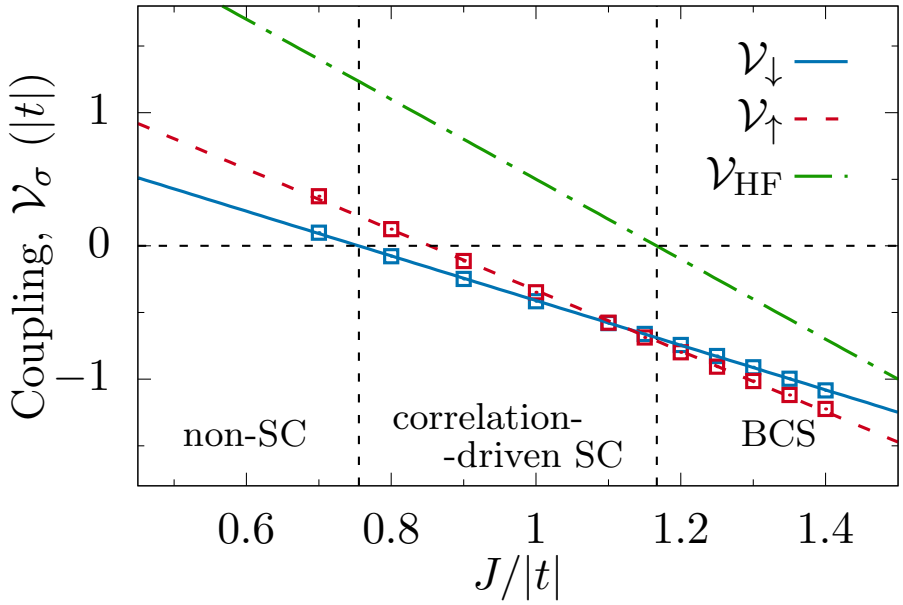

Figure 3.10.: Comparison of pairing potential in different approximations: Hartree-Fock-BCS value $\mathcal{V}_{\mathrm{HF}} = U' - J$ and renormalized due to correlations in SGA, spin-dependent values $\mathcal{V}_\sigma = g_{1\sigma}U' + g_{2\sigma}(U' - J)$ as a function of Hund's coupling amplitude J for $U/|t| = 3.5$ and $V/t = 1.32$.

- correlation-driven SC: for higher Hund's coupling values of at least one of $\mathcal{V}_\sigma$ becomes negative, making pair creation possible. In the SGA approach f-electrons pairing appears, whereas in HF-BCS it does not;

- BCS: for $J > U/3$ the $\mathcal{V}_{\mathrm{HF}}$ pairing potential becomes negative, pairs can exist even in the Hartree-Fock-BCS approximation.

Note that Hund's coupling value $J/|t| = 1.1$ employed in Chapter 3, falls into the correlation-driven regime. This is happens due to strong on-site electronic correlations and would not be possible otherwise.

To discuss other issues of correlation we present in Figure 3.11 phase diagram calculated in HF-BCS approximation. It is obtained for the same set of parameters as Figure 3.8. In the HF-BCS approximation the equal-gap A phase has much larger amplitude of pairing than in A_1 phase, as depicted in Figure 3.11. Furthermore, A_2 phase does not appear (in calculation with accuracy 10^{-8}).

Correlations appear to shift maximum of gap parameter in A_1 phase to magnetic FM2→FM1 phase transition. Additionally, it is enhanced by the pairing potential $\mathcal{V}_\sigma$ dependent on f-c hybridization, which has the larger value on FM2+A_2 →FM1+A_1 phase transition.

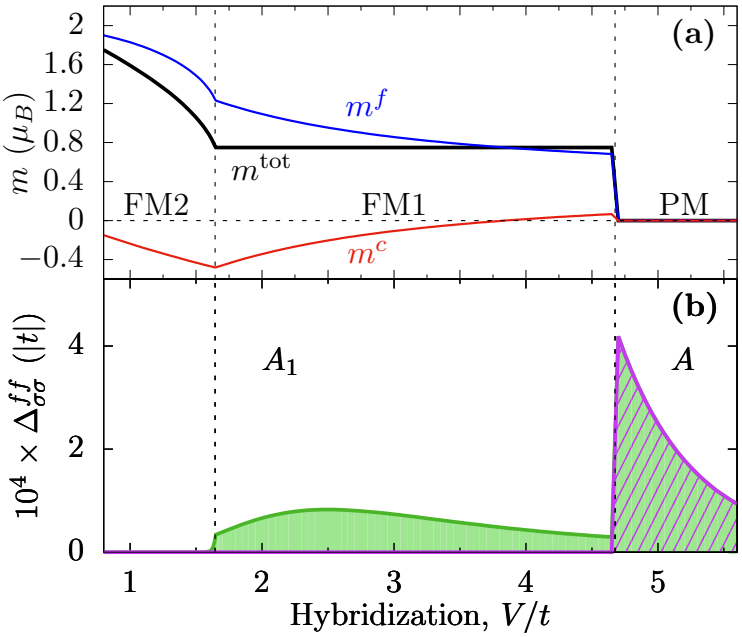

Figure 3.11.: Calculated phase diagram for temperature $T/|t| = 0$, Hund's coupling $J/|t| = 1.6$, and Coulomb interaction $U/|t| = 4.0$ in Hartree-Fock approximation. (a) Magnetic moments: total m^{tot} per formula unit – black solid line, f-component m^f – blue and c m^c – red. Similarly as before there are marked three different magnetic phases: FM2, FM1, PM. (b) Triplet f-f superconducting gap components: $\Delta^{ff}_{\uparrow\uparrow}$ – purple, $\Delta^{ff}_{\downarrow\downarrow}$ – green.

3.2.4. UGe_2 as Hund's metal

In this section the term "Hund's metal" is discussed, which was originally introduced in the context of studies of iron-based superconductors [87] and then investigated in the Ruthenates [88, 89]. In the Hund's metal the correlated state is induced by Hund's coupling J under a moderate intraorbital Coulomb interaction U.

In Figure 3.12 we present comparison of two interactions involved in the system: intraorbital Coulomb ($U\sum_l \langle \hat{n}^f_{il\uparrow}\hat{n}^f_{il\downarrow}\rangle_G$) and Hund's ($2J\langle \hat{\mathbf{S}}^f_{i1}\cdot\hat{\mathbf{S}}^f_{i2} + \frac{1}{4}\hat{n}^f_{i1}\hat{n}^f_{i2}\rangle_G$) contributions to the ground-state energy, calculated in correlated state as a function of f-c hybridization. For small hybridization values, for which the system is in ferromagnetic FM2 phase, Coulomb interaction is small due to fact that majority of spins is oriented up and double occupancies are almost suppressed (compare d^2 on Figure 3.5(a)). Just before FM2→FM1 phase transition occurs, the contribution from Coulomb interaction becomes dominant. This region, near FM2/FM1 border is the most interesting, since here metamagnetic phase transition takes place together with the superconductivity having the largest amplitude.

Moreover, for different Hund's coupling values the charge fluctuations per orbital

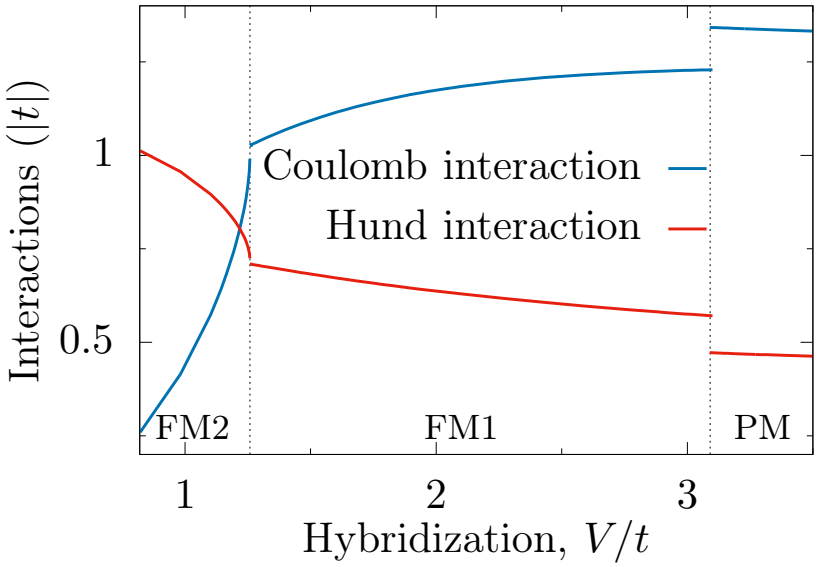

Figure 3.12.: Comparison of renormalized intraorbital Coulomb and interorbital Hund's interactions. One can observe that near FM2 + A_2 → FM1 + A_1 phase transition, the Coulomb interaction becomes dominant as the hybridization increases. In the FM2 phase, due to rarely occurring double occupancies, the Hund interaction is the largest energy scale in the system.

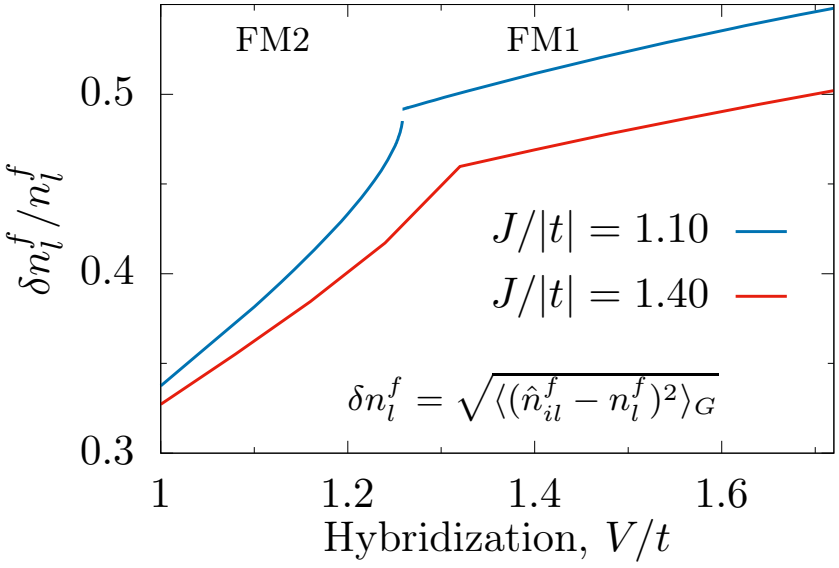

Figure 3.13.: Normalized charge fluctuations for two choices of the Hund's coupling values and $U/|t| = 3.5$. The f-electrons number operator per orbital $\hat{n}_{il}^f = \sum_\sigma \hat{n}_{il\sigma}^f$ and its expectation value $n_l^f = \langle \hat{n}_{il}^f \rangle_0$. Hybridization value for which FM2→FM1 transition takes place is not marked, because for different Hund's coupling values J transition occurs for different hybridizations. For $J/|t| = 1.4$ fewer number of points was calculated, so that the curve has different shape near FM2→FM1 phase transition.

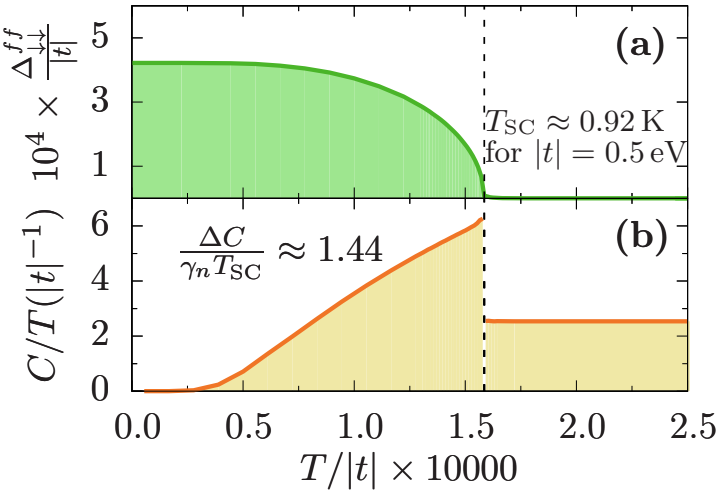

Figure 3.14.: Temperature dependence of (a) the dominant spin-down superconducting gap parameter $\Delta^{ff}_{\downarrow\downarrow}$ (b) the specific heat.

was calculated, i.e.,

$$\frac{\delta n^f_l}{n^f_l} = \frac{\sqrt{\left\langle \left(\hat{n}^f_{il} - n^f_l\right)^2 \right\rangle_G}}{n^f_l}. \tag{3.1}$$

The results are presented in Figure 3.13. For smaller value of Hund's coupling $J/|t| = 1.1$ the normalized charge fluctuations are larger.

3.2.5. Temperature dependence of superconducting gap parameter and related properties

In the SGA approximation, the finite-temperature properties of the system can be also calculated. The temperature dependence of the dominant spin-down superconducting gap parameter $\Delta^{ff}_{\downarrow\downarrow}$ is presented in Figure 3.14(a) for $U/|t| = 3.5$, $J/|t| = 1.1$, $V/t = 1.3$, $\epsilon^f/|t| = -4$ and $t'/|t| = 0.25$. For the given set of parameters, the system is in FM1+A_1 phase. For specific choice of kinetic term $|t| = 0.5$ eV, the superconducting transition temperature is obtained as $T_{\mathrm{SC}} \simeq 0.92$ K. The value is close to the values measured for high-quality UGe_2 samples $T_{\mathrm{SC}} \simeq 0.8$ K.

The specific heat as a function of temperature was also calculated, as presented in Figure 3.14(b). It does not agree with experiment, since we do not get the residual value at $T = 0$ K. However, the normalized specific heat jump $\Delta C/\gamma_n T_{\mathrm{SC}} \simeq 1.44$, which is not far from $\Delta C/\gamma_n T_{\mathrm{SC}} \simeq 0.97$ measured in experiment [86].

3.3. Results for non-zero magnetic field

In this Section the effects of non-zero applied magnetic field $\mu_0 H \neq 0$ are studied. These are included in the model (2.2) via the Zeeman term (2.13), defined at the page 18.

We are motivated by the experiments for UGe_2 with applied magnetic field [29, 42] discussed briefly in Chapter 1 (cf. Figure 1.2(c), page 7, and Figure 1.5, page 9).

3.3.1. Influence of magnetic field on phase transitions

Here we examine influence of the magnetic field on the f-c hybridization value for which phase transition FM2+A_2 →FM1+A_1 occurs. In Figure 3.15 we show (a) total magnetization, as well as equal-spin superconducting gap parameters (b) dominant spin-down and (c) minority spin-up pairing components as functions of hybridization without magnetic field (lighter colors and dashed lines) and with $h/|t| = 0.002$ (darker colors and solid lines). Reduced magnetic field $h = \frac{1}{2} g \mu_B \mu_0 H = 0.002\ |t|$ corresponds to $\mu_0 H \approx 17.3$ T for c-electron nearest-neighbor hopping $|t| = 0.5$ eV. The main effect of switching on magnetic field is a shift of FM2→FM1 phase transition for larger values of hybridization: from $V_{PT}/t = 1.25852$ for zero magnetic field to $V_{\mathrm{PT}}/t = 1.260515$ for above value of magnetic field. The change $\Delta V/t = 0.001995$. The applied magnetic field neither changes the character of transition (the first order), nor influences the values of magnetization or gap parameter after phase transition.

To obtain the proper value of hybridization, for which the phase transition occurs, we have compared energies in both FM2+A_2 and FM1+A_1 phases. Calculations are presented in Appendix D.5 (cf. Table D.5 and Figure D.10).

3.3.2. Characteristic transition field $\mu_0 H_x$ for different hybridization values

We now investigate, what happens in the system in applied magnetic field for a given hybridization value. We choose such a f-c hybridization, $V/t = 1.26$, that without magnetic field the system is in FM1+A_1 phase. Then we apply magnetic field and check how the system evolves. It turns out that the state of the system does not change, until we reach magnetic field value $\mu_0 H_x$, known as characteristic transition field. Then phase transition of the first order occurs and the system goes to FM2+A_2 phase with two unequal gap parameters.

To find proper value of the characteristic transition field we compare energies of the system in both phases: FM1+A_1 and FM2+A_2. Detailed calculations are presented in Appendix D.5, cf. Table D.6.

In Figure 3.16 the resulting phase diagram is presented. In Figure 3.16(a) there are shown magnetizations: total m^{tot} – black, for f-electrons – blue and for c-electrons – red. Regions of the ferromagnetic phases are marked (FM1, FM2). The inset shows enclose to the jump of total magnetization. We have also investigated the superconducting properties: In Figure 3.16(b) equal-spin triplet superconducting gap ampli-

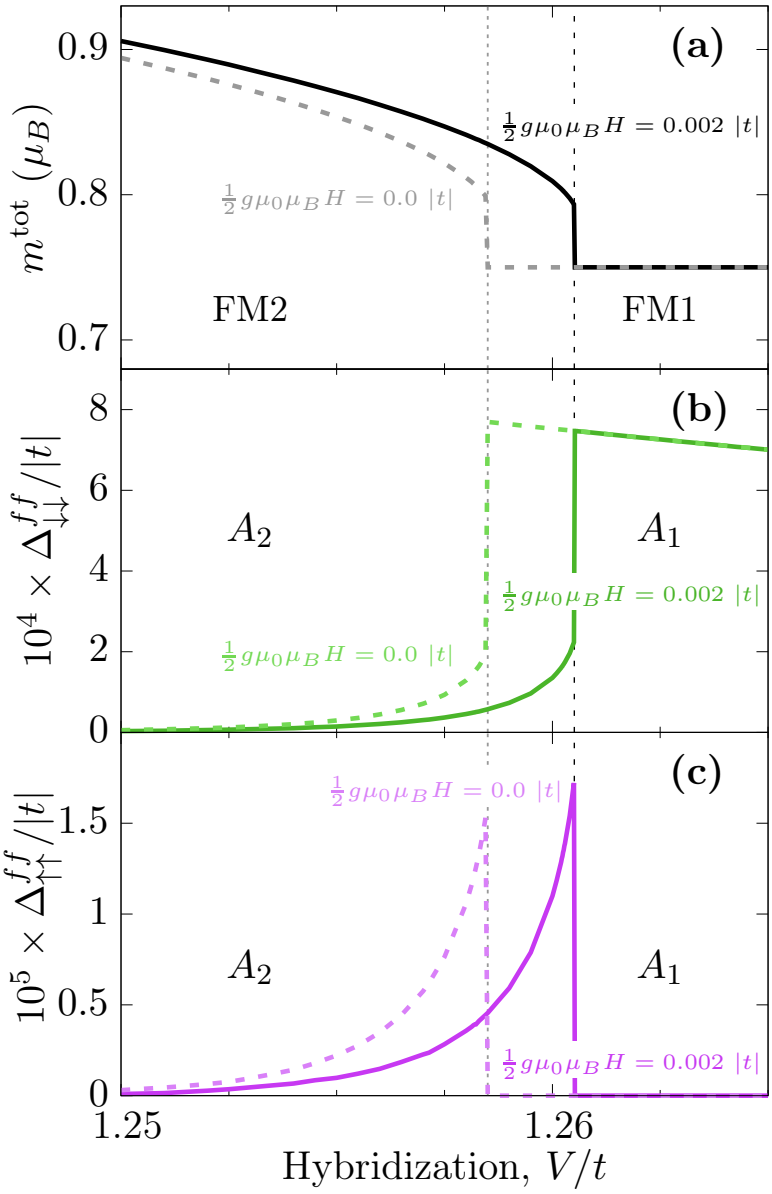

Figure 3.15.: (a) Total magnetization. (b) and (c) Superconducting gap parameters as functions of hybridization. Solid lines correspond to applied field $h = 0.002|t|$, whereas dashed lines represent the zero-field situation. Shift of phase transition point for non-zero magnetic field ($h/|t| = 0.002$) as compared to zero magnetic field can be seen. The set of parameters is the same as that used in Figure 3.1: $U/|t| = 3.5$, $J/|t| = 1.1$, $T = 0$ K, $t'/|t| = 0.25$, $\epsilon^f/|t| = -4$, $n^{\mathrm{tot}} = 3.25$.

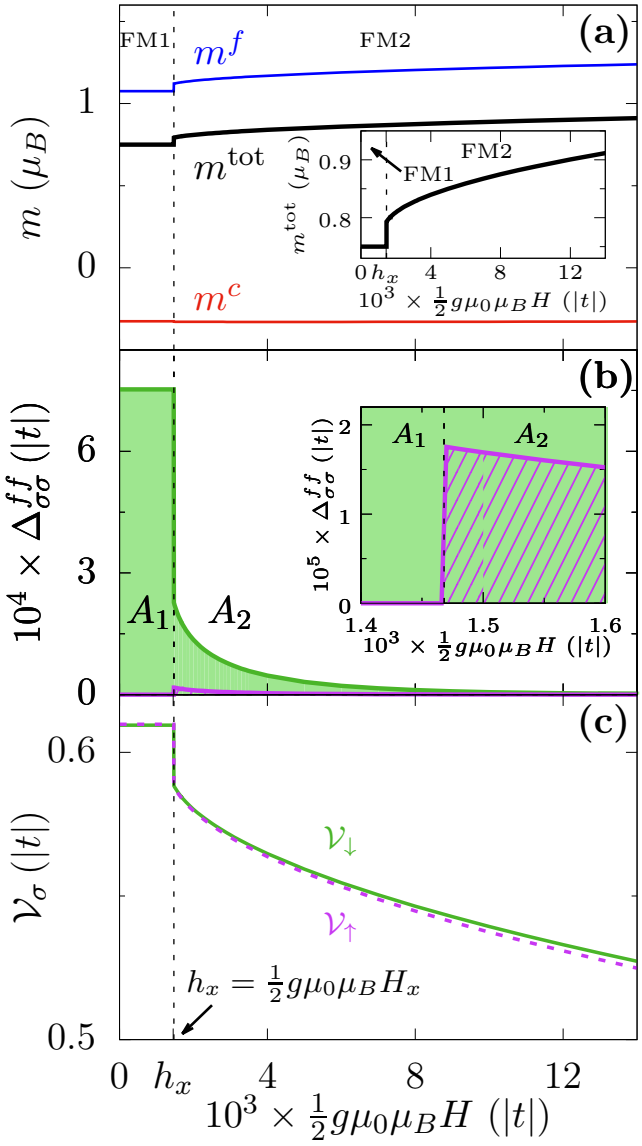

Figure 3.16.: Phase diagram obtained for non-zero applied magnetic field at zero temperature. (a) Magnetizations: $m^{\rm tot}$ – total (black line), m^f – f-electron component (blue), m^c – c-electron component (red). (b) Triplet f-f superconducting gap components: $\Delta^{ff}_{\uparrow\uparrow}$ – purple, $\Delta^{ff}_{\downarrow\downarrow}$ – green. (c) Spin-dependent pairing potential $\mathcal{V}_\sigma$. Phase transition from FM1+A_1 to FM2+A_2 at $h_x/|t| = 0.001468$, which corresponds to magnetic field $\mu_0 H_x \approx 12.7$ T. The results are obtained for the set of parameters: $U/|t| = 3.5$, $J/|t| = 1.1$, $T = 0$ K, $V/t = 1.26$, $t'/|t| = 0.25$, $\epsilon^f/|t| = -4$, $n^{\rm tot} = 3.25$.

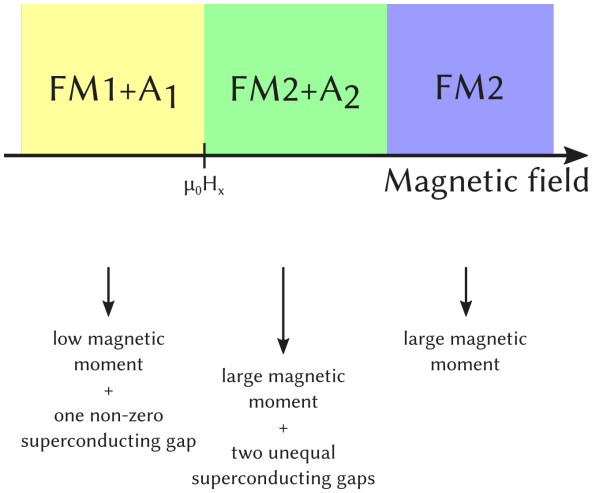

Figure 3.17.: Sequence of superconducting and magnetic phases with increasing magnetic field and fixed f-c hybridization V, at zero temperature.

tudes $\Delta^{ff}_{\uparrow\uparrow}$ – purple, $\Delta^{ff}_{\downarrow\downarrow}$ – green are shown. The superconducting phases are marked: A_1 phase with one non-zero gap parameter and A_2 with two non-equal gap parameters. The inset shows enclose to $A_1 \rightarrow A_2$ phase transition region. We have also plotted the coupling constant $\mathcal{V}_\sigma$ in Figure 3.16(c).

Both metamagnetic and superconducting phase transitions are of the first order and take place for the same value of applied magnetic field $\mu_0 H_x \approx 12.7$ T. Calculated characteristic transition field is too large, comparing with experiments [29]. This could be related to the neglected orbital effects of the applied magnetic field. Schematic diagram of phases, which the system passes with growing magnetic field, is depicted in Figure 3.17.

The superconducting gap parameters in A_2 phase are disappearing for larger values of applied magnetic field.

The characteristic transition field $\mu_0 H_x$ was also specified for other hybridization values, just over FM2→FM1 phase transition in zero magnetic field. Obtained values of the characteristic transition fields are presented in Table 3.2 and in Figure 3.18. Detailed calculations are included in Appendix D.5, cf. Table D.7.

In Figure 3.18 we see linear dependence of the characteristic transition field on the f-c hybridization. The obtained result agrees with experiment [29] qualitatively (linear dependence). However, the calculated characteristic transition fields are far too large, cf. Figure 1.2 in Chapter 1 (page 7).

Table 3.2.: Characteristic transition field, i.e., the magnetic field value for which FM1+A_1 →FM2+A_2 transition takes place as a function of hybridization and for $|t| = 0.5$ eV. The following results are also shown in Figure 3.18.

V/t	$h_x/\|t\|$	$\mu_0 H_x$ (T)
1.25852	0.0	0.0
1.2590	0.000435	3.8
1.2595	0.000951	8.2
1.2600	0.001468	12.7
1.2605	0.001984	17.1
1.2610	0.002501	21.6

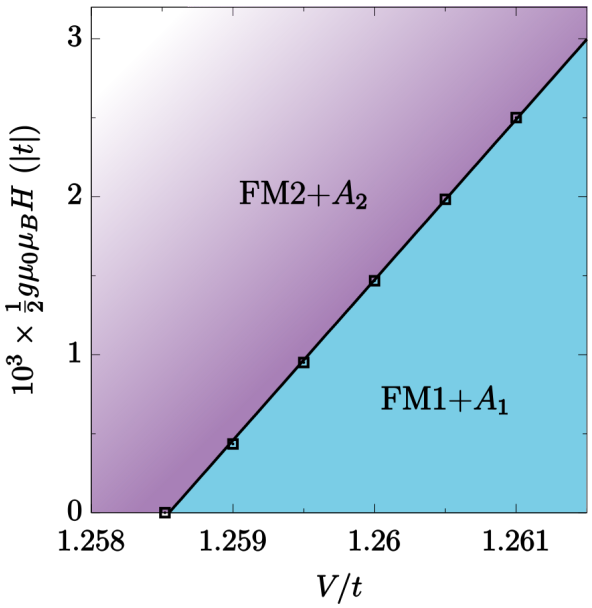

Figure 3.18.: Linear dependence of the characteristic transition field $\mu_0 H_x$ on f-c hybridization.

3.4. Summary of results

In this Chapter we have discussed calculated phase diagram for UGe_2 with reproduced magnetic phase transitions (FM2→FM1→PM) together with superconductivity having peak at FM2→FM1 phase transition. We have also discussed the appearing superconducting phases: A_2, A_1, and A at zero temperature. Results presented here were obtained within SGA method and compared with the Hartree-Fock-BCS solution. It turns out, that correlations have a significant influence on the ground state of the system, i.e., they allow for superconductivity to exist in broader regime of parameters. We have also tested evolution of superconducting gap at non-zero temperature and in non-zero Zeeman magnetic field.

4. Modified Schrieffer-Wolff transformation and exchange interactions

4.1. Introduction

In this Chapter we consider explicitly the strong-correlation limit of the Anderson lattice model to determine emerging kinetic-exchange interactions. Explicitly, we discuss modified Schrieffer-Wolff transformation. The presented results were obtained for the non-degenerate Anderson lattice model [63]; we also sketch the situation for the orbital degeneracy. The considered canonical perturbation expansion is applied for both models in real space. The transformation is carried up to the fourth order of expansion in the non-degenerate case and up to the second order in the orbitally degenerate situation. The modified Schrieffer-Wolff transformation leaves intact the residual hybridization and provides the spin-spin antiferromagnetic Kondo and f-f interactions. It is important to mention that we are working now in the strong correlation limit, i.e., the intraorbital Coulomb interaction of f-electrons U is large, but finite. Also, the hybridization term is decomposed into two parts. Namely, the part of the c-f hybridization term responsible for the high-energy processes is replaced with the virtual processes in higher orders. On the other hand, the effective Hamiltonian for the degenerate model is discussed in two different cases, i.e., when f-occupancy per site n^f is $0 < n^f \leqslant 1$ and $1 < n^f \leqslant 2$, respectively.

The transformation presented in this Chapter was originally proposed for the non-degenerate Hubbard model [90] and subsequently, extended into the case of orbital degeneracy [91, 92]. Later, it has been also applied in the non-degenerate Anderson lattice model [50, 62, 63].

The obtained result was the introduction of spin-singlet pairing mediated by antiferromagnetic exchange interactions between conduction and f-electrons (the Kondo exchange interaction). This is because spin-singlet correlations in real space can lead to pairing in heavy-fermion systems. The idea of exchange-mediated pairing in narrow bands was originally proposed by Anderson [49]. The transformation presented in this chapter is also compared to the original Schrieffer-Wolff transformation [64].

4.2. The canonical perturbation expansion (CPE)

The basic feature of the Anderson model is the differentiation between two electron types: localized f-electrons and the conduction c states, which can be mixed via the hybridization term $\hat{\mathcal{H}}^{cf}$ (2.4). Since the hybridization term can create new double

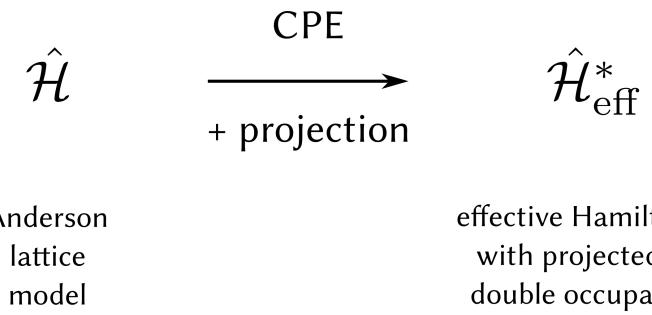

Figure 4.1.: The idea of obtaining the effective Hamiltonian using the canonical perturbation expansion (CPE) with projection onto the Fock subspace with the lowest possible number of double occupancies.

f-occupancies, which involve large intraatomic Coulomb interaction U, one can say that the hybridization connects two Fock subspaces: low-energy and high-energy parts. It is assumed, that the parameter U is the largest energy scale in the system and $|V_{ij}| \ll U$. The aim of the canonical perturbation expansion is schematically depicted in Figure 4.1.

Let us consider a Hamiltonian $\hat{\mathcal{H}}$, which can be divided in two terms: $\hat{\mathcal{H}} = \hat{\mathcal{H}}_0 + \varepsilon\hat{\mathcal{H}}_1$, where $\hat{\mathcal{H}}_0$ describes both low- and high-energy subspaces, whereas $\hat{\mathcal{H}}_1$ corresponds to mixing of these subspaces and can be treated as a perturbation; ε is an expansion parameter. We introduce the canonical transformation of the Hamiltonian $\hat{\mathcal{H}}$ in the following manner

$$\hat{\mathcal{H}}^*(\varepsilon) = e^{-i\varepsilon\hat{\mathcal{S}}}(\hat{\mathcal{H}}_0 + \varepsilon\hat{\mathcal{H}}_1)e^{+i\varepsilon\hat{\mathcal{S}}}, \tag{4.1}$$

where $\hat{\mathcal{S}}$ is the transformation generator. Expanding $\hat{\mathcal{S}}$ in Taylor series and taking into account physical condition, which eliminates linear term $\sim \varepsilon$ by the requirement, i. e.,

$$\hat{\mathcal{H}}_1 = i[\hat{\mathcal{S}}, \hat{\mathcal{H}}_0], \tag{4.2}$$

we obtain up to the fourth order

$$\hat{\mathcal{H}}^*(\varepsilon) = \hat{\mathcal{H}}_0 - \frac{i}{2}\varepsilon^2[\hat{\mathcal{S}}, \hat{\mathcal{H}}_1] - \frac{1}{3}\varepsilon^3[\hat{\mathcal{S}}, [\hat{\mathcal{S}}, \hat{\mathcal{H}}_1]] + \frac{i}{8}\varepsilon^4[\hat{\mathcal{S}}, [\hat{\mathcal{S}}, [\hat{\mathcal{S}}, \hat{\mathcal{H}}_1]]] + \mathcal{O}(\varepsilon^5). \tag{4.3}$$

Next, we introduce projection operator $\hat{\mathcal{P}}_0$, which ensures that there is the lowest possible number of double f-occupancies present in the system, whereas $\hat{\mathcal{P}}_m$ creates m additional double occupancies. For the case, when mean f-occupancy $n^f \leqslant 1$, the operator $\hat{\mathcal{P}}_0$ projects to the subspace without double occupancies. Operators $\hat{\mathcal{P}}_m$ have following properties

$$\sum_m \hat{\mathcal{P}}_m = \mathbb{1} \qquad \text{and} \qquad \hat{\mathcal{P}}_m\hat{\mathcal{P}}_{m'} = \delta_{mm'}\hat{\mathcal{P}}_m. \tag{4.4}$$

Using these operators one can define parts of the initial Hamiltonian $\hat{\mathcal{H}}$ as

$$\hat{\mathcal{H}}_0 = \sum_m \hat{\mathcal{P}}_m \hat{\mathcal{H}} \hat{\mathcal{P}}_m, \tag{4.5}$$

$$\hat{\mathcal{H}}_1 = \sum_m \left(\hat{\mathcal{P}}_m \hat{\mathcal{H}} \hat{\mathcal{P}}_{m+1} + \hat{\mathcal{P}}_{m+1} \hat{\mathcal{H}} \hat{\mathcal{P}}_m \right). \tag{4.6}$$

Since we assume, that the initial Hamiltonian $\hat{\mathcal{H}}$ does not contain pair-hopping terms, the part $\hat{\mathcal{H}}_1$ connects only subspaces, in which numbers of double occupancies differ by one. The assumption is valid for U values large in relation to other energy scales.

Using projection operators $\hat{\mathcal{P}}_m$ and $\hat{\mathcal{P}}_{m+1}$, the condition (4.2) can be solved by putting $\hat{\mathcal{P}}_m \hat{\mathcal{S}}^{(0)} \hat{\mathcal{P}}_{m+1} = 0$ and iterating the solution. In this manner the projected version of (4.2) is obtained in the form

$$\hat{\mathcal{P}}_m \hat{\mathcal{S}}^{(n\to\infty)} \hat{\mathcal{P}}_{m+1} = -i \left(\hat{\mathcal{P}}_m \hat{\mathcal{H}}_1 \hat{\mathcal{P}}_{m+1} \right) \cdot \left(\hat{\mathcal{P}}_{m+1} \hat{\mathcal{H}}_0 \hat{\mathcal{P}}_{m+1} - \hat{\mathcal{P}}_m \hat{\mathcal{H}}_0 \hat{\mathcal{P}}_m \right)^{-1}. \tag{4.7}$$

Note, that projecting (4.2) with operator $\hat{\mathcal{P}}_m$ on both sides we obtain that $\hat{\mathcal{P}}_m \hat{\mathcal{S}} \hat{\mathcal{P}}_m$ commutes with $\hat{\mathcal{H}}_0$. It means that $\hat{\mathcal{P}}_m \hat{\mathcal{S}} \hat{\mathcal{P}}_m \sim \hat{\mathcal{P}}_m$, so we can choose $\hat{\mathcal{S}}$ in such a way, that $\hat{\mathcal{P}}_m \hat{\mathcal{S}} \hat{\mathcal{P}}_m = 0$.

In the atomic limit the difference $\hat{\mathcal{P}}_{m+1} \hat{\mathcal{H}}_0 \hat{\mathcal{P}}_{m+1} - \hat{\mathcal{P}}_m \hat{\mathcal{H}}_0 \hat{\mathcal{P}}_m$ can be approximated by the average energy difference

$$\Delta E_{m+1,m} \equiv \langle \hat{\mathcal{P}}_{m+1} \hat{\mathcal{H}}_0 \hat{\mathcal{P}}_{m+1} \rangle - \langle \hat{\mathcal{P}}_m \hat{\mathcal{H}}_0 \hat{\mathcal{P}}_m \rangle. \tag{4.8}$$

By making this approximation, a renormalization of the low-energy hybridization processes by the higher order contributions is neglected (terms $\sim V_{im}$ in the denominator of (4.7) are omitted).

Moreover, our goal is to obtain the effective Hamiltonian, which is the transformed Hamiltonian $\hat{\mathcal{H}}^* = \hat{\mathcal{H}}^*(\varepsilon = 1)$ projected by the operator $\hat{\mathcal{P}}_0$:

$$\hat{\mathcal{H}}_{\text{eff}} = \hat{\mathcal{P}}_0 \hat{\mathcal{H}}^* \hat{\mathcal{P}}_0. \tag{4.9}$$

Using (4.7), the effective Hamiltonian in the subspace with the lowest possible number of double occupancies acquires the following form

$$\begin{aligned} \hat{\mathcal{H}}_{\text{eff}} \approx\ & \hat{\mathcal{P}}_0 \hat{\mathcal{H}}_0 \hat{\mathcal{P}}_0 - \frac{1}{\Delta E_{10}} \hat{\mathcal{P}}_0 \hat{\mathcal{H}}_1 \hat{\mathcal{P}}_1 \hat{\mathcal{H}}_1 \hat{\mathcal{P}}_0 \\ & + \frac{1}{(\Delta E_{10})^3} \hat{\mathcal{P}}_0 \hat{\mathcal{H}}_1 \hat{\mathcal{P}}_1 \hat{\mathcal{H}}_1 \hat{\mathcal{P}}_0 \hat{\mathcal{H}}_1 \hat{\mathcal{P}}_1 \hat{\mathcal{H}}_1 \hat{\mathcal{P}}_0 \\ & - \frac{1}{2} \frac{1}{(\Delta E_{10})^2 \, \Delta E_{21}} \hat{\mathcal{P}}_0 \hat{\mathcal{H}}_1 \hat{\mathcal{P}}_1 \hat{\mathcal{H}}_1 \hat{\mathcal{P}}_2 \hat{\mathcal{H}}_1 \hat{\mathcal{P}}_1 \hat{\mathcal{H}}_1 \hat{\mathcal{P}}_0. \end{aligned} \tag{4.10}$$

Note that the third-order term is always zero, because we have put $\left(\hat{\mathcal{P}}_m \hat{\mathcal{S}} \hat{\mathcal{P}}_m \right) = 0$. The term $\hat{\mathcal{P}}_0 \hat{\mathcal{H}}_1 \hat{\mathcal{P}}_1 \hat{\mathcal{H}}_1 \hat{\mathcal{P}}_0$ describes virtual process in the second order, in which in intermediate state one additional double occupancy occurs. In the fourth order of

expansion different types of processes appear: with passing through the subspace without double occupancies, the subspace characterized by $\hat{\mathcal{P}}_0$ and with two additional double f-occupancies, by $\hat{\mathcal{P}}_2$.

The expression (4.10) will be discussed in details for both the non-degenerate and orbitally degenerate Anderson lattice models, because it is helpful in determining the ground state for different magnetic and superconducting phases of heavy fermions.

4.3. Results for the non-degenerate Anderson lattice model

The non-degenerate Anderson lattice model can be used for modeling the heavy fermion systems, such as the cerium compounds (approximate $4f^1$ configuration for Ce^{3+} ions). The initial Hamiltonian has the same form as that in Chapter 2 with subtracted the chemical-potential part (μ), namely

$$\hat{\mathcal{H}} = \sum_{ij\sigma} \left(t_{ij} - \delta_{ij}\mu\right) \hat{c}^{\dagger}_{i\sigma}\hat{c}_{j\sigma} + \sum_{ij\sigma} \left(V_{ij}\hat{f}^{\dagger}_{i\sigma}\hat{c}_{j\sigma} + V^{*}_{ij}\hat{c}^{\dagger}_{i\sigma}\hat{f}_{j\sigma}\right) + \left(\epsilon^{f} - \mu\right) \sum_{i\sigma} \hat{n}^{f}_{i\sigma} + U \sum_{i} \hat{n}^{f}_{i\uparrow}\hat{n}^{f}_{i\downarrow}. \tag{4.11}$$

It is assumed that the hybridization strength is much smaller than the intraatomic Coulomb interaction, i.e., the calculations presented below are carried out in the regime $|V_{ij}| \ll U$. In the regime of strong correlations (large U values), if f-level is located shallow, the relative hybridization strength V_{ij}/ϵ^{f} cannot be transformed out, as it would be in the Schrieffer-Wolff transformation [64]; this is because it cannot be regarded as small value. The hybridization term changes f-electron occupancies, either by creating a double f-electron occupancy (if on the site was electron with the opposite spin) or a single f-occupancy (if the site was empty before). Decomposing the hybridization term into two parts according to the identity

$$\hat{f}^{\dagger}_{i\sigma}\hat{c}_{j\sigma} \equiv \left(1 - \hat{n}^{f}_{i\bar{\sigma}}\right) \hat{f}^{\dagger}_{i\sigma}\hat{c}_{j\sigma} + \hat{n}^{f}_{i\bar{\sigma}}\hat{f}^{\dagger}_{i\sigma}\hat{c}_{j\sigma}, \tag{4.12}$$

we differentiate processes as those, that do not involve large U energy (the first term) and those, that create double f-occupancy on one site (the second term). Those two distinct situations are depicted in Figure 4.2. In presented here approach only f-electron double occupancies (high-energy states) are projected out.

We can define the projection operators for the non-degenerate Anderson lattice

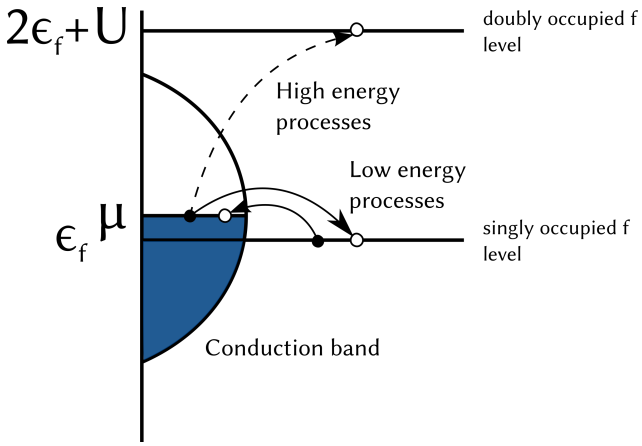

Figure 4.2.: High- and low-energy interorbital hopping processes induced by the f-c hybridization. Only the high-energy mixing (involving U, the largest energy scale in the system) are transformed out and replaced by the virtual hopping processes. Low-energy part remains unchanged in the effective Hamiltonian, with a residual hybridization. Figure taken from [63].

model, in the case $n^f \leqslant 1$:

$$\hat{\mathcal{P}}_0 = \prod_i \left(\left(1 - \hat{n}^f_{i\uparrow}\right)\left(1 - \hat{n}^f_{i\downarrow}\right) + \sum_\sigma \hat{n}^f_{i\sigma}\left(1 - \hat{n}^f_{i\bar{\sigma}}\right) \right) = \prod_i \left(1 - \hat{n}^f_{i\uparrow}\hat{n}^f_{i\downarrow}\right), \tag{4.13}$$

$$\hat{\mathcal{P}}_1 = \sum_j \left(\hat{n}^f_{j\uparrow}\hat{n}^f_{j\downarrow} \times \prod_{i\neq j} \left(1 - \hat{n}^f_{i\uparrow}\hat{n}^f_{i\downarrow}\right) \right), \tag{4.14}$$

$$\hat{\mathcal{P}}_2 = \sum_{\substack{j,k \\ j\neq k}} \left(\hat{n}^f_{j\uparrow}\hat{n}^f_{j\downarrow}\hat{n}^f_{k\uparrow}\hat{n}^f_{k\downarrow} \times \prod_{\substack{i\neq j \\ i\neq k}} \left(1 - \hat{n}^f_{i\uparrow}\hat{n}^f_{i\downarrow}\right) \right). \tag{4.15}$$

The idea of projection operators construction is presented in Figure 4.3. The operator $\hat{\mathcal{P}}_0$ defined by (4.13) suppresses double f-occupancies, $\hat{\mathcal{P}}_1$ defined by (4.14) creates one additional double occupancy, and $\hat{\mathcal{P}}_2$ (4.15) creates two additional double occupancies.

Using (4.13) – (4.15) the effective Hamiltonian defined as (4.10) is calculated. We carry out a careful analysis of possible two- and three-site processes, examples of them are depicted in Figure 4.4. The energy difference given by (4.8) for the non-degenerate Anderson lattice model is connected with appearance of double f-occupancy

$$\Delta E = \langle \hat{\mathcal{P}}_{m+1}\hat{\mathcal{H}}_0\hat{\mathcal{P}}_{m+1}\rangle - \langle \hat{\mathcal{P}}_m\hat{\mathcal{H}}_0\hat{\mathcal{P}}_m\rangle = U + \epsilon^f - \mu. \tag{4.16}$$

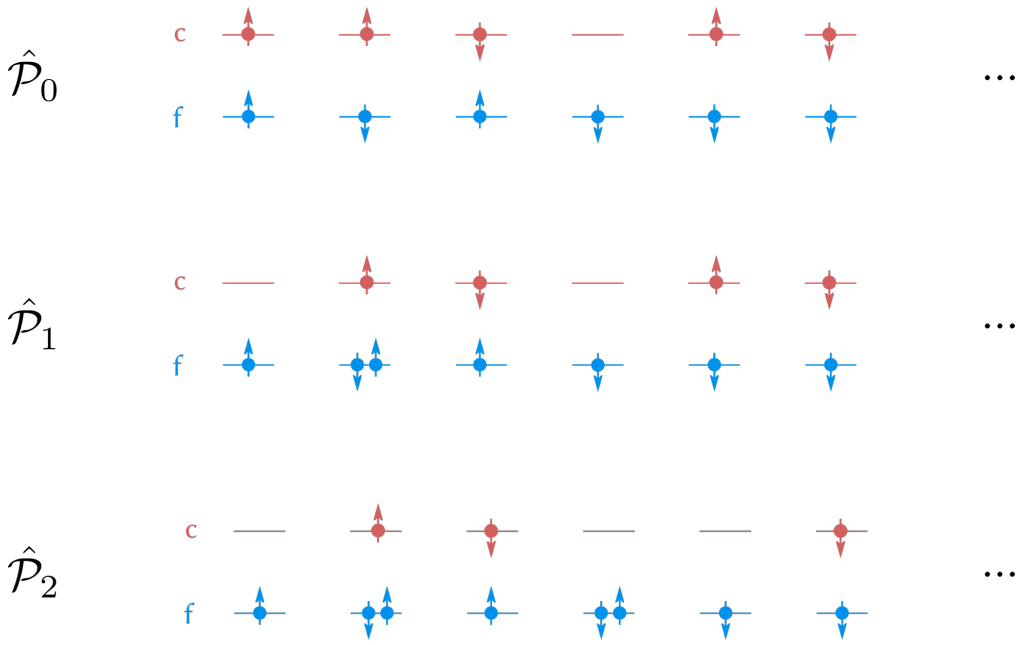

Figure 4.3.: Schematic description different local contribution to the projection operators (4.13) – (4.15). The operator $\hat{\mathcal{P}}_0$ suppresses double f-occupancies, whereas $\hat{\mathcal{P}}_1$ creates one additional double f-occupancy, and $\hat{\mathcal{P}}_2$ (4.15) creates two additional double f-occupancies in the system.

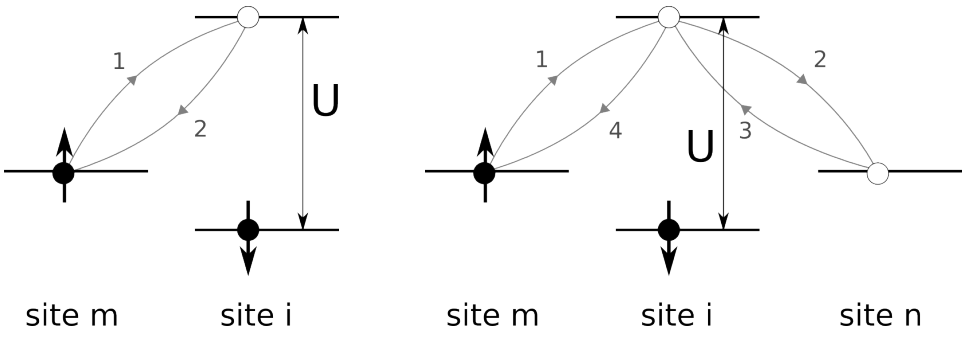

Figure 4.4.: Examples of processes in the second (left) and the fourth (right) orders of the CPE expansion. Figure taken from [63].

4.3.1. Kondo f-c and superexchange f-f integrals

The form of the effective Hamiltonian is found by carrying out an analysis of possible processes, which can show up in the second and the fourth orders of the expansion. After rather tedious calculations and collecting all possible terms (diagrams) the following result is obtained

$$\begin{aligned}\hat{\mathcal{H}}_{\text{eff}} \simeq & \sum_{ij\sigma}\left(t_{ij}-\mu\delta_{ij}\right)\hat{c}^{\dagger}_{i\sigma}\hat{c}_{j\sigma}+\left(\epsilon^{f}-\mu\right)\sum_{i,\sigma}\hat{\nu}^{f}_{i\sigma} \\ & +\sum_{i,m,\sigma}\left(V_{im}\left(1-\hat{n}^{f}_{i\bar{\sigma}}\right)\hat{f}^{\dagger}_{i\sigma}\hat{c}_{m\sigma}+H.c.\right) \\ & +\sum_{i,m}J^{(\mathrm{K})}_{im}\left(\hat{\mathbf{S}}^{f}_{i}\cdot\hat{\mathbf{S}}^{c}_{m}-\frac{\hat{n}^{c}_{m}\hat{\nu}^{f}_{i}}{4}\right)+\sum_{i\neq j,\sigma}J^{(\mathrm{H})}_{ij}\left(\hat{\mathbf{S}}^{f}_{i}\cdot\hat{\mathbf{S}}^{f}_{j}-\frac{\hat{\nu}^{f}_{i}\hat{\nu}^{f}_{j}}{4}\right) \\ & +2i\sum_{\langle mi\rangle\langle mj\rangle}J^{(\mathrm{H})}_{ij}\left(1+\frac{n^{f}}{n^{c}}\right)\hat{\mathbf{S}}^{c}_{m}\cdot\left(\hat{\mathbf{S}}^{f}_{j}\times\hat{\mathbf{S}}^{f}_{i}\right),\end{aligned} \tag{4.17}$$

where $\hat{\nu}^{f}_{i\sigma}\equiv\left(1-\hat{n}^{f}_{i\bar{\sigma}}\right)\hat{n}^{f}_{i\sigma}$, $\hat{\nu}^{f}_{i}\equiv\sum_{\sigma}\hat{\nu}^{f}_{i\sigma}$, $\hat{\mathbf{S}}^{f}_{i}$ and $\hat{\mathbf{S}}^{c}_{m}$ are spin operators in the fermion representation for f and c electrons, respectively (the formal definition see Chapter 2, page 15). The symbols $\langle mi\rangle\langle mj\rangle$ in the last term mean a summation over indexes i, j, m, where i,m and j,m are pairs of nearest neighbors.

The first three terms in (4.17) represent the projected initial Hamiltonian with residual (projected) hybridization part only. The next three correspond respectively to the f-c Kondo interaction, the f-f superexchange part and the interaction of Dzyaloshinskii-Moriya-type appearing only if the c-electrons are present (the anti-symmetric exchange). The noncollinearity of the magnetic ordering of c electrons ($\sim\hat{\mathbf{S}}^{f}_{i}\cdot\left(\hat{\mathbf{S}}^{c}_{n}\times\hat{\mathbf{S}}^{c}_{m}\right)$), as well as the superexchange interaction between them, were neglected in effective Hamiltonian (4.17), since the c-electron bandwidth $W=2z|t|$ is by far the largest energy in the c-electron system, where z is the number of the nearest neighbors (in the considered case of two-dimensional square lattice $z=4$) and the hopping integral is

$$t_{ij}=\begin{cases}t & \text{for } i,j \text{ – nearest neighbors,}\\ 0 & \text{otherwise.}\end{cases} \tag{4.18}$$

The corresponding exchange integrals have the following forms

$$\begin{aligned}J^{(\mathrm{K})}_{im}\equiv & \,2\frac{|V_{im}|^{2}}{U+\epsilon^{f}}-4\frac{|V_{im}|^{4}}{\left(U+\epsilon^{f}\right)^{3}}-4\sum_{n(i)}\frac{|V_{im}|^{2}|V_{in}|^{2}}{\left(U+\epsilon^{f}\right)^{3}}\left(1-\frac{n^{c}}{2}\right) \\ & -2\sum_{n(i)}\frac{|V_{im}|^{2}|V_{in}|^{2}}{\left(U+\epsilon^{f}\right)^{3}}n^{c}-2\sum_{j(m)}\frac{|V_{im}|^{2}|V_{jm}|^{2}}{\left(U+\epsilon^{f}\right)^{3}}n^{f},\end{aligned} \tag{4.19}$$

$$J_{ij}^{(\mathrm{H})} \equiv \sum_{m(i)} \frac{|V_{jm}|^2 |V_{im}|^2}{\left(U + \epsilon^f\right)^3} n^c. \tag{4.20}$$

Note that the effective Hamiltonian contains the Dzyaloshinskii-Moriya interaction as induced purely by the electron-electron interaction, i.e., without any degenerate orbital structure, as in the original case [93, 94].

Estimates of exchange integrals The estimates of the exchange integrals appearing in (4.19) and (4.20) are shown in Figures 4.5 and 4.6 for $U + \epsilon^f = 3\ |t|$ and $U + \epsilon^f = 5\ |t|$, respectively. Purely onsite hybridization cannot lead to f-electron itineracy; therefore, we have assumed the interatomic form of hybridization

$$V_{ij} = \begin{cases} V & \text{for } i,j \text{ – nearest neighbors,} \\ 0 & \text{otherwise,} \end{cases} \tag{4.21}$$

and reference number of electrons per site for the cerium-based compounds is $n^f = 1$ and $n^c = 1$. Let us note that in order to estimate exchange integral $J_{ij}^{(\mathrm{H})}$ it is assumed that the sites i and j are next nearest neighbors, such that summation in Eq. (4.20) allows only such m that $\langle i, m\rangle$ and $\langle m, j\rangle$ are the nearest neighbors.

All exchange integrals are antiferromagnetic. The fourth-order correction reduces the second-order values (Figures 4.5(a) and 4.6(b)). The Kondo exchange integral $J^{(\mathrm{K})}$ in Figure 4.5(a) is more than an order of magnitude larger than the f-f superexchange counterpart, which contains solely the fourth-order processes. Note that the canonical perturbation expansion is valid only for $|V| \ll U$; therefore, for larger hybridization values the series in Equation (4.10) is divergent. For the larger U value the integrals $J^{(\mathrm{H})}$ and $J^{(\mathrm{K})}$ are smaller, as presented in Figure 4.6.

Comparison to original Schrieffer-Wolff transformation In the case of the original Schrieffer-Wolff transformation, the whole hybridization term is transformed out. Energetically favorable is to have single f-occupancies on all system sites, since the f-level is located deeply below the Fermi surface. Processes perturbing such a situation can be schematically written as

$$c + f^1 \leftrightarrow f^2, \tag{4.22}$$

$$f^1 \leftrightarrow f^0 + c, \tag{4.23}$$

and both of them are transferring the system to high-energy subspace, as it is depicted in Figure 4.7(a). On the contrary, the modified version of Schrieffer-Wolff transformation is valid for such systems, where f-electron energy level ϵ^f is located shallowly, as presented in Figure 4.7(b).

It is important to mention that after the Schrieffer-Wolff transformation has been carried out, the number of c-electrons, n^c, and the number of f-electrons, n^f, are conserved separately, whereas in the modified version only their total number, $n^{\mathrm{tot}} = n^f + n^c$, is unchanged. In the effective Anderson-Kondo Hamiltonian (4.17) part of

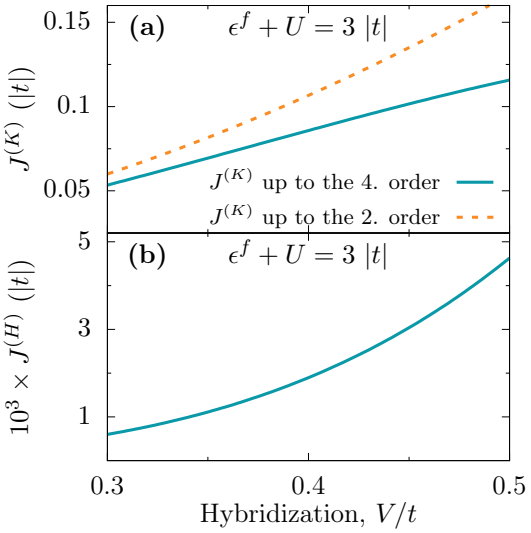

Figure 4.5.: Values of (a) the Kondo exchange integral $J^{(\mathrm{K})}$, with and without correction from the fourth order of expansion, and (b) the f-f superexchange integral $J^{(\mathrm{H})}$, for the case with $n^c = 1$, $n^f = 1$, the nearest neighbor hybridization only, and $U + \epsilon^f = 3\ |t|$. Figure taken from [63].

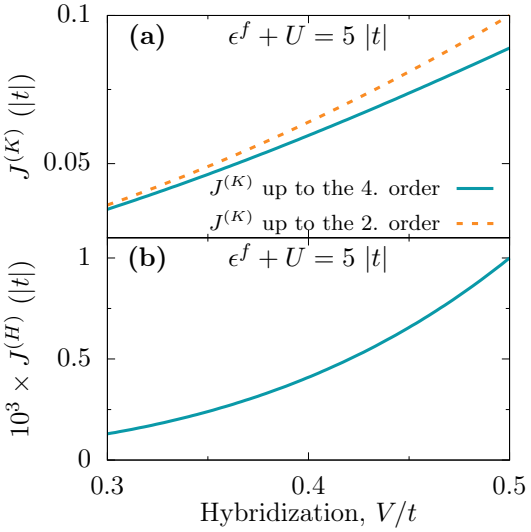

Figure 4.6.: Values of (a) the Kondo exchange integral $J^{(\mathrm{K})}$, with and without correction from the fourth order of expansion, and (b) the f-f superexchange integral $J^{(\mathrm{H})}$, for the case with $n^c = 1$, $n^f = 1$, the nearest neighbor hybridization only, and $U + \epsilon^f = 5\ |t|$. Figure taken from [63].

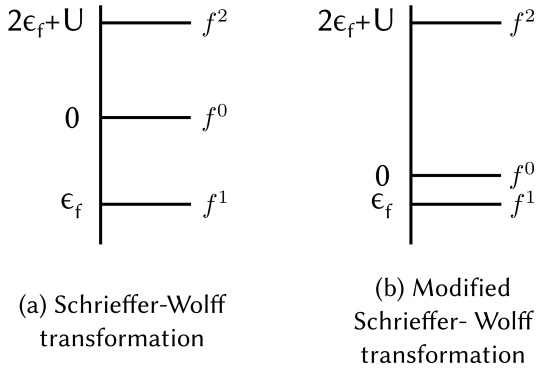

Figure 4.7.: Comparison of energy levels, which indicates the choice of the transformation type. In the left panel (a) both processes $c + f^1 \leftrightarrow f^2$ and $f^1 \leftrightarrow f^0 + c$ involve high-energy scales; therefore, both of them are transformed out (the case of *the Schrieffer-Wolff transformation*). In the right panel (b) the f-level is shallowly located. Thus, V/ϵ^f cannot be treated as small perturbation. Such a situation requires here a division of hybridization term to low- and high-energy processes (as presented in Figure 4.2).

the hybridization $\sim V_{im}\left(1-\hat{n}^f_{i\bar{\sigma}}\right)\hat{f}^\dagger_{i\sigma}\hat{c}_{m\sigma}$ remains unaltered and is called the residual hybridization. This feature provides an important difference between those two approaches and it allows for an itineracy of strongly correlated and originally localized f-electrons in the latter situation.

Numerical results The present results (4.17) provide an effective model for subsequent consideration of the magnetism and the real-space pairing in the heavy-fermion systems [59, 60]. Phase diagram obtained within above Anderson-Kondo model without Dzyaloshinskii-Moriya type of interaction, i.e., the last term in (4.17), is presented in Figure 4.8. The most important feature of the phase diagram is two regimes of coexistence of anitferromagnetism and superconductivity.

The effective Hamiltonian (4.17) with the Dzyaloshinskii-Moriya type of interaction needs a further detailed analysis, because it may introduce a noncollinearity of the spins in the magnetic heavy-fermion state. This subject will not be treated any further in the present Thesis.

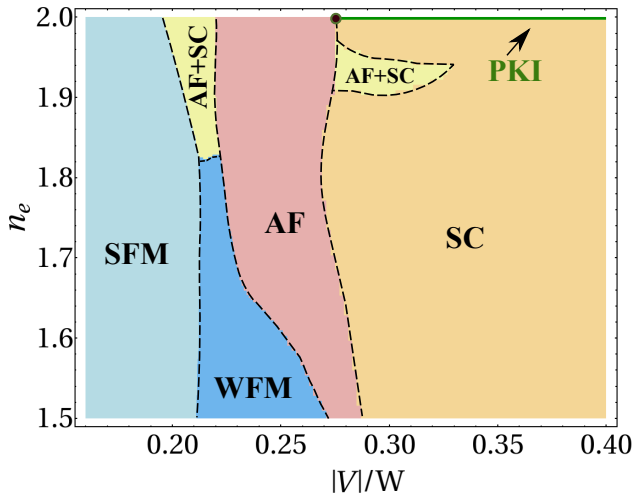

Figure 4.8.: Phase diagram obtained using Anderson-Kondo lattice model (4.17). It contains magnetic and superconducting phases on the plane: hybridization ($|V|$) – number of electrons per site ($n_e = n^c + n^f$) in the case with interatomic hybridization of extended s-wave form and anisotropic superconducting gap of d-wave type. W is the c-band width $W = 2z|t|$, z – number of nearest neighbors, t – nearest neighbors hopping integral for c-electrons. Symbols: WFM, SFM – weak and strong ferromagnetic phases, respectively; AF – antiferromagnetic metal; PKI – paramagnetic Kondo insulator; SC – d-wave superconducting phase. In the phase diagram two regimes of coexistence of antiferromagnetism and superconductivity (AF+SC) occur. Figure taken from [60].

4.4. Results for the orbitally degenerate Anderson lattice model

We now sketch the situation in the analogous case for an orbitally degenerate Anderson lattice model and present briefly the results.

4.4.1. Site-projection operators

Since we would like to apply the canonical perturbation expansion to the orbitally degenerate Anderson lattice model (2.2) up to the second order of expansion, a proper construction of the projection operators $\hat{\mathcal{P}}_0$ and $\hat{\mathcal{P}}_1$ is needed. Incorporation of the degeneracy in the system requires that somehow possible double f-electron occupancies must be distinguishable, because they have different energies, as shown schematically in Figure 4.9. Therefore, site-projection operators are introduced, which act on individual site i. As in Chapters 2 and 3, the double degeneracy is labelled by index $l = 1, 2$, so that the number of f-electrons on i-th site is $\nu \in \{0, 1, 2, 3, 4\}$. The site-projection operator $\hat{P}^{\nu}_{i\mu}$ is introduced similarly to [91, 92]. The index μ corresponds to the configuration of f-electrons. All possible configurations of the single-site f-electron Hamiltonian $\hat{\mathcal{H}}^f$ (2.5) are discussed in Appendix A. For an empty site, $\nu = 0$

$$\hat{P}^0_{i0} = \prod_{l\sigma} \left(1 - \hat{n}^f_{il\sigma}\right) = \left(1 - \hat{n}^f_{i1\uparrow}\right)\left(1 - \hat{n}^f_{i1\downarrow}\right)\left(1 - \hat{n}^f_{i2\uparrow}\right)\left(1 - \hat{n}^f_{i2\downarrow}\right). \tag{4.24}$$

For one electron on i-th site, $\nu = 1$

$$\hat{P}^1_{i1} = \sum_{l\sigma} \hat{n}^f_{il\sigma}\left(1 - \hat{n}^f_{il\bar{\sigma}}\right)\left(1 - \hat{n}^f_{il'\uparrow}\right)\left(1 - \hat{n}^f_{il'\downarrow}\right), \tag{4.25}$$

where l' denotes orbital other than l. The most complex part is for two electrons on i-th site ($\nu = 2$), then there are 6 possible states: 3 singlets (s, $+$, $-$) and the triplet (t) as described in Appendix A. Site-projection operators are defined as

$$\hat{P}^2_{it} = \frac{3}{4}\sum_{\sigma,\sigma'} \hat{n}^f_{i1\sigma}\hat{n}^f_{i2\sigma'}\left(1 - \hat{n}^f_{i1\bar{\sigma}}\right)\left(1 - \hat{n}^f_{i2\bar{\sigma}'}\right) + \hat{\mathbf{S}}^f_{i1}\cdot\hat{\mathbf{S}}^f_{i2}, \tag{4.26}$$

$$\hat{P}^2_{is} = \frac{1}{4}\sum_{\sigma,\sigma'} \hat{n}^f_{i1\sigma}\hat{n}^f_{i2\sigma'}\left(1 - \hat{n}^f_{i1\bar{\sigma}}\right)\left(1 - \hat{n}^f_{i2\bar{\sigma}'}\right) - \hat{\mathbf{S}}^f_{i1}\cdot\hat{\mathbf{S}}^f_{i2}, \tag{4.27}$$

$$\hat{P}^2_{i\pm} = \frac{1}{2}\sum_{l} \left(\hat{n}^f_{il\uparrow}\hat{n}^f_{il\downarrow}\left(1 - \hat{n}^f_{il'\uparrow}\right)\left(1 - \hat{n}^f_{il'\downarrow}\right) \pm \hat{f}^{\dagger}_{il\uparrow}\hat{f}^{\dagger}_{il\downarrow}\hat{f}_{il'\uparrow}\hat{f}_{il'\downarrow}\right). \tag{4.28}$$

For three electrons on i-th site

$$\hat{P}^3_{i1} = \sum_{l\sigma} \hat{n}^f_{il\uparrow}\hat{n}^f_{il\downarrow}\hat{n}^f_{il'\sigma}\left(1 - \hat{n}^f_{il'\bar{\sigma}}\right). \tag{4.29}$$

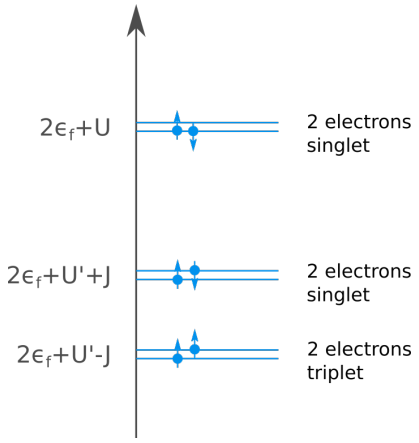

Figure 4.9.: Eigenvalues of single-site f-electron Hamiltonian $\hat{\mathcal{H}}^f$ for site occupied by two electron ($n^f = 2$).

The fully occupied site, $\nu = 4$

$$\hat{P}^4_{i1} = \prod_{l\sigma} \hat{n}^f_{il\sigma} = \hat{n}^f_{i1\uparrow}\hat{n}^f_{i1\downarrow}\hat{n}^f_{i2\uparrow}\hat{n}^f_{i2\downarrow}. \tag{4.30}$$

The site-projection operators have following properties

$$\sum_{\mu\nu} \hat{P}^\nu_{i\mu} = 1 \qquad \text{and} \qquad \hat{P}^\nu_{i\mu}\hat{P}^{\nu'}_{i\mu'} = \delta_{\mu\mu'}\delta_{\nu\nu'}\hat{P}^\nu_{i\mu}. \tag{4.31}$$

One can check the action of site-projection operators, e.g.,

$$\hat{P}^2_{it}\hat{f}^\dagger_{i1\uparrow}\hat{f}^\dagger_{i2\uparrow}\left|\phi\right\rangle = \hat{f}^\dagger_{i1\uparrow}\hat{f}^\dagger_{i2\uparrow}\left|\phi\right\rangle, \tag{4.32}$$

$$\hat{P}^2_{it}\left(\hat{f}^\dagger_{i1\uparrow}\hat{f}^\dagger_{i2\downarrow} - \hat{f}^\dagger_{i1\downarrow}\hat{f}^\dagger_{i2\uparrow}\right)\left|\phi\right\rangle = 0, \tag{4.33}$$

$$\hat{P}^2_{it}\hat{f}^\dagger_{i1\uparrow}\left|\phi\right\rangle = 0, \tag{4.34}$$

where $|\phi\rangle$ is the vacuum state. Let us denote part of the hybridization term connected with a creation or annihilation of f-electron on the i-th site

$$\hat{\mathcal{H}}^{cf}_i = \sum_{jl\sigma} V_{ij}\hat{f}^\dagger_{il\sigma}\hat{c}_{jl\sigma}, \tag{4.35}$$

$$\left(\hat{\mathcal{H}}^{cf}_i\right)^\dagger = \sum_{jl\sigma} V^*_{ij}\hat{c}^\dagger_{jl\sigma}\hat{f}_{il\sigma}. \tag{4.36}$$

Using properties of single-site projection operators given by (4.31), we can divide the hybridization term $\hat{\mathcal{H}}^{cf}$ (2.4) in processes, which include all possible configurations

$$\hat{\mathcal{H}}^{cf} = \sum_i \left(\hat{\mathcal{H}}_i^{cf} + \left(\hat{\mathcal{H}}_i^{cf} \right)^\dagger \right) = \sum_i \left[\left(\sum_{\mu\nu} \hat{P}_{i\mu}^{\nu} \right) \left(\hat{\mathcal{H}}_i^{cf} + \left(\hat{\mathcal{H}}_i^{cf} \right)^\dagger \right) \left(\sum_{\mu\nu} \hat{P}_{i\mu}^{\nu} \right) \right] \quad (4.37)$$

$$= \sum_i \Big(\hat{P}_{i1}^1 \hat{\mathcal{H}}_i^{cf} \hat{P}_{i0}^0 + \hat{P}_{it}^2 \hat{\mathcal{H}}_i^{cf} \hat{P}_{i1}^1 + \hat{P}_{is}^2 \hat{\mathcal{H}}_i^{cf} \hat{P}_{i1}^1 + \hat{P}_{i+}^2 \hat{\mathcal{H}}_i^{cf} \hat{P}_{i1}^1 + \hat{P}_{i-}^2 \hat{\mathcal{H}}_i^{cf} \hat{P}_{i1}^1 \quad (4.38)$$

$$+ \hat{P}_{i1}^3 \hat{\mathcal{H}}_i^{cf} \hat{P}_{it}^2 + \hat{P}_{i1}^3 \hat{\mathcal{H}}_i^{cf} \hat{P}_{is}^2 + \hat{P}_{i1}^3 \hat{\mathcal{H}}_i^{cf} \hat{P}_{i+}^2 + \hat{P}_{i1}^3 \hat{\mathcal{H}}_i^{cf} \hat{P}_{i-}^2 + \hat{P}_{i1}^4 \hat{\mathcal{H}}_i^{cf} \hat{P}_{i1}^3 + H.c. \Big) .$$

We are going to treat only the part $\hat{\mathcal{H}}_1$ of $\hat{\mathcal{H}}^{cf}$ as a perturbation within the canonical perturbation expansion. Also, the remaining part of hybridization term $\hat{\mathcal{H}}^{cf}$ enters into the unperturbed Hamiltonian $\hat{\mathcal{H}}_0$. The Hamiltonian $\hat{\mathcal{H}}_1$ will be presented after discussion of possible processes that can occur in the second order of the expansion in two separate cases: $0 < n^f \leqslant 1$ and $1 < n^f \leqslant 2$.

Since the canonical perturbation expansion for the orbitally degenerate Anderson lattice model is obtained up to the second order, only the projection operators $\hat{\mathcal{P}}_0$, $\hat{\mathcal{P}}_1$ will matter. Another point is to define exact forms of projection operators $\hat{\mathcal{P}}_0$, $\hat{\mathcal{P}}_1$, by means of which our Hamiltonian (2.2) can be divided into two parts $\hat{\mathcal{H}}_0$ and $\hat{\mathcal{H}}_1$ as defined in the Section 4.2.

First, we need to discuss, which part of the hybridization causes virtual processes and which will stay as a residual hybridization. In Table 4.1 we draw all possibilities of processes for f-electron occupancy $n^f \leqslant 2$:

We have to take into account two different cases:

1. $0 < n^f \leqslant 1$
2. $1 < n^f \leqslant 2$

for each of the two cases the projection operators $\hat{\mathcal{P}}_0$, $\hat{\mathcal{P}}_1$, and hence the effective Hamiltonian, will have a different form, as discussed next.

4.4.2. Results for the case: $0 < n^f \leqslant 1$

Only the processes numbered as 1, 2, and 3 in Table 4.1 are possible, if n^f occupancy is less or equal than 1. Since a creation of single f-electron does not lead to double occupancy appearance (process no. 1 in Table 4.1) and $\Delta E = \epsilon^f$ is small, it must not be transformed out. In result, this type of process remains in the effective Hamiltonian as a residual hybridization term. Creation of triple f-electron occupancy (process no. 4 in Table 4.1) is not possible, because in the ground state sites are unoccupied or occupied by one f-electron and we do not include in our calculations a pair-hopping term. Only processes with double-occupancy occurrence are taken into account. However, they might have different energies depending on the f-electron configuration, as it is described in Appendix A and depicted in Figure 4.9. As the process is $\sim 1/\Delta E$, the largest contribution has the process with the smallest energy difference, i.e., with the triplet intermediate state.

Table 4.1.: Virtual processes appearing in the second order of CPE expansion (see main text).

No.	Figure	Math	Description
1	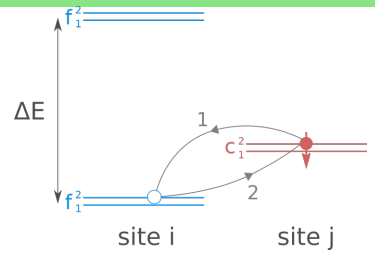	1: $\hat{P}^1_{i1}\hat{\mathcal{H}}^{cf}_i\hat{P}^0_{i0}$ 2: $\hat{P}^0_{i0}\left(\hat{\mathcal{H}}^{cf}_i\right)^\dagger\hat{P}^1_{i1}$ $=\left(\hat{P}^1_{i1}\hat{\mathcal{H}}^{cf}_i\hat{P}^0_{i0}\right)^\dagger$	Starting configuration: empty site, no double occupancies, $\Delta E=\epsilon^f$, therefore it should not be treated as a virtual process.
2	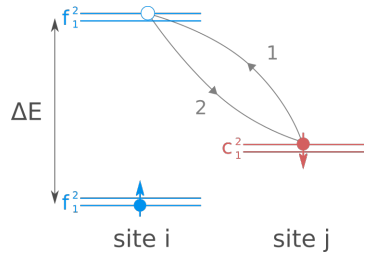	1: $\hat{P}^2_{i\mu}\hat{\mathcal{H}}^{cf}_i\hat{P}^1_{i1}$, where $\mu=s,t$; 2: $\hat{P}^1_{i1}\left(\hat{\mathcal{H}}^{cf}_i\right)^\dagger\hat{P}^2_{i\mu}$	Starting configuration: 1 f-electron on i-th site, double occupancy in intermediate state $\Delta E=\{\epsilon^f+U'-J,\epsilon^f+U'+J\}$ for interorbital triplet and singlet configurations, respectively
3	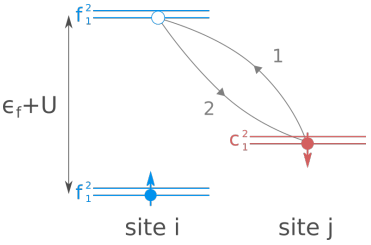	1: $\hat{P}^2_{i\mu}\hat{\mathcal{H}}^{cf}_i\hat{P}^1_{i1}$, where $\mu=+,-$; 2: $\hat{P}^1_{i1}\left(\hat{\mathcal{H}}^{cf}_i\right)^\dagger\hat{P}^2_{i\mu}$	Starting configuration: 1 f-electron on i-th site, double occupancy in intermediate state: intraorbital singlet
4	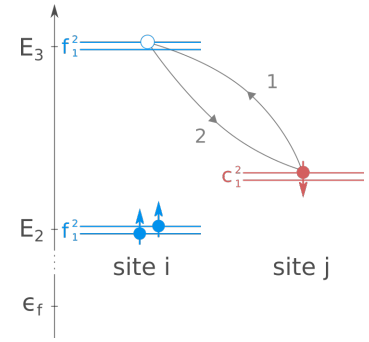	1: $\hat{P}^3_{i1}\hat{\mathcal{H}}^{cf}_i\hat{P}^2_{i\mu}$, where $\mu=s,t,+,-$; 2: $\hat{P}^2_{i\mu}\left(\hat{\mathcal{H}}^{cf}_i\right)^\dagger\hat{P}^3_{i1}$	Starting configuration: 2 f-electron on i-th site, $E_2=\{2\epsilon^f+U'-J,2\epsilon^f+U'+J,2\epsilon^f+U\}$, $E_3=3\epsilon^f+U+2U'-J$, 3 electrons on i-th site in intermediate state

For example, taking $J/U = 0.25$ and recalling that we assume that $U' = U - 2J$, the energy difference is

$$\Delta E = \begin{cases} \epsilon^f + \frac{1}{4}U & \text{for triplet,} \\ \epsilon^f + \frac{3}{4}U & \text{for interorbital singlet,} \\ \epsilon^f + U & \text{for intraoribtal singlet.} \end{cases} \tag{4.39}$$

From above considerations, the perturbation part is

$$\hat{\mathcal{H}}_1 = \sum_i \left(\hat{P}^2_{it} \hat{\mathcal{H}}^{cf}_i \hat{P}^1_{i1} + H.c. \right). \tag{4.40}$$

Analogously to the orbitally non-degenerate case projection operators: $\hat{\mathcal{P}}_0$ and $\hat{\mathcal{P}}_1$ are defined as

$$\hat{\mathcal{P}}_0 = \prod_i \left(\hat{P}^0_{i0} + \hat{P}^1_{i1} \right), \tag{4.41}$$

$$\hat{\mathcal{P}}_1 = \sum_j \left[\hat{P}^2_{jt} \prod_{i \neq j} \left(\hat{P}^0_{i0} + \hat{P}^1_{i1} \right) \right]. \tag{4.42}$$

The projection operator $\hat{\mathcal{P}}_0$ ensures us that there are no double occupancies in the f-system. Empty or single-occupied sites are the only possibilities. The operator $\hat{\mathcal{P}}_1$ creates one double occupancy in the triplet state, which leads to virtual process. With the definitions (4.41)-(4.42) the effective Hamiltonian can be obtained by straightforward, but cumbersome manner. The results are:

- **In the first order of expansion:**

$$\hat{\mathcal{H}}_0 = \hat{\mathcal{P}}_0 \hat{\mathcal{H}} \hat{\mathcal{P}}_0 = \prod_i \left(\hat{P}^0_{i0} + \hat{P}^1_{i1} \right) \left(\hat{\mathcal{H}}^c + \hat{\mathcal{H}}^f + \hat{\mathcal{H}}^{cf} \right) \prod_j \left(\hat{P}^0_{j0} + \hat{P}^1_{j1} \right) \tag{4.43}$$

$$= \sum_{\langle i,j \rangle l\sigma} t_{ij} \hat{c}^\dagger_{il\sigma} \hat{c}_{jl\sigma} + \epsilon^f \sum_{il\sigma} \hat{P}^1_{i1} \hat{n}^f_{il\sigma} \hat{P}^1_{i1} + \sum_{ijl\sigma} \left(V_{ij} \hat{P}^1_{i1} \hat{f}^\dagger_{il\sigma} \hat{P}^0_{i0} \hat{c}_{jl\sigma} + H.c. \right) \tag{4.44}$$

- **In the second order of expansion** for the triplet in the intermediate state: $\Delta E = \epsilon^f + U' - J$.

$$\hat{\mathcal{P}}_1 \hat{\mathcal{H}}_1 \hat{\mathcal{P}}_0 = \sum_j \left(\hat{P}^2_{jt} \prod_{i \neq j} \left(\hat{P}^0_{i0} + \hat{P}^1_{i1} \right) \left(\sum_m \hat{P}^2_{mt} \hat{\mathcal{H}}^{cf}_m \hat{P}^1_{m1} \right) \prod_{\mathbf{i}'} \left(\hat{P}^0_{\mathbf{i}'0} + \hat{P}^1_{\mathbf{i}'1} \right) \right) \tag{4.45}$$

$$= \sum_j \hat{P}^2_{jt} \hat{\mathcal{H}}^{cf}_j \hat{P}^1_{j1} \prod_{i \neq j} \left(\hat{P}^0_{i0} + \hat{P}^1_{i1} \right), \tag{4.46}$$

$$\hat{\mathcal{P}}_0 \hat{\mathcal{H}}_1 \hat{\mathcal{P}}_1 \hat{\mathcal{H}}_1 \hat{\mathcal{P}}_0 = \sum_j \hat{P}^1_{j1} \left(\hat{\mathcal{H}}^{cf}_j \right)^\dagger \hat{P}^2_{jt} \hat{\mathcal{H}}^{cf}_j \hat{P}^1_{j1} \prod_{i \neq j} \left(\hat{P}^0_{i0} + \hat{P}^1_{i1} \right). \tag{4.47}$$

Next, our goal is to obtain the explicit form of the expression $\sum_{ll'\sigma\sigma'} \hat{P}^1_{i1}\hat{c}^\dagger_{jl\sigma}\hat{f}_{il\sigma}\hat{P}^2_{it}\hat{f}^\dagger_{il'\sigma'}\hat{c}_{jl'\sigma'}\hat{P}^1_{i1}$, using the fermionic anticommutation relations. The algebraic calculations were done in *Mathematica with SNEG package* [95]. Due to complexity of the problem, our consideration are restricted only to the case of two-site processes. Inclusion of the three-site processes requires a further analysis, which will not be performed here.

- **Analytical results:** Using (4.10), we obtain the effective Hamiltonian in the second order of the expansion, taking into account only the two-site processes. It has the following form

$$\begin{aligned}\hat{\mathcal{H}}_{\text{eff}} = &\sum_{ijl\sigma} t_{ij}\hat{c}^\dagger_{il\sigma}\hat{c}_{jl\sigma} + \epsilon^f \sum_{il\sigma}\hat{P}^1_{i1}\hat{n}^f_{il\sigma}\hat{P}^1_{i1} + \sum_{ijl\sigma}\left(V_{ij}\hat{P}^1_{i1}\hat{f}^\dagger_{il\sigma}\hat{P}^0_{i0}\hat{c}_{jl\sigma} + H.c.\right) \\ &+ \frac{1}{\epsilon^f + U' - J}\sum_{ij}|V_{ij}|^2 \times \sum_m\left(\left(\hat{a}^{cf}_{ij12m}\right)^\dagger \hat{a}^{cf}_{ij21m} + \left(\hat{a}^{cf}_{ij21m}\right)^\dagger \hat{a}^{cf}_{ij12m}\right) \\ &- \frac{1}{\epsilon^f + U' - J}\sum_{ij}|V_{ij}|^2\Bigg(\left(\hat{\mathbf{T}}^c_{j\downarrow}\cdot\hat{\mathbf{T}}^f_{i\uparrow} - \frac{1}{4}\hat{n}^c_{j\downarrow}\hat{\pi}^f_{i\uparrow}\right)\left(1-\hat{n}^f_{i1\downarrow}\right)\left(1-\hat{n}^f_{i2\downarrow}\right) \\ &+ \left(\hat{\mathbf{T}}^c_{j\uparrow}\cdot\hat{\mathbf{T}}^f_{i\downarrow} - \frac{1}{4}\hat{n}^c_{j\uparrow}\hat{\pi}^f_{i\downarrow}\right)\left(1-\hat{n}^f_{i1\uparrow}\right)\left(1-\hat{n}^f_{i2\uparrow}\right) \\ &+ \hat{n}^c_{j2}\hat{\nu}^f_{i1}\left(1-\hat{n}^f_{i2\uparrow}\right)\left(1-\hat{n}^f_{i2\downarrow}\right) + \hat{n}^c_{j1}\hat{\nu}^f_{i2}\left(1-\hat{n}^f_{i1\uparrow}\right)\left(1-\hat{n}^f_{i1\downarrow}\right)\Bigg),\end{aligned} \tag{4.48}$$

where $\hat{\mathbf{T}}^f_{i\sigma}$ is the orbital ordering operator for f-electrons $\hat{\mathbf{T}}^f_{i\sigma} \equiv \left(\left(\hat{\mathbf{T}}^f_{i\sigma}\right)^+, \left(\hat{\mathbf{T}}^f_{i\sigma}\right)^-, \left(\hat{\mathbf{T}}^f_{i\sigma}\right)^z\right)$:

$$\left(\hat{\mathbf{T}}^f_{i\sigma}\right)^+ = \hat{f}^\dagger_{i1\sigma}\hat{f}_{i2\sigma}, \tag{4.49}$$

$$\left(\hat{\mathbf{T}}^f_{i\sigma}\right)^- = \hat{f}^\dagger_{i2\sigma}\hat{f}_{i1\sigma}, \tag{4.50}$$

$$\left(\hat{\mathbf{T}}^f_{i\sigma}\right)^z = \frac{1}{2}\left(\hat{n}^f_{i1\sigma} - \hat{n}^f_{i2\sigma}\right). \tag{4.51}$$

The orbital ordering operators for c-electrons $\hat{\mathbf{T}}^c_{j\sigma}$ are defined similarly. Projected number operators for f-electrons are

$$\hat{\pi}^f_{il\sigma} = \hat{n}^f_{il\sigma}\left(1-\hat{n}^f_{il'\sigma}\right), \tag{4.52}$$

$$\hat{\pi}^f_{i\sigma} = \hat{\pi}^f_{i1\sigma} + \hat{\pi}^f_{i2\sigma}, \tag{4.53}$$

$$\hat{\nu}^f_{il\sigma} = \hat{n}^f_{il\sigma}\left(1-\hat{n}^f_{il\bar{\sigma}}\right), \tag{4.54}$$

$$\hat{\nu}^f_{il} = \hat{\nu}^f_{il\uparrow} + \hat{\nu}^f_{il\downarrow}. \tag{4.55}$$

The projected hybrid (f-c) spin-triplet pairing operators are

$$\left(\hat{a}^{cf}_{ij12m}\right)^{\dagger} = \begin{cases} \hat{f}^{\dagger}_{i1\uparrow}\hat{P}^{0}_{i0}\hat{c}^{\dagger}_{i2\uparrow} & \text{for } m=1, \\ \frac{1}{\sqrt{2}}\left(\hat{f}^{\dagger}_{i1\uparrow}\hat{P}^{0}_{i0}\hat{c}^{\dagger}_{i2\downarrow} + \hat{f}^{\dagger}_{i1\downarrow}\hat{P}^{0}_{i0}\hat{c}^{\dagger}_{i2\uparrow}\right) & \text{for } m=0, \\ \hat{f}^{\dagger}_{i1\downarrow}\hat{P}^{0}_{i0}\hat{c}^{\dagger}_{i2\downarrow} & \text{for } m=-1. \end{cases} \tag{4.56}$$

The first term in the effective Hamiltonian (4.48) is the unchanged hopping term of c-electrons, the second is the projected atomic energy of f-electrons, the third is the residual hybridization (processes no. 1 in Table 4.1, which include the smallest energy difference, therefore we cannot treat it as perturbation). Then, we have also the consecutive corrections in the second order: the hybrid f-c triplet pairing ($\left(\hat{a}^{cf}_{ij12m}\right)^{\dagger}$) and orbital ordering $\hat{T}^{c}_{j\sigma}\cdot\hat{T}^{f}_{i\tilde{\sigma}}$. Note that the hybrid pairing operator $\left(\hat{a}^{cf}_{ij12m}\right)^{\dagger}$ pairs electrons f and c from different sites (indexes i, j) and different orbitals (indexes 1, 2). The last term expresses the Coulomb attraction among the two electron subsystems and may also contribute to pairing. However, these processes are of the second order and can be neglected, since we have already neglected direct f-c Coulomb repulsion (the Falicov-Kimball term).

The form of the effective Hamiltonian is quite complicated. It describes hybridized itinerant quasiparticles with renormalized (residual) hybridization in a multiorbital situation. Furthermore, it includes the attractive interorbital interaction, here represented as favoring orbital ordering augmented by the interorbital f-c spin-triplet pairing under proper conditions. No further analytical or numerical analysis of this very complicated effective Hamiltonian will be undertaken here.

4.4.3. Results for the case: $1 < n^f \leqslant 2$

Once again, an explicit construction of $\hat{\mathcal{P}}_0$ and $\hat{\mathcal{P}}_1$ is required. All the processes presented in Table 4.1 are possible now, however the new perturbation term is only the last one, i.e.,

$$\hat{\mathcal{H}}_1 = \sum_i \left(\hat{P}^{3}_{i1}\hat{\mathcal{H}}^{cf}_{i}\hat{P}^{2}_{it} + H.c.\right). \tag{4.57}$$

In this case we always have double occupancies in the system (because $n^f > 1$). Let us define projection operator $\hat{\mathcal{P}}_0$ with the lowest possible number of double f-occupancies present in the system and $\hat{\mathcal{P}}_1$:

$$\hat{\mathcal{P}}_0 = \prod_i \left(\hat{P}^{1}_{i1} + \hat{P}^{2}_{it}\right), \tag{4.58}$$

$$\hat{\mathcal{P}}_1 = \sum_j \left[\hat{P}^{3}_{j1}\prod_{i\neq j}\left(\hat{P}^{1}_{i1} + \hat{P}^{2}_{it}\right)\right]. \tag{4.59}$$

The projection operator $\hat{\mathcal{P}}_0$ ensures, that in the system there are either single or doubly occupied sites. If two f-electrons occupy single site, they are in triplet state. The operator $\hat{\mathcal{P}}_1$ creates one triply occupied site out of triplet state, which leads to virtual process. Once again, the effective Hamiltonian is obtained by means of $\hat{\mathcal{P}}_0$ and $\hat{\mathcal{P}}_1$ definitions (4.58)-(4.59).

- **In the first order of expansion** for $1 < n^f \leqslant 2$ we obtain thus

$$\begin{aligned}\hat{\mathcal{H}}_0 = \hat{\mathcal{P}}_0\hat{\mathcal{H}}\hat{\mathcal{P}}_0 &= \prod_i \left(\hat{P}^1_{i1} + \hat{P}^2_{it}\right)\left(\hat{\mathcal{H}}^c + \hat{\mathcal{H}}^f + \hat{\mathcal{H}}^{cf}\right)\prod_j \left(\hat{P}^1_{j1} + \hat{P}^2_{jt}\right) \\ &= \sum_{ijl\sigma} t_{ij}\hat{c}^\dagger_{il\sigma}\hat{c}_{jl\sigma} + \epsilon^f \sum_{il\sigma}\left(\hat{P}^1_{i1}\hat{n}^f_{il\sigma}\hat{P}^1_{i1} + \hat{P}^2_{it}\hat{n}^f_{il\sigma}\hat{P}^2_{it}\right) \\ &\quad + \sum_{ijl\sigma}\left(V_{ij}\hat{P}^2_{it}\hat{f}^\dagger_{il\sigma}\hat{P}^1_{i1}\hat{c}_{jl\sigma} + H.c.\right) \\ &\quad + U'\sum_i \hat{P}^2_{it}\hat{n}^f_{i1}\hat{n}^f_{i2}\hat{P}^2_{it} - 2J\sum_i \hat{P}^2_{it}\left(\hat{\mathbf{S}}^f_{i1}\cdot\hat{\mathbf{S}}^f_{i2} + \frac{1}{4}\hat{n}^f_{i1}\hat{n}^f_{i2}\right)\hat{P}^2_{it}.\end{aligned} \tag{4.60}$$

- **In the second order of expansion** for $1 < n^f \leqslant 2$ and $\Delta E = \epsilon^f + U + U'$ we have

$$\begin{aligned}\hat{\mathcal{P}}_1\hat{\mathcal{H}}_1\hat{\mathcal{P}}_0 &= \sum_j\left(\hat{P}^3_{j1}\prod_{i\neq j}\left(\hat{P}^1_{i1} + \hat{P}^2_{it}\right)\left(\sum_m \hat{P}^3_{m1}\hat{\mathcal{H}}^{cf}_m\hat{P}^2_{mt}\right)\prod_{i'}\left(\hat{P}^1_{i'1} + \hat{P}^2_{i't}\right)\right) \\ &= \sum_j \hat{P}^3_{j1}\hat{\mathcal{H}}^{cf}_j\hat{P}^2_{jt}\prod_{i\neq j}\left(\hat{P}^1_{i1} + \hat{P}^2_{it}\right),\end{aligned} \tag{4.61}$$

$$\hat{\mathcal{P}}_0\hat{\mathcal{H}}_1\hat{\mathcal{P}}_1\hat{\mathcal{H}}_1\hat{\mathcal{P}}_0 = \sum_j \hat{P}^2_{jt}\left(\hat{\mathcal{H}}^{cf}_j\right)^\dagger\hat{P}^3_{j1}\hat{\mathcal{H}}^{cf}_j\hat{P}^2_{jt}\prod_{i\neq j}\left(\hat{P}^1_{i1} + \hat{P}^2_{it}\right). \tag{4.62}$$

- **Analytical results:** Now the term $\sum_{ll'\sigma\sigma'}\hat{P}^2_{it}\hat{c}^\dagger_{jl\sigma}\hat{f}_{il\sigma}\hat{P}^3_{i1}\hat{f}^\dagger_{il'\sigma'}\hat{c}_{jl'\sigma'}\hat{P}^2_{it}$ is evaluated. As in the case $0 < n^f \leqslant 1$, the calculations were performed using *Mathematica with SNEG package* [95]. Using (4.10) and the definition of pairing

operators we obtain the effective Hamiltonian in the form

$$\begin{aligned}\hat{\mathcal{H}}_{\text{eff}} = &\sum_{ijl\sigma} t_{ij}\hat{c}^{\dagger}_{il\sigma}\hat{c}_{jl\sigma} + \epsilon^f \sum_{il\sigma} \hat{n}^f_{il\sigma}\left(1-\hat{n}^f_{il\bar{\sigma}}\right)\left(1-\hat{n}^f_{il'\uparrow}\right)\left(1-\hat{n}^f_{il'\downarrow}\right) \\ &+ \sum_{ijl\sigma}\left(V_{ij}\left(\sum_m \hat{A}^{\dagger}_{im}\hat{A}_{im}\right)\hat{f}^{\dagger}_{il\sigma}\hat{c}_{jl\sigma} + H.c.\right) \\ &+ \left(2\epsilon^f + U' - J\right)\sum_{im}\hat{A}^{\dagger}_{im}\hat{A}_{im} \\ &+ \sum_{ij}\frac{1}{2}\frac{|V_{ij}|^2}{\epsilon^f + U + U'}\left(\hat{n}^c_{j1} + \hat{n}^c_{j2}\right)\hat{B}^{\dagger}_i\hat{B}_i \\ &- \sum_{ij}\frac{|V_{ij}|^2}{\epsilon^f + U + U'}\hat{\nu}^f_{i1}\left(\hat{b}^{\dagger}_{ij22}\hat{b}_{ij22} + \hat{b}^{\dagger}_{ij21}\hat{b}_{ij21}\right) \\ &- \sum_{ij}\frac{|V_{ij}|^2}{\epsilon^f + U + U'}\hat{\nu}^f_{i2}\left(\hat{b}^{\dagger}_{ij12}\hat{b}_{ij12} + \hat{b}^{\dagger}_{ij11}\hat{b}_{ij11}\right),\end{aligned} \tag{4.63}$$

where the projected pairing operators now have the following form

$$\hat{A}^{\dagger}_{im} = \begin{cases} \hat{f}^{\dagger}_{i1\uparrow}\left(1-\hat{n}^f_{i1\downarrow}\right)\hat{f}^{\dagger}_{i2\uparrow}\left(1-\hat{n}^f_{i2\downarrow}\right) & m=1 \\ \frac{1}{\sqrt{2}}\sum_{\sigma}\hat{f}^{\dagger}_{i1\sigma}\left(1-\hat{n}^f_{i1\bar{\sigma}}\right)\hat{f}^{\dagger}_{i2\bar{\sigma}}\left(1-\hat{n}^f_{i2\sigma}\right) & m=0 \\ \hat{f}^{\dagger}_{i1\downarrow}\left(1-\hat{n}^f_{i1\uparrow}\right)\hat{f}^{\dagger}_{i2\downarrow}\left(1-\hat{n}^f_{i2\uparrow}\right) & m=-1 \end{cases} \tag{4.64}$$

$$\begin{aligned}\hat{B}^{\dagger}_i = \frac{1}{\sqrt{2}}&\left(\hat{f}^{\dagger}_{i1\uparrow}\left(1-\hat{n}^f_{i1\downarrow}\right)\hat{f}^{\dagger}_{i2\downarrow}\left(1-\hat{n}^f_{i2\uparrow}\right)\right. \\ &\left.-\hat{f}^{\dagger}_{i1\downarrow}\left(1-\hat{n}^f_{i1\uparrow}\right)\hat{f}^{\dagger}_{i2\uparrow}\left(1-\hat{n}^f_{i2\downarrow}\right)\right),\end{aligned} \tag{4.65}$$

$$\hat{b}^{\dagger}_{ijl_1l_2} = \frac{1}{\sqrt{2}}\left(\hat{f}^{\dagger}_{il_1\uparrow}\left(1-\hat{n}^f_{il_1\downarrow}\right)\hat{c}^{\dagger}_{jl_2\downarrow} - \hat{f}^{\dagger}_{il_1\downarrow}\left(1-\hat{n}^f_{il_1\uparrow}\right)\hat{c}^{\dagger}_{jl_2\uparrow}\right). \tag{4.66}$$

The most important in the effective Hamiltonian (4.63) is the two last terms, which introduces the spin-singlet hybrid f-c pairing, lowering the energy of the system. Therefore, one can expect a transformation for the spin-triplet to the spin-singlet pairing in the regime $1 < n^f \leqslant 2$, before Kondo insulating state may be achieved. This however, should be analyzed in detail separately.

4.5. Summary of results

In this Chapter we have discussed the canonical perturbation expansion (CPE) for the Anderson lattice models: in the non-degenerate and in the orbitally degenerate cases. The effective Hamiltonians were obtained and described. The most important results are

1. In the non-degenerate Anderson lattice model: the effective Hamiltonian contains Kondo f-c and f-f superexchange interactions, as well as the antisymmet-

ric exchange between f-electrons appearing only if the c-electrons are present, i.e., Dzyaloshinkii-Moriya type of interaction.

2. In the orbitally degenerate Anderson lattice model, for $n^f \leqslant 1$: the effective Hamiltonian includes the attractive interorbital interaction, leading to orbital ordering.

3. In the orbitally degenerate Anderson lattice model, for $1 < n^f \leqslant 2$: the effective Hamiltonian introduces the spin-singlet hybrid f-c pairing, lowering the energy of the system.

Effective Hamiltonians for the orbitally degenerate Anderson lattice model, obtained in both cases, require further analysis, however it has not been done yet.

5. Summary and conclusions

In this Thesis selected topics of strongly correlated and hybridized electronic states have been raised for the first time.

In the first part we have focused on the problem of theoretical description of UGe_2 compound, representing an example of system with tightly connected and coexistent ferromagnetism and spin-triplet superconductivity. This has been accomplished by using a four-orbital model, i.e., orbitally degenerate Anderson lattice model.

The main results achieved in the first part of the Thesis are:

- construction of the phase diagram for UGe_2 comprising all the observed phases within a single theoretical framework,
- determination of the temperature dependence of the gap parameter in FM1+A_1 phase,
- description of the system behavior in non-zero magnetic field,
- identification of the *Hund's metal limit*, i.e., that correlations complement the pairing part coming from the Hund's rule coupling and that the two contributions are of comparable magnitude.

The principal points that require a future analysis are:

- inclusion of the spin-orbit coupling,
- a proper inclusion of the applied magnetic field, particularly in the superconducting phase,
- incorporation of quantum spin fluctuations in the SGA method.

In the second part, in Chapter 4 we have outlined the situation in the strong-correlation limit by calculating explicitly an effective Hamiltonian up to the fourth order in the non-degenerate Anderson lattice model and to the second order in the degenerate case, with the help of *modified Schrieffer-Wolff transformation* (CPE). We have shown explicitly how the part leading to the renormalized quasiparticle states can be introduced via the presence of residual hybridization part and the spin-triplet pairing part is derived microscopically for the orbitally degenerate situation. The results obtained in the second part (cf. Chapter 4) confirm principal features of the concrete considerations in Chapters 2 and 3. Namely, the decisive role of the Hund's rule in stabilization of the triplet pairing in the case $n^f > 1$. The detailed analysis of the results of Chapter 4 requires an extensive and separate studies. In particular, the transformation of the dominant spin-triplet pairing into its spin-singlet correspondant, as well as the corresponding ferromagnetism $\rightarrow$ antiferromagnetism transition, both with the increasing band filling, would complete the picture.

A. Energies of the single-site f-electron Hamiltonian with addition of the pair-hopping

One-site f-electron Hamiltonian $\hat{\mathcal{H}}^f$

In definition of orbitally degenerate Anderson lattice model the most complex part is the term for f-electrons only (2.5). In this Appendix the energies of one-site $\hat{\mathcal{H}}^f$ are discussed depending on the f electrons occupancy per site $n^f = \sum_{l\sigma}\langle\hat{n}^{\mathrm{f}}_{il\sigma}\rangle$.

The simplest case is an empty site, $n^f = 0$. Vacuum is the eigenstate of Hamiltonian: $|\phi\rangle = |0,0\rangle$ and

$$\frac{\langle\hat{\mathcal{H}}^f\rangle}{\Lambda} = 0. \tag{A.1}$$

Afterwards, if one electron is occupying i-th site, $n^f = 1$, the Hamiltonian has 4 eigenstates: $|\uparrow,0\rangle$, $|\downarrow,0\rangle$, $|0,\uparrow\rangle$, $|0,\downarrow\rangle$. All eigenstates can be written as $|n\rangle = f^\dagger_{il\sigma}|\phi\rangle$, where $n = 1,...,4$ for different l and σ combinations. Eigenvalues of the Hamiltonian are ϵ^f, because one electron does not interact.

$$\frac{\langle\hat{\mathcal{H}}^f\rangle}{\Lambda} = \epsilon^f\mathbb{1}, \tag{A.2}$$

where $\mathbb{1}$ is the identity matrix. Due to the electron-hole symmetry, similar situation is in the case when $n^f = 3$. The Hamiltonian has four possible eigenstates

$$|1\rangle = \hat{f}^\dagger_{i1\uparrow}\hat{f}^\dagger_{i1\downarrow}\hat{f}^\dagger_{i2\uparrow}|\phi\rangle, \tag{A.3}$$
$$|2\rangle = \hat{f}^\dagger_{i1\uparrow}\hat{f}^\dagger_{i1\downarrow}\hat{f}^\dagger_{i2\downarrow}|\phi\rangle, \tag{A.4}$$
$$|3\rangle = \hat{f}^\dagger_{i1\uparrow}\hat{f}^\dagger_{i2\uparrow}\hat{f}^\dagger_{i2\downarrow}|\phi\rangle, \tag{A.5}$$
$$|4\rangle = \hat{f}^\dagger_{i1\downarrow}\hat{f}^\dagger_{i2\uparrow}\hat{f}^\dagger_{i2\downarrow}|\phi\rangle \tag{A.6}$$

and eigenvalues

$$\frac{\langle\hat{\mathcal{H}}^f\rangle}{\Lambda} = \Big(3\epsilon^f + U + 2U' - J\Big)\,\mathbb{1}. \tag{A.7}$$

The fully occupied site $|\uparrow\downarrow,\uparrow\downarrow\rangle$ has energy

$$\frac{\langle\hat{\mathcal{H}}^f\rangle}{\Lambda} = 4\epsilon^f + 2U + 4U' - 2J. \tag{A.8}$$

The most interesting case is when two electrons sit on the same site, $n^f = 2$. In systems there are 6 possible states: $|\uparrow\downarrow,0\rangle$, $|0,\uparrow\downarrow\rangle$, $|\uparrow,\downarrow\rangle$, $|\downarrow,\uparrow\rangle$, $|\uparrow,\uparrow\rangle$, $|\downarrow,\downarrow\rangle$. Eigenstates of Hamiltonian can be constructed as follows

$$|1\rangle = \hat{f}^\dagger_{i1\uparrow}\hat{f}^\dagger_{i2\uparrow}|\phi\rangle, \tag{A.9}$$

$$|2\rangle = \hat{f}^\dagger_{i1\downarrow}\hat{f}^\dagger_{i2\downarrow}|\phi\rangle, \tag{A.10}$$

$$|3\rangle = \frac{1}{\sqrt{2}}\left(\hat{f}^\dagger_{i1\uparrow}\hat{f}^\dagger_{i2\downarrow} + \hat{f}^\dagger_{i1\downarrow}\hat{f}^\dagger_{i2\uparrow}\right)|\phi\rangle, \tag{A.11}$$

$$|4\rangle = \frac{1}{\sqrt{2}}\left(\hat{f}^\dagger_{i1\uparrow}\hat{f}^\dagger_{i2\downarrow} - \hat{f}^\dagger_{i1\downarrow}\hat{f}^\dagger_{i2\uparrow}\right)|\phi\rangle, \tag{A.12}$$

$$|5\rangle = \frac{1}{\sqrt{2}}\left(\hat{f}^\dagger_{i1\uparrow}\hat{f}^\dagger_{i1\downarrow} + \hat{f}^\dagger_{i2\uparrow}\hat{f}^\dagger_{i2\downarrow}\right)|\phi\rangle, \tag{A.13}$$

$$|6\rangle = \frac{1}{\sqrt{2}}\left(\hat{f}^\dagger_{i1\uparrow}\hat{f}^\dagger_{i1\downarrow} - \hat{f}^\dagger_{i2\uparrow}\hat{f}^\dagger_{i2\downarrow}\right)|\phi\rangle. \tag{A.14}$$

Eigenstates $|1\rangle$, $|2\rangle$, $|3\rangle$ are composing triplet, $|4\rangle$ is interorbital singlet, $|5\rangle$ and $|6\rangle$ are intraorbital singlets. Corresponding eigenvalues (energies) of the Hamiltonian:

$$\frac{\langle\hat{\mathcal{H}}^f\rangle}{\Lambda} = 2\epsilon^f\mathbb{1} + \begin{pmatrix} U'-J & 0 & 0 & 0 & 0 & 0 \\ 0 & U'-J & 0 & 0 & 0 & 0 \\ 0 & 0 & U'-J & 0 & 0 & 0 \\ 0 & 0 & 0 & U'+J & 0 & 0 \\ 0 & 0 & 0 & 0 & U & 0 \\ 0 & 0 & 0 & 0 & 0 & U \end{pmatrix} \tag{A.15}$$

From the above considerations follows that triplet has the lowest energy, because of the Hund's coupling J.

Inclusion of the pair-hopping term

We add to the Hamiltonian $\hat{\mathcal{H}}^f$ (2.5) the pair-hopping term:

$$\hat{\mathcal{H}}^f \to \hat{\mathcal{H}}^f + J'\sum_i\left(\hat{f}^\dagger_{i1\uparrow}\hat{f}^\dagger_{i1\downarrow}\hat{f}_{i2\downarrow}\hat{f}_{i2\uparrow} + \hat{f}^\dagger_{i2\uparrow}\hat{f}^\dagger_{i2\downarrow}\hat{f}_{i1\downarrow}\hat{f}_{i1\uparrow}\right) \tag{A.16}$$

Afterwards, intraorbital singlet pairing operators are introduced:

$$\hat{b}^{\dagger}_{i+} = \frac{1}{\sqrt{2}}\left(\hat{f}^{\dagger}_{i1\uparrow}\hat{f}^{\dagger}_{i1\downarrow} + \hat{f}^{\dagger}_{i2\uparrow}\hat{f}^{\dagger}_{i2\downarrow}\right), \tag{A.17}$$

$$\hat{b}^{\dagger}_{i-} = \frac{1}{\sqrt{2}}\left(\hat{f}^{\dagger}_{i1\uparrow}\hat{f}^{\dagger}_{i1\downarrow} - \hat{f}^{\dagger}_{i2\uparrow}\hat{f}^{\dagger}_{i2\downarrow}\right). \tag{A.18}$$

Similarly to identities (2.9) and (2.10) for interorbital triplet- and singlet-pairing operators, one can show that operators $\hat{b}^{\dagger}_{i+}$ and $\hat{b}^{\dagger}_{i-}$ obey following relations

$$\hat{b}^{\dagger}_{i+}\hat{b}_{i+} + \hat{b}^{\dagger}_{i-}\hat{b}_{i-} \equiv \hat{n}^{f}_{il\uparrow}\hat{n}^{f}_{il\downarrow}, \tag{A.19}$$

$$\hat{b}^{\dagger}_{i+}\hat{b}_{i+} - \hat{b}^{\dagger}_{i-}\hat{b}_{i-} \equiv \hat{f}^{\dagger}_{i1\uparrow}\hat{f}^{\dagger}_{i1\downarrow}\hat{f}_{i2\downarrow}\hat{f}_{i2\uparrow} + \hat{f}^{\dagger}_{i2\uparrow}\hat{f}^{\dagger}_{i2\downarrow}\hat{f}_{i1\downarrow}\hat{f}_{i1\uparrow}. \tag{A.20}$$

Using (A.19) and (A.20) the Hamiltonian $\hat{\mathcal{H}}^{f}$ (2.5) can be re-written as

$$\begin{aligned}\hat{\mathcal{H}}^{f} = \epsilon^{f}\sum_{il\sigma}\hat{n}^{f}_{il\sigma} + (U-J')\sum_{i}\hat{b}^{\dagger}_{i-}\hat{b}_{i-} + (U+J')\sum_{i}\hat{b}^{\dagger}_{i+}\hat{b}_{i+} \\ + (U'+J)\sum_{i}\hat{B}^{\dagger}_{i}\hat{B}_{i} + (U'-J)\sum_{im}\hat{A}^{\dagger}_{im}\hat{A}_{im},\end{aligned} \tag{A.21}$$

where $\hat{A}^{\dagger}_{im}$ and $\hat{B}^{\dagger}_{i}$ are the interorbital triplet- and singlet-pairing operators defined (2.7), (2.8). The addition of pair-hopping term J' affects only energy of intraorbital spin-singlet pairing ($\sim J'\langle\hat{f}^{\dagger}_{i1\uparrow}\hat{f}^{\dagger}_{i1\downarrow}\rangle\langle\hat{f}_{i2\downarrow}\hat{f}_{i2\uparrow}\rangle$). It is additionally suppressed by large and positive value of U.

B. Statistically consistent Gutzwiller approximation – details

Since it is wearisome to follow all calculations in statistically consistent Gutzwiller approximation for degenerate Anderson model in the main text, for sake of completeness they should be presented in this Appendix. Therefore, here we will focus on the details of the approach.

Similarly to (2.21), we obtain the action of Gutzwiller correlator $\hat{P}_{\mathrm{G}}$ on the f-electron number operator $\hat{n}^f_{il\sigma}$:

$$\hat{\mathcal{P}}_{il}\hat{n}^f_{il\sigma}\hat{\mathcal{P}}_{il} = n^f_{l\sigma} + p_\sigma \hat{n}^{f\ \mathrm{HF}}_{il\sigma} + a_\sigma \hat{n}^{f\ \mathrm{HF}}_{il\bar{\sigma}} + \left(\lambda_d^2 - \lambda_\sigma^2\right)\hat{n}^{f\ \mathrm{HF}}_{il\uparrow}\hat{n}^{f\ \mathrm{HF}}_{il\downarrow}, \tag{B.1}$$

where factors p_σ and a_σ are given below. The orbital index l is omitted in factors names (a_σ, p_σ), since it is assumed that orbitals are equivalent and $n^f_{1\sigma} = n^f_{2\sigma}$.

$$p_\sigma = \lambda_\sigma^2 + \left(\lambda_d^2 - \lambda_\sigma^2\right) n^f_{l\bar{\sigma}}, \tag{B.2}$$

$$a_\sigma = \left(\lambda_d^2 - \lambda_\sigma^2\right) n^f_{l\sigma}. \tag{B.3}$$

As a result of (B.1) we get, that the expectation value of the f-electron number operator $\hat{n}^f_{il\sigma}$ calculated in correlated state is the same as in uncorrelated:

$$\langle \hat{n}^f_{il\sigma}\rangle_{\mathrm{G}} = \langle \hat{\mathcal{P}}_{il}\hat{n}^f_{il\sigma}\hat{\mathcal{P}}_{il}\rangle_0 = n^f_{l\sigma}. \tag{B.4}$$

To calculate terms containing four creation/annihilation operators the Wick theorem is applied (summation over all possible contractions). The easiest term to calculate is the Coulomb interaction between two f-electrons with opposite spins on one orbital, because the intraorbital pairing does not arise in the system $\langle f^\dagger_{il\uparrow} f^\dagger_{il\downarrow}\rangle_0 = 0$ (the state is not favored due to involving large energy scale U):

$$\hat{\mathcal{P}}_{il}\hat{n}^f_{il\uparrow}\hat{n}^f_{il\downarrow}\hat{\mathcal{P}}_{il} = \lambda_d^2\left(n^f_{l\uparrow}n^f_{l\downarrow} + n^f_{l\uparrow}\hat{n}^{f\ \mathrm{HF}}_{il\downarrow} + n^f_{l\downarrow}\hat{n}^{f\ \mathrm{HF}}_{il\uparrow} + \hat{n}^{f\ \mathrm{HF}}_{il\uparrow}\hat{n}^{f\ \mathrm{HF}}_{il\downarrow}\right), \tag{B.5}$$

$$d^2 = \langle \hat{n}^f_{il\uparrow}\hat{n}^f_{il\downarrow}\rangle_{\mathrm{G}} = \langle \hat{\mathcal{P}}_{il}\hat{n}^f_{il\uparrow}\hat{n}^f_{il\downarrow}\hat{\mathcal{P}}_{il}\rangle_0 \simeq \lambda_d^2 n^f_{l\uparrow}n^f_{l\downarrow}. \tag{B.6}$$

The factor λ_d is the renormalization of double occupancies. Subsequently:

$$\hat{\mathcal{P}}_{i1}\hat{\mathcal{P}}_{i2}\hat{n}^f_{i1\uparrow}\hat{n}^f_{i2\downarrow}\hat{\mathcal{P}}_{i2}\hat{\mathcal{P}}_{i1} = \hat{\mathcal{P}}_{i1}\hat{n}^f_{i1\uparrow}\hat{\mathcal{P}}_{i1} \times \hat{\mathcal{P}}_{i2}\hat{n}^f_{i2\downarrow}\hat{\mathcal{P}}_{i2} \tag{B.7}$$

$$\begin{aligned}\langle \hat{n}^f_{i1\uparrow}\hat{n}^f_{i2\downarrow}\rangle_{\mathrm{G}} = \langle \hat{\mathcal{P}}_{i1}\hat{\mathcal{P}}_{i2}\hat{n}^f_{i1\uparrow}\hat{n}^f_{i2\downarrow}\hat{\mathcal{P}}_{i2}\hat{\mathcal{P}}_{i1}\rangle_0 &\simeq n^f_{1\uparrow}n^f_{2\downarrow} + p_\uparrow a_\downarrow \langle \hat{f}^\dagger_{i1\uparrow}\hat{f}^\dagger_{i2\uparrow}\rangle_0\langle \hat{f}_{i2\uparrow}\hat{f}_{i1\uparrow}\rangle_0 \\ &+ a_\uparrow p_\downarrow \langle \hat{f}^\dagger_{i1\downarrow}\hat{f}^\dagger_{i2\downarrow}\rangle_0\langle \hat{f}_{i2\downarrow}\hat{f}_{i1\downarrow}\rangle_0.\end{aligned} \tag{B.8}$$

Similarly, it is obtained

$$\hat{\mathcal{P}}_{i1}\hat{\mathcal{P}}_{i2}\hat{n}^f_{i1\sigma}\hat{n}^f_{i2\sigma}\hat{\mathcal{P}}_{i2}\hat{\mathcal{P}}_{i1} = \hat{\mathcal{P}}_{i1}\hat{n}^f_{i1\sigma}\hat{\mathcal{P}}_{i1} \times \hat{\mathcal{P}}_{i2}\hat{n}^f_{i2\sigma}\hat{\mathcal{P}}_{i2}, \tag{B.9}$$

$$\begin{aligned}\langle \hat{n}^f_{i1\sigma}\hat{n}^f_{i2\sigma}\rangle_{\mathrm{G}} = \langle \hat{\mathcal{P}}_{i1}\hat{\mathcal{P}}_{i2}\hat{n}^f_{i1\sigma}\hat{n}^f_{i2\sigma}\hat{\mathcal{P}}_{i2}\hat{\mathcal{P}}_{i1}\rangle_0 \simeq n^f_{1\sigma}n^f_{2\sigma} + p_\sigma p_\sigma \langle \hat{f}^\dagger_{i1\sigma}\hat{f}^\dagger_{i2\sigma}\rangle_0 \langle \hat{f}_{i2\sigma}\hat{f}_{i1\sigma}\rangle_0 \\ + a_\sigma a_\sigma \langle \hat{f}^\dagger_{i1\bar{\sigma}}\hat{f}^\dagger_{i2\bar{\sigma}}\rangle_0 \langle \hat{f}_{i2\bar{\sigma}}\hat{f}_{i1\bar{\sigma}}\rangle_0.\end{aligned} \tag{B.10}$$

In our considerations we have chosen, that only equal spin components of pairing operator are non-zero, thus $\langle \hat{f}^\dagger_{i1\sigma}\hat{f}^\dagger_{i2\bar{\sigma}}\rangle_0 = 0$. Therefore, $\langle \hat{\mathbf{S}}^+_{i1}\hat{\mathbf{S}}^-_{i2}\rangle_0 = \langle \hat{\mathbf{S}}^-_{i1}\hat{\mathbf{S}}^+_{i2}\rangle_0 = 0$ and mean values of $m = 0$ component of spin-triplet pairing operator (2.7), as well as singlet-pairing operator (2.8) are zero: $\langle A^\dagger_{i0}\rangle_0 = 0$, $\langle B^\dagger_i\rangle_0 = 0$.

$$g_{1\sigma} = 2 \times p_\sigma a_{\bar{\sigma}} = 2 \times (\lambda^2_d - \lambda^2_{\bar{\sigma}}) \times (\lambda^2_\sigma + (\lambda^2_d - \lambda^2_\sigma) n^f_{l\bar{\sigma}}) \times n^f_{l\bar{\sigma}}, \tag{B.11}$$

$$g_{2\sigma} = p_\sigma p_\sigma + a_{\bar{\sigma}} a_{\bar{\sigma}} = (\lambda^2_d - \lambda^2_{\bar{\sigma}})^2 \times \left(n^f_{l\bar{\sigma}}\right)^2 + \left(\lambda^2_\sigma + (\lambda^2_d - \lambda^2_\sigma) n^f_{l\bar{\sigma}}\right)^2, \tag{B.12}$$

In the Table B.1 a comparison of initial and effective Hamiltonians is presented, both in SGA and in Hartree-Fock approximations.

Table B.1.: Comparison of the initial (2.2) and the obtained effective Hamiltonian in SGA approximation (2.30) and in Hartree-Fock-BCS approximation. Note that $\mathcal{V}_\sigma = g_{1\sigma}U' + g_{2\sigma}(U' - J)$ and $n^f_{l\sigma}$, $\langle \hat{f}^\dagger_{i1\sigma}\hat{f}^\dagger_{i2\sigma}\rangle_0$, $\langle \hat{f}_{i2\sigma}\hat{f}_{i1\sigma}\rangle_0$ are calculated in uncorrelated state. Correlations renormalize hybridization (factor q_σ) and the f-orbital energy, furthermore they influence superconductivity by changing coupling $(U' - J)$ to $\mathcal{V}_\sigma$.

Initial Hamiltonian	Effective SGA Hamiltonian	Effective HF-BCS Hamiltonian
$V_{ij}\hat{f}^\dagger_{il\sigma}\hat{c}_{jl\sigma}$	$q_\sigma V_{ij}\hat{f}^\dagger_{il\sigma}\hat{c}_{jl\sigma}$	$V_{ij}\hat{f}^\dagger_{il\sigma}\hat{c}_{jl\sigma}$
$\epsilon^f \hat{n}^f_{il\sigma}$	$\epsilon^f_\sigma \hat{n}^f_{il\sigma}$	$\left(\epsilon^f + (U+U')n^f_{l\bar{\sigma}} + (U'-J)n^f_{l\sigma}\right)\hat{n}^f_{il\sigma}$
$U\hat{n}^f_{il\uparrow}\hat{n}^f_{il\downarrow}$	$Ud^2 = U\lambda_d^2 n^f_{l\uparrow}n^f_{l\downarrow}$	$Un^f_{l\uparrow}n^f_{l\downarrow}$
$U'\left(\hat{n}^f_{i1\uparrow}\hat{n}^f_{i2\downarrow} + \hat{n}^f_{i1\downarrow}\hat{n}^f_{i2\uparrow}\right)$	$U'\Big(n^f_{1\uparrow}n^f_{2\downarrow} + n^f_{1\downarrow}n^f_{2\uparrow} + \sum_\sigma g_{1\sigma}\langle \hat{f}^\dagger_{i1\sigma}\hat{f}^\dagger_{i2\sigma}\rangle \hat{f}_{i2\sigma}\hat{f}_{i1\sigma}\Big)$	$U'\left(n^f_{1\uparrow}n^f_{2\downarrow} + n^f_{1\downarrow}n^f_{2\uparrow}\right)$
$(U'-J)\sum_\sigma \hat{n}^f_{i1\sigma}\hat{n}^f_{i2\sigma}$	$(U'-J)\sum_\sigma\Big(n^f_{1\sigma}n^f_{2\sigma} + g_{2\sigma}\langle \hat{f}^\dagger_{i1\sigma}\hat{f}^\dagger_{i2\sigma}\rangle \hat{f}_{i2\sigma}\hat{f}_{i1\sigma}\Big)$	$(U'-J)\left(n^f_{1\sigma}n^f_{2\sigma} + \langle \hat{f}^\dagger_{i1\sigma}\hat{f}^\dagger_{i2\sigma}\rangle_0 \hat{f}_{i2\sigma}\hat{f}_{i1\sigma}\right)$

C. Stoner-like magnetism

In Hartree-Fock-BCS approximation Stoner criterion for the orbitally degenerate Anderson lattice model:

$$\rho^f_{l\sigma}\,(U+J) > 1, \tag{C.1}$$

$\rho^f_{l\sigma}$ is the density of f-electrons per orbital per spin in the paramagnetic phase with suppressed superconductivity.

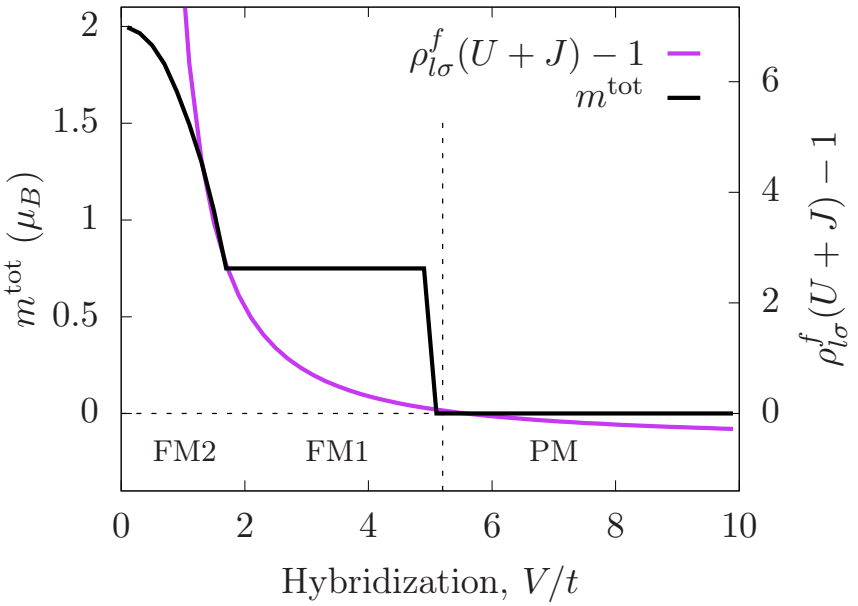

Figure C.1.: Stoner criterion for $U/|t| = 4$, $J/|t| = 1.7$, $\epsilon^f/|t| = -4$, $t' = 0.25|t|$, in Hartree-Fock-BCS approximation.

D. Details of numerical calculation

D.1. Numerical results

In this Section we show numerical results obtained for the orbitally degenerate Anderson model in SGA approximation with precision at least 10^{-8} for the set of parameters: $U/|t| = 3.5$, $J/|t| = 1.1$, $U' = U - 2J$, $U'/|t| = 1.3$, temperature: $k_B T = 0|t|$, $n^{\mathrm{tot}} = 3.25$, $t'/|t| = 0.25$, $\epsilon^f/|t| = -4$.

In Table D.1 raw numerical data calculated with numerical precision at least 10^{-8} are presented. The Table contains: hybridization V/t, for which calculations were done (1st column), f-electron occupancy per orbital for spin up and spin down (2nd and 3rd column), c-electron occupancy per orbital for both spin directions (4th and 5th column), expectation values for pairing for both spin directions (6th and 7th column), expectation value for mixing f-c states for both spin directions (8th and 9th column). The last column stands for the phase type.

In Table D.2 for the same hybridization values as in Table D.1, are presented: chemical potential μ and factors λ_α from SGA approximation.

Table D.1.: Raw numerical data from SGA approximation for selected hybridization values. Numerical precision for dimensionless expectation values has been set at least 10^{-8} (points in the PM+A phase, where calculated with precision 10^{-10}), $t'/|t| = 0.25$, $\epsilon^f/|t| = -4$, $U/|t| = 3.5$, $J/|t| = 1.1$, $U' = U - 2J$, $U'/|t| = 1.3$, temperature: $k_BT = 0|t|$, $n^{\mathrm{tot}} = 3.25$.

V/t	$n^f_{l\uparrow}$	$n^f_{l\downarrow}$	$n^c_{l\uparrow}$	$n^c_{l\downarrow}$	$\langle \hat{f}_{i2\uparrow}\hat{f}_{i1\uparrow}\rangle_0$	$\langle \hat{f}_{i2\downarrow}\hat{f}_{i1\downarrow}\rangle_0$	$\langle \hat{f}^\dagger_{i1\uparrow}\hat{c}_{i1\uparrow}\rangle_0$	$\langle \hat{f}^\dagger_{i1\downarrow}\hat{c}_{i1\downarrow}\rangle_0$	Phase
1.100 00	0.897 251 54	0.102 251 08	0.239 126 25	0.386 371 13	0.000 000 00	0.000 000 00	0.256 121 42	0.193 034 34	FM2
1.200 00	0.852 339 87	0.146 944 03	0.231 782 96	0.393 933 14	0.000 000 00	0.000 000 00	0.304 210 63	0.232 277 19	FM2
1.250 00	0.806 346 41	0.193 145 07	0.229 689 82	0.395 818 70	0.000 000 57	0.000 010 42	0.343 101 61	0.264 739 90	FM2+A_2
1.254 00	0.798 571 95	0.201 020 38	0.229 749 04	0.395 658 62	0.000 002 57	0.000 036 85	0.348 809 13	0.269 576 16	FM2+A_2
1.258 00	0.785 346 74	0.214 468 26	0.230 093 34	0.395 091 67	0.000 018 23	0.000 222 48	0.357 976 37	0.277 393 74	FM2+A_2
1.258 40	0.782 528 56	0.217 342 55	0.230 205 20	0.394 923 69	0.000 024 92	0.000 310 95	0.359 842 41	0.278 993 46	FM2+A_2
1.258 45	0.782 071 11	0.217 809 40	0.230 224 61	0.394 894 88	0.000 026 11	0.000 327 84	0.360 142 42	0.279 250 94	FM2+A_2
1.258 50	0.769 047 38	0.231 126 93	0.230 952 62	0.393 873 07	0.000 000 00	0.001 260 40	0.368 362 01	0.286 322 14	FM1+A_1
1.260 00	0.768 914 78	0.231 224 56	0.231 085 22	0.393 775 44	0.000 000 00	0.001 235 03	0.368 510 08	0.286 379 70	FM1+A_1
1.261 00	0.768 826 40	0.231 289 60	0.231 173 60	0.393 710 40	0.000 000 00	0.001 218 39	0.368 608 67	0.286 417 99	FM1+A_1
1.264 00	0.768 561 36	0.231 484 50	0.231 438 64	0.393 515 50	0.000 000 00	0.001 169 79	0.368 903 79	0.286 532 44	FM1+A_1
1.625 00	0.738 607 03	0.251 991 60	0.261 392 97	0.373 008 40	0.000 000 00	0.000 006 89	0.398 507 16	0.296 718 17	FM1+A_1
1.896 00	0.719 235 67	0.263 571 52	0.280 764 33	0.361 428 48	0.000 000 00	0.000 000 00	0.414 807 90	0.301 183 99	FM1
2.950 00	0.664 710 46	0.288 915 47	0.335 289 54	0.336 084 53	0.000 000 00	0.000 000 00	0.452 221 80	0.308 385 61	FM1
3.125 00	0.462 855 72	0.462 855 72	0.349 644 28	0.349 644 28	0.000 000 01	0.000 000 01	0.394 216 92	0.394 216 92	PM+A
3.250 00	0.461 341 47	0.461 341 47	0.351 158 53	0.351 158 53	0.000 000 00	0.000 000 00	0.394 997 32	0.394 997 32	PM

Table D.2.: Raw numerical data from SGA approximation for selected hybridization values. Numerical precision for dimensionless expectation values has been set at least 10^{-8} (points in the PM+A phase were calculated with precision 10^{-10}), $t'/|t| = 0.25$, $\epsilon^f/|t| = -4$, $U/|t| = 3.5$, $J/|t| = 1.1$, $U' = U - 2J$, $U'/|t| = 1.3$, temperature: $k_BT = 0|t|$, $n^{\mathrm{tot}} = 3.25$.

V/t	$\mu/\lvert t\rvert$	$\lambda_\emptyset$	$\lambda_\uparrow$	$\lambda_\downarrow$	λ_d	Phase
1.100 00	−1.425 436 06	0.889 323 88	1.011 901 86	1.684 010 95	0.888 686 30	FM2
1.200 00	−1.443 255 42	0.864 280 93	1.021 681 53	1.571 257 84	0.863 443 62	FM2
1.250 00	−1.448 290 90	0.842 277 87	1.034 303 30	1.487 896 12	0.841 714 48	FM2+A_2
1.254 00	−1.448 293 48	0.838 663 68	1.036 737 14	1.476 158 56	0.838 214 44	FM2+A_2
1.258 00	−1.447 879 27	0.832 485 54	1.041 105 83	1.457 507 96	0.832 283 00	FM2+A_2
1.258 40	−1.447 729 75	0.831 158 38	1.042 076 10	1.453 737 17	0.831 017 42	FM2+A_2
1.258 45	−1.447 703 60	0.830 942 46	1.042 234 96	1.453 131 62	0.830 811 81	FM2+A_2
1.258 50	−1.447 155 74	0.824 792 60	1.046 907 00	1.436 516 54	0.824 982 64	FM1+A_1
1.260 00	−1.448 779 53	0.825 018 78	1.046 887 68	1.435 881 27	0.825 170 44	FM1+A_1
1.261 00	−1.449 862 33	0.825 169 22	1.046 874 83	1.435 458 64	0.825 295 34	FM1+A_1
1.264 00	−1.453 112 00	0.825 618 90	1.046 836 42	1.434 195 05	0.825 668 61	FM1+A_1
1.625 00	−1.851 628 42	0.866 609 03	1.043 128 52	1.318 747 49	0.859 322 03	FM1+A_1
1.896 00	−2.152 954 63	0.886 772 83	1.040 862 71	1.263 685 51	0.875 780 11	FM1
2.950 00	−3.304 103 38	0.929 993 67	1.033 514 55	1.154 356 87	0.912 284 02	FM1
3.125 00	−3.436 449 41	0.922 772 78	1.082 738 74	1.082 738 74	0.894 437 73	PM+A
3.250 00	−3.550 469 62	0.926 468 15	1.079 535 68	1.079 535 68	0.898 266 92	PM

D.2. Calculation of the density of states

In Figure 3.2 of Chapter 3 we present calculated spin- and orbital-resolved density of states in three phases: FM2, FM1, and PM. Here, we want to explain shortly, how it was done. The local density of states can be defined as

$$\rho_{\sigma}^{(l)}(\omega) = \sum_{\mathbf{k}} \frac{\mathcal{A}_{\sigma}^{(l)}(\mathbf{k},\omega)}{2\pi}, \tag{D.1}$$

where index l labels type of electron: c or f and $\mathcal{A}_{\sigma}^{(l)}(\mathbf{k},\omega)$ is the spectral function. For f-electrons it can be calculated as

$$\begin{aligned}\mathcal{A}_{\sigma}^{f}(\mathbf{k},\omega) = (2\pi)\sum_{n}\Big(&\langle 0|\,\hat{f}_{\mathbf{k}\sigma}^{\dagger}\,|n\rangle\langle n|\,\hat{f}_{\mathbf{k}\sigma}\,|0\rangle\,\delta(\omega+E_n-E_0) \\ &+\langle 0|\,\hat{f}_{\mathbf{k}\sigma}\,|n\rangle\langle n|\,\hat{f}_{\mathbf{k}\sigma}^{\dagger}\,|0\rangle\,\delta(\omega-E_n+E_0)\Big),\end{aligned} \tag{D.2}$$

where $|n\rangle$ is the eigenstate of the effective Hamiltonian (2.32), E_n – the corresponding eigenvalue, and E_0 corresponds to the ground state energy. Similarly we construct the spectral function for c-electrons. Dirac delta function are smeared out by adding a small imaginary part to the spectral function: the Lorentzian form of the typical width $\epsilon = 10^{-3}|t|$. Calculations are done using CQUAD doubly-adaptive integration (from GSL Library).

D.3. Band structure

On the basis of eigenvalues of the effective Hamiltonian (2.32), i.e., Equation (2.37), the band structure can be calculated for different hybridization values, and standard set of parameters: $U/|t| = 3.5$, $J/|t| = 1.1$, $T = 0$ K, $n^{\mathrm{tot}} = 3.25$, $t'/|t| = 0.25$, $\epsilon^{f}/|t| = -4$. Since the band structure describes energies of quasiparticles, one can restore the contribution from f- and c-electrons:

$$\Psi_{\mathbf{k}\sigma}^{\dagger} = \Phi_{\mathbf{k}\sigma}^{\dagger} Q^{-1}, \tag{D.3}$$

where $\Psi_{\mathbf{k}\sigma}^{\dagger} = \left(\hat{c}_{\mathbf{k}1\sigma}^{\dagger}, \hat{c}_{-\mathbf{k}2\sigma}, \hat{f}_{\mathbf{k}1\sigma}^{\dagger}, \hat{f}_{-\mathbf{k}2\sigma}\right)$, $\Phi_{\mathbf{k}\sigma}^{\dagger}$ describes quasiparticles, and Q^{-1} is the inversed transition matrix. An explicit form of transformation matrix Q is quite involved, so it is not given here. All Figures: D.1, D.2, and D.3 contain contribution from f- (marked in blue) and c-electrons (marked in red) for both spin directions.

Note that in the FM2 phase (cf. Figure D.1), the f-electrons are located in narrow bands (weak dependence on the $\mathbf{k}$-vector) for both spin directions, whereas the conduction electrons are practically uncorrelated. Thus, the f-electrons acquire itinerant, but an almost localized nature. Similar situation takes place in the FM1 phase.

For larger values of hybridization the system is in paramagnetic (PM) state (cf. Figure D.3). Then, the results for both spin directions are the same.

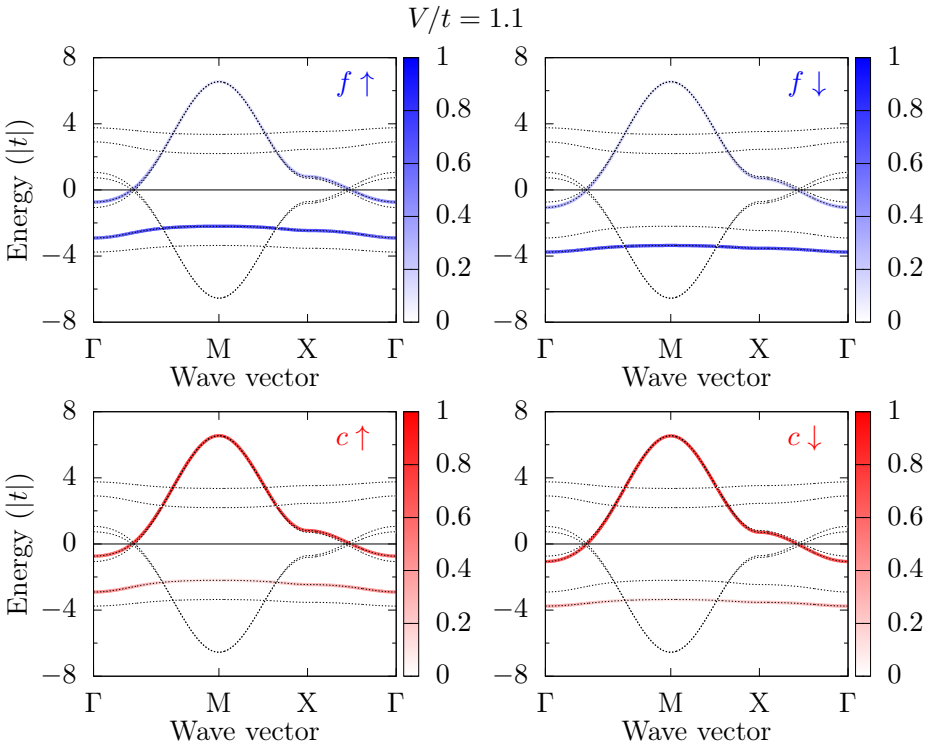

Figure D.1.: Band structure (black dashed lines) for $V/t = 1.1$ in the FM2 phase. Contributions from f-electrons are marked in blue, whereas for c-electrons in red. Color intensity represents the spectral weight.

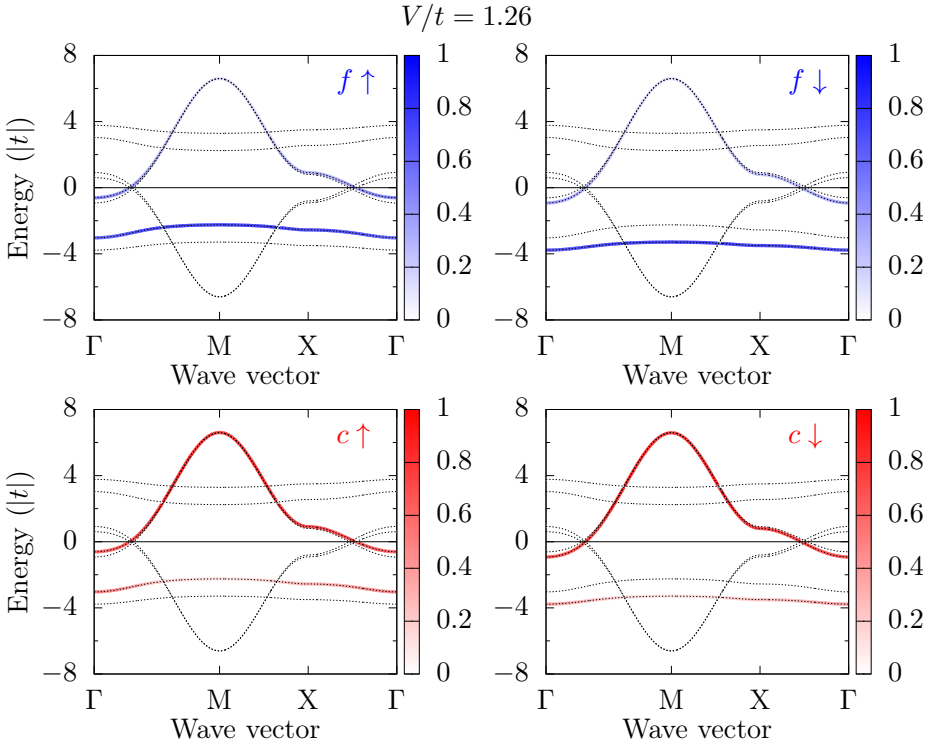

Figure D.2.: Band structure for $V/t = 1.26$ in the FM1+A_1 phase. Colors the same as in Figure D.1.

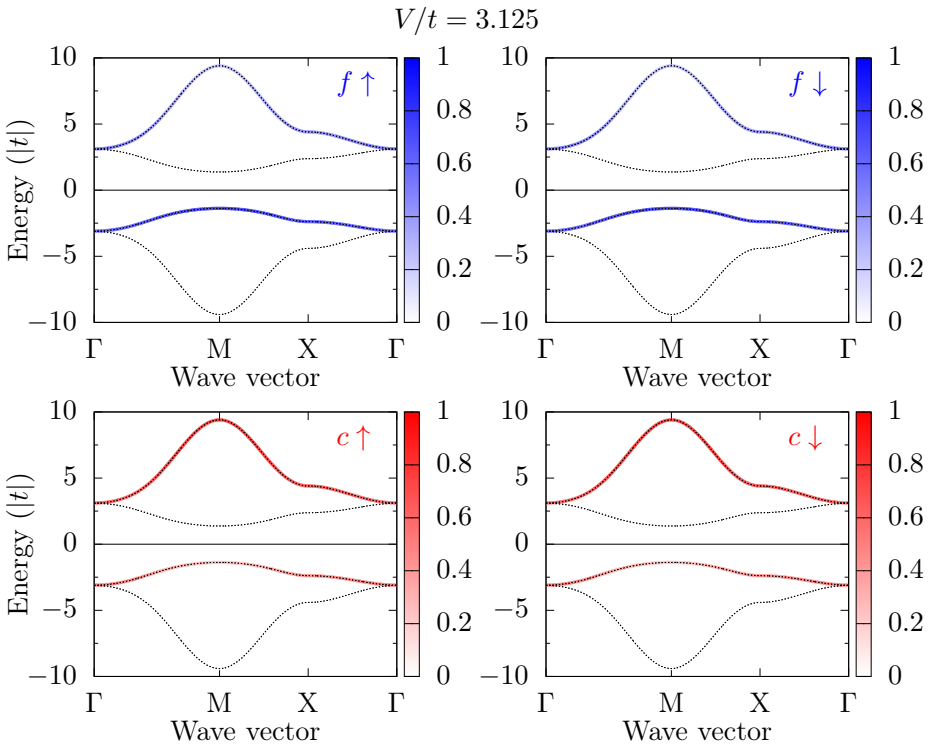

Figure D.3.: Band structure for $V/t = 3.125$ in the PM+A phase. Colors the same as in Figure D.1.

D.4. Summation versus integration over the Brillouin zone

In this Chapter we explain carefully problems, which we encounter during performing numerical simulation of the orbitally degenerate Anderson lattice model.

Results presented in Chapter 3 are obtained in thermodynamic limit with number of sites $\Lambda \to \infty$ (Brillouin zone integration). However, performing calculations with large, but finite number of lattice sites Λ and $k_{\mathrm{B}}T \neq 0$ (but really small $\sim 10^{-8}|t|$), leads to large speed-up. Unfortunately, since we want to describe superconductivity with gap parameters in range $\sim 10^{-4}|t| \div 10^{-9}|t|$ (the case of $U/|t| = 3.5$, $J/|t| = 1.1$, studied in Chapter 3 and [82]) it is not sufficient, because of finite size effect on the superconducting state.

Having in mind the Anderson criterion [96]: equal-spin-triplet superconducting gap is of order of mean level spacing between discrete energy levels $\Delta^{ff}_{\sigma\sigma} \sim d$ and $d \sim W/\Lambda$ ($W \sim$ several t is bandwidth, Λ – number of lattice sites) to get appropriate accuracy, we would need summation over $\Lambda = 10^{10}$ lattice sites. Therefore, an integration over the Brillouin zone was applied to obtain satisfying results. Specifically, we employed GNU Scientific Library QAGS adaptive integration with singularities algorithm.

Previous works in the non-degenerate Anderson model [51, 40, 52] concern phenomenon of magnetism without superconductivity, so the problem was not encountered before. In [53] calculation was performed with accuracy $\epsilon = 10^{-6}$ with finite number of points in the numerical integration over density states. However, superconducting gaps $\Delta^{ff}_{\sigma\sigma}$ are large for chosen there set of parameters.

Similar problem, i.e. dependence on the system size of superconducting gap parameters in Fulde-Ferrell-Larkin-Ovchinnikov (FFLO) phase, was described in the paper [97].

In Figures D.4 and D.5 are presented results for different sets of parameters, nevertheless in both calculations a summation over the Brillouin zone has been applied, with lattice size 256×256. In Figure D.4 results are obtained in Hartree-Fock-BCS approximation for parameters: $U/|t| = 8$, $J/|t| = 4$, $k_B T/|t| = 10^{-8}$, $t'/|t| = 0.25$, $\epsilon^f/|t| = -4$. Large U value and ratio $J/U = 0.5$ are dictated to compare results with [53]. For those parameters FM2→FM1 phase transition is continuous and superconducting phase A_2 with two non-zero gap parameters is not observed, therefore phase transition from the normal state to A_1 phase is also continuous. FM1+A_1 →PM+A phase transition stays of the first order.

Figure D.4(a) contains total magnetization and partial for f- and c-electron contributions, Figure D.4(b): two equal-spin superconducting gap parameters $\Delta^{ff}_{\sigma\sigma}$, and Figure D.4(c): f- and c-electron occupancies per site. In Figure D.4(d) the condensation energy is presented. The condensation energy between FM1+A_1 and PM+A phases are calculated as the difference in energies

$$E_{\mathrm{cond}} = \min(E_{\mathrm{FM1+A1}}, E_{\mathrm{PM+A}}) - \min(E_{\mathrm{FM1}}, E_{\mathrm{PM}}) \tag{D.4}$$

In the inset of Figure D.4(d) it is shown, that to calculate the condensation energy properly, it is needed to determine a right ground state with and without su-

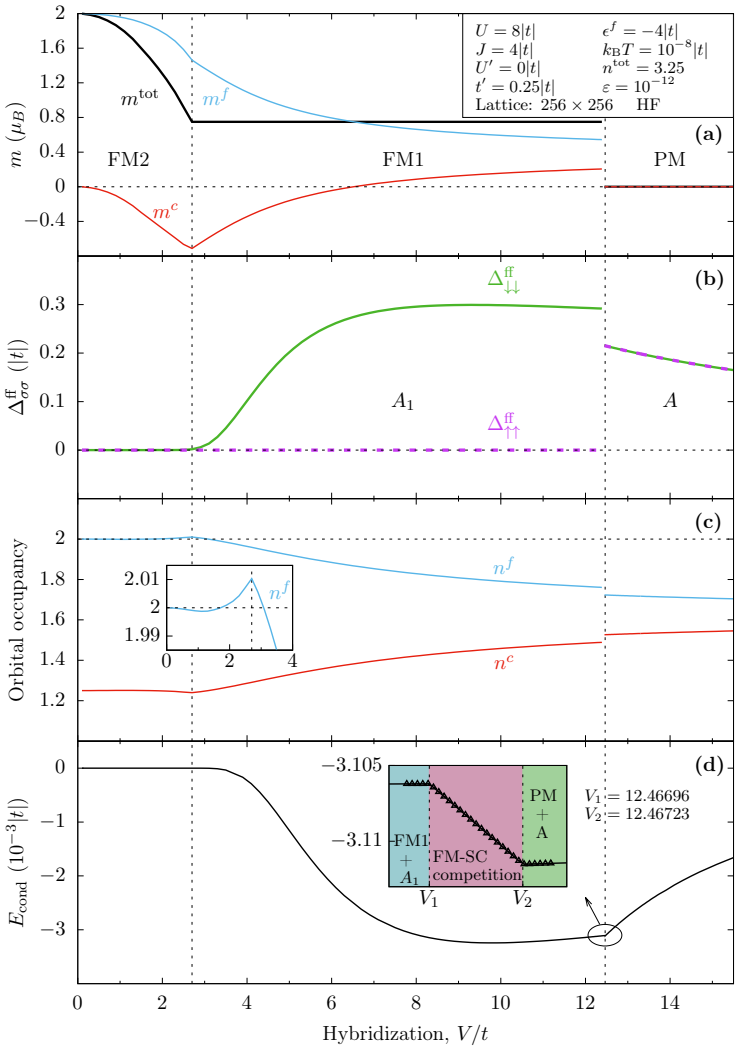

Figure D.4.: Phase diagram for $U/|t| = 8$, $J/|t| = 4$, $k_BT/|t| = 10^{-8}$, $t'/|t| = 0.25$, $\epsilon^f/|t| = -4$, summation over lattice 256×256, precision 10^{-12}, Hartree-Fock approximation. Compare with [53].

perconductivity. On the left from V_1 the condensation energy is simply $E_{\mathrm{cond}} = E_{\mathrm{FM1+A1}} - E_{\mathrm{FM1}}$, on the right from V_2 it is $E_{\mathrm{cond}} = E_{\mathrm{PM+A}} - E_{\mathrm{PM}}$, whereas between in the system with switched on superconductivity PM+A is the ground state, but without it is FM1. Note, that the difference $V_2 - V_1$ is small $\sim 3 \cdot 10^{-4}|t|$.

Going to lower U values and lower ratio J/U, superconducting gap parameters become smaller. The phase diagram in Figure D.5 is obtained for the same set of parameters as Figure 3.8 in the main text, however summation over the Brillouin zone does not cover properly superconducting properties in A_2 phase (cf. with inset of Figure D.5(d)).

Subsequently, we compare results obtained using integration and summation over the Brillouin zone for set of parameters: $U/|t| = 4$, $J/|t| = 1.6$, $k_BT/|t| = 10^{-8}$, $t'/|t| = 0.25$, $\epsilon^f/|t| = -4$. In Figure D.6(a) small spin-up gap parameter $\Delta^{ff}_{\uparrow\uparrow} \sim 10^{-4}$ in A_2 phase is presented: obtained using integration (purple dots) and summation on the lattice 256×256 (black triangles) over the Brillouin zone. Failure of approach with summation manifests itself in fluctuations of gap parameter value. In both A_2 and A_1 phases parameter $\Delta^{ff}_{\downarrow\downarrow}$, which is two orders of magnitude larger than $\Delta^{ff}_{\uparrow\uparrow}$ in A_2 phase, does not reveal any unusual behavior, as presented in Figure D.6(b) and (c), respectively.

The total magnetization calculated for the same set of parameters, but obtained using either integration or summation, does not change significantly (Figure D.7). E.g. in the FM2 phase for the hybridization $V/t = 1.4$ the difference is about 0.05%, whereas in the FM1 phase $m^{\mathrm{tot}} = 0.75$ in both approaches.

In Figure D.8 convergence through iterations of gap parameters is presented for all three distinct superconducting phases: A, A_1, A_2.

Despite the fact that summation over the Brillouin zone gives wrong behavior of superconductivity in regime of small gap parameters, it can speed up the calculations, if we include in the first few iterations summation over the Brillouin zone, then the system approaches to the solution (proper magnetization values) and next, in solving of the model we switch to integration.

We also supply Table with exemplary results, calculated using summation over the Brillouin zone (cf. Table D.3). Note, that the total magnetization multiplied by the lattice size gives integer value, what is a good test of correctness of summation approach.

Table D.3.: $U/|t| = 4$, $J/|t| = 1.6$, lattice sites 256×256

V/t	$m^{\mathrm{tot}} \times 256^2$ (μ_B)	$\mathcal{V}_\uparrow/\lvert t\rvert$	$\mathcal{V}_\downarrow/\lvert t\rvert$	$\Delta^{ff}_{\uparrow\uparrow}$ ($\lvert t\rvert$)	$\Delta^{ff}_{\downarrow\downarrow}/\lvert t\rvert$
0.2	130092	−0.809380	−0.806110	0.0	0.0
1.45	49152	−1.386500	−1.289000	0.0	0.058776
4.1	49152	−1.007600	−1.020300	0.0	0.001031
4.2	0	−1.052500	−1.052500	0.007893	0.007893

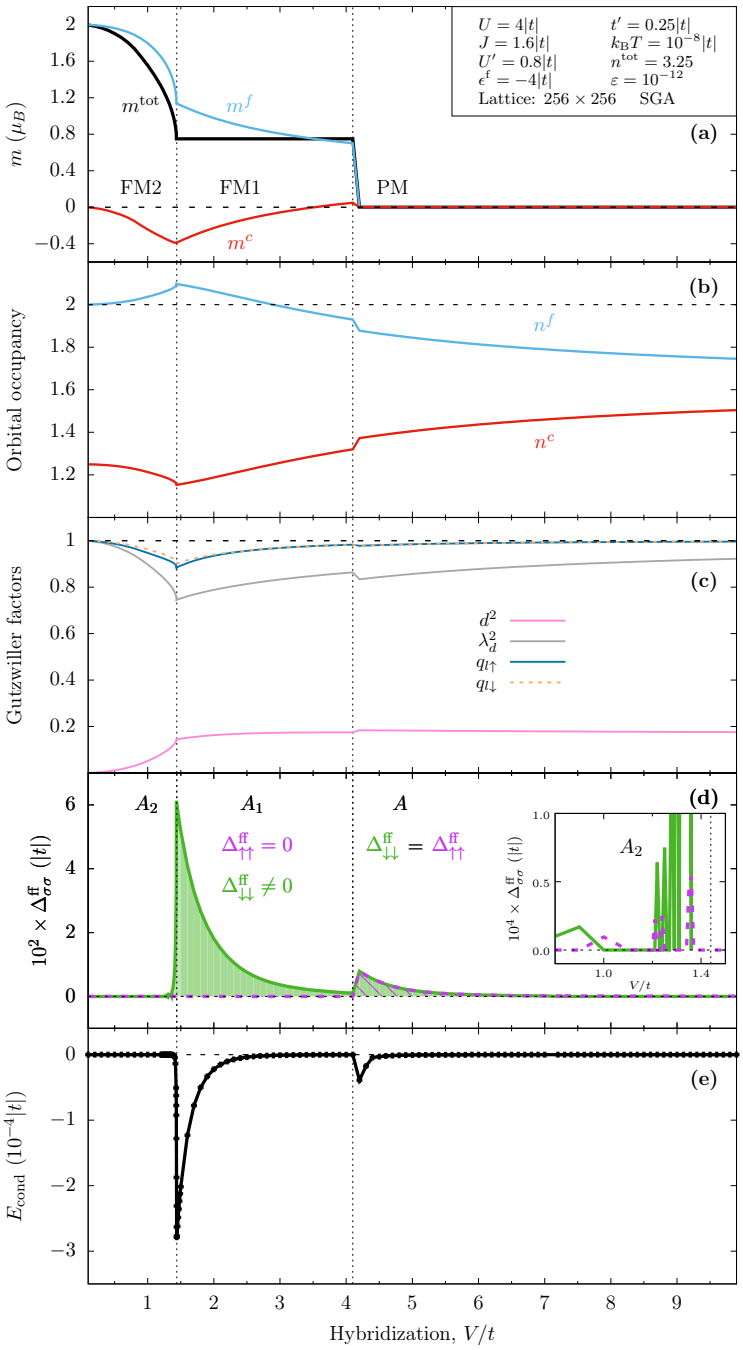

Figure D.5.: Phase diagram for $U/|t| = 4$, $J/|t| = 1.6$, $k_BT/|t| = 10^{-8}$, $t'/|t| = 0.25$, $\epsilon^f/|t| = -4$ summation over lattice 256×256, precision 10^{-12}, SGA approximation. Figure 3.8 in the Section 3.2.2 is calculated for the same set of parameters, but with the integration applied instead of summation. Summation over the Brillouin zone does not affect magnetization, but we cannot calculate properly superconducting gaps, due to finite-size scaling.

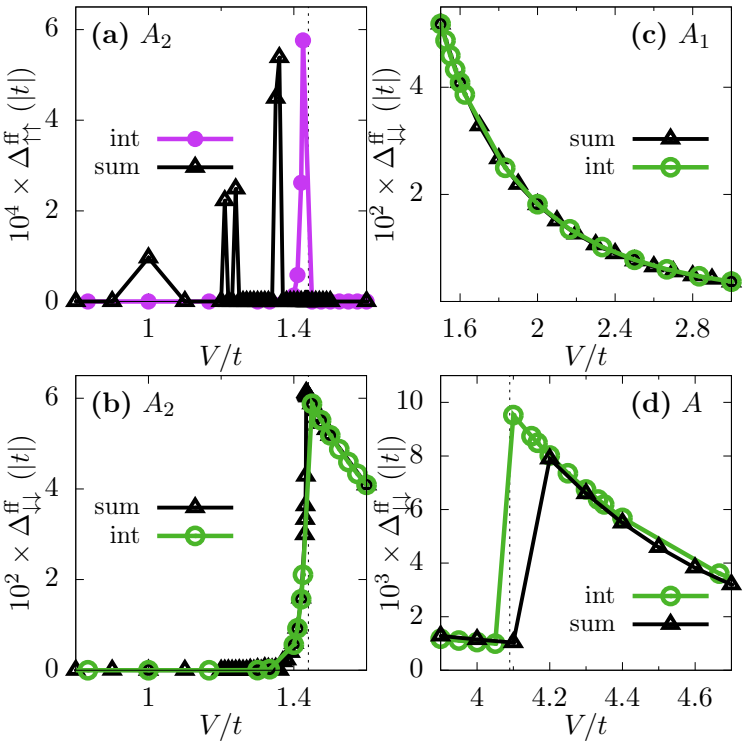

Figure D.6.: Comparison of superconducting gap parameters obtained for $U/|t| = 4$, $J/|t| = 1.6$, $k_BT/|t| = 10^{-8}$, $t'/|t| = 0.25$, $\epsilon^f/|t| = -4$ using integration (purple or green dots) or summation over 256×256 lattice (black triangles): (a) $\Delta^{ff}_{\uparrow\uparrow}$ in A_2 phase, (b) $\Delta^{ff}_{\downarrow\downarrow}$ in A_2 phase, (c) $\Delta^{ff}_{\downarrow\downarrow}$ in A_1 phase, (d) $\Delta^{ff}_{\sigma\sigma}$ in A phase.

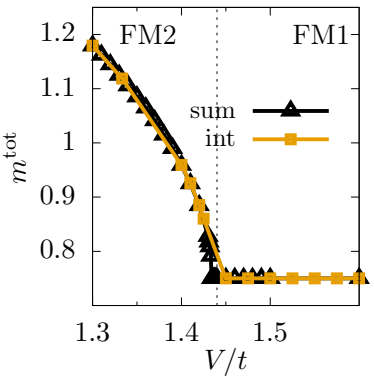

Figure D.7.: Comparison of total magnetization obtained for $U/|t| = 4$, $J/|t| = 1.6$, $k_BT/|t| = 10^{-8}$, $t'/|t| = 0.25$, $\epsilon^f/|t| = -4$ using integration (orange squares) or summation over 256×256 lattice (black triangles) in region of FM2→FM1 phase transition.

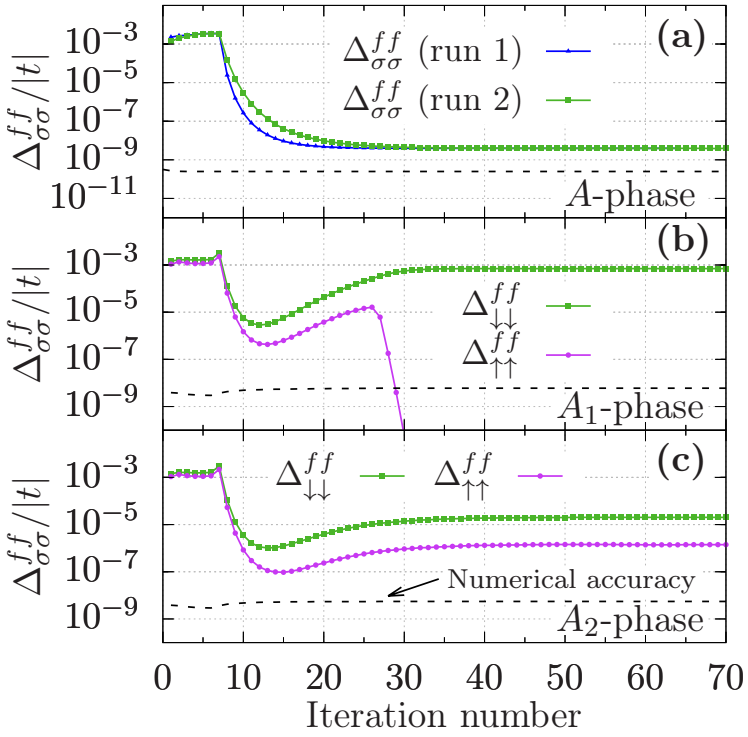

Figure D.8.: Convergence of gap parameters in (a) A, (b) A_1, (c) A_2 superconducting phases for $U/|t| = 3.5$, $J/|t| = 1.1$, $U'/|t| = 1.3$, temperature: $k_BT = 0|t|$, $n^{\text{tot}} = 3.25$, $t'/|t| = 0.25$, $\epsilon^f/|t| = -4$. In the first few iterations a summation over the Brillouin zone was applied, with $k_BT/|t| = 10^{-8}$ and forced $\Delta^{ff}_{\sigma\sigma} \sim 10^{-3}$. Afterwards, we established $k_BT/|t| = 0$, simultaneously the integration procedure was incorporated and gap parameters $\Delta^{ff}_{\sigma\sigma}$ was released to converge.

D.5. Determination of the ground state

D.5.1. The case without applied magnetic field

The condensation energy is the difference between energy for the superconducting state and for the normal state (with suppressed superconductivity). E.g., for the FM1 phase:

$$E_{\mathrm{cond}} = E_{\mathrm{FM1+A1}} - E_{\mathrm{FM1}} \tag{D.5}$$

Calculated condensation energies for different Hund's rule values are presented in Table D.4.

Table D.4.: The ground-state energies in superconducting and normal states for set of parameters: $U/|t| = 3.5$, $V/t = 1.32$, $t'/|t| = 0.25$, $\epsilon^f/|t| = -4$, $n^{\mathrm{tot}} = 3.25$, and selected values of Hund's coupling J. Here E_{FM1} denotes the energy of the ferromagnetic FM1 phase without superconductivity, and $E_{\mathrm{FM1}+A_1}$ is the FM1 phase coexisting with the A_1-type superconductivity. In the last column condensation energy $E_{\mathrm{cond}} \equiv E_{\mathrm{FM1}+A_1} - E_{\mathrm{FM1}}$ is presented. The numerical accuracy of the energy difference is of the order of 2×10^{-8}.

$J/\lvert t\rvert$	$E_{\mathrm{FM1}}/\lvert t\rvert$	$E_{\mathrm{FM1}+A_1}/\lvert t\rvert$	$10^4 \times E_{\mathrm{cond}}/\lvert t\rvert$
1.10	-11.663 459 37	-11.663 459 39	-0.0003
1.15	-11.796 917 55	-11.796 917 77	-0.0022
1.20	-11.934 039 49	-11.934 041 79	-0.0230
1.25	-12.074 935 82	-12.074 951 80	-0.1598
1.30	-12.219 724 82	-12.219 802 79	-0.7797
1.35	-12.368 534 05	-12.368 822 15	-2.8810
1.40	-12.521 501 70	-12.522 354 69	-8.5299

Since obtaining results with suppressed superconductivity is numerically expensive, we did not do it for whole range of hybridization.

To determine the ground state near the phase transition, energies in both phases have to be calculated, as presented in Figure D.9. It supplements the phase diagram presented in the main text, i.e., Figure 3.1.

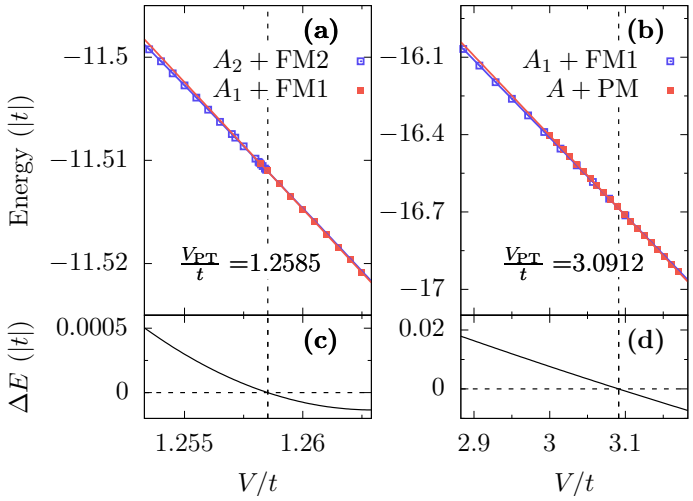

Figure D.9.: Calculated energies differences, which marks the hybridizations, for which FM2+A_2 →FM1+A_1 and FM1+A_1 →PM+A phase transitions take place, in absence of magnetic field.

D.5.2. The case with non-zero applied magnetic field

Calculations to Figure 3.15, i.e., the influence of magnetic field on phase transitions: The energy difference between A_1 and A_2 state tells us, which phase is preferred:

$$\Delta E = E_{\mathrm{FM1}+A_1} - E_{\mathrm{FM2}+A_2}. \tag{D.6}$$

Values of energies differences are presented in table D.5.

Table D.5.: Energy difference between FM1+A_1 and FM2+A_2 phases in $h/|t| = 0.002$.

V/t	$10^6 \times \Delta E$ ($\|t\|$)	Phase
1.26030	10.5022	FM2+A_2
1.26040	5.3856	FM2+A_2
1.26050	0.6728	FM2+A_2
1.26052	−2.1111	FM1+A_1
1.26058	−2.7285	FM1+A_1
1.26060	−3.5130	FM1+A_1

Energy difference setting the characteristic magnetic field $\mu_0 H_x$

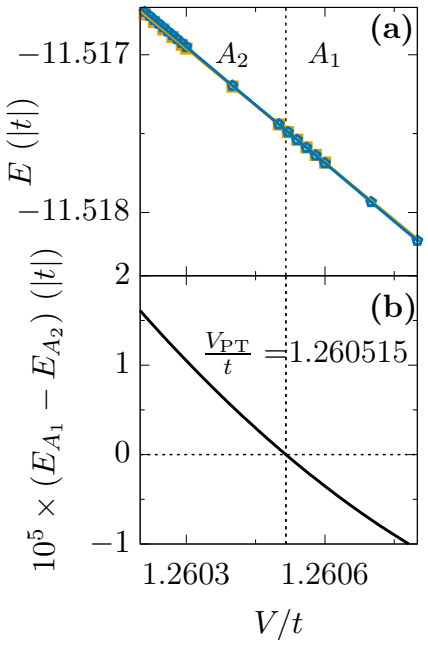

Figure D.10.: Energy difference between FM1+A_1 and FM2+A_2 phases for reduced magnetic field $h/|t| = 0.002$.

Table D.6.: Energy difference between FM1+A_1 and FM2+A_2 phases for different hybridization values $V/t = 1.26$, $h_x/|t| = 0.001468$.

$10^3 \times H/t$	$10^6 \times \Delta E\ (|t|)$	Phase
1.40	−2.7885	FM1+A_1
1.41	−2.3944	FM1+A_1
1.42	−1.9943	FM1+A_1
1.43	−1.5868	FM1+A_1
1.44	−1.1767	FM1+A_1
1.45	−0.7588	FM1+A_1
1.46	−0.3366	FM1+A_1
1.47	0.0917	FM2+A_2
1.48	0.5235	FM2+A_2
1.49	0.9608	FM2+A_2
1.5	1.4035	FM2+A_2
1.6	6.0461	FM2+A_2
1.66	9.0068	FM2+A_2
1.67	9.5121	FM2+A_2
1.68	10.0197	FM2+A_2
1.7	11.0452	FM2+A_2

Table D.7.: Energy difference between FM1+A_1 and FM2+A_2 phases for different hybridization values.

(a) $V/t = 1.259$, $h_x/|t| = 0.000435$

$10^3 \times H/t$	$10^6 \times \Delta E$ ($\|t\|$)	Phase
0.38	−2.3106	FM1+A_1
0.40	−1.4878	FM1+A_1
0.42	−0.6434	FM1+A_1
0.44	0.2208	FM2+A_2
0.46	1.1046	FM2+A_2
0.48	2.0070	FM2+A_2
0.50	2.9250	FM2+A_2
0.52	3.8600	FM2+A_2

(b) $V/t = 1.2595$, $h_x/|t| = 0.000951$

$10^3 \times H/t$	$10^6 \times \Delta E$ ($\|t\|$)	Phase
0.90	−2.1515	FM1+A_1
0.92	−1.3312	FM1+A_1
0.94	−0.4906	FM1+A_1
0.96	0.3729	FM2+A_2
0.98	1.2550	FM2+A_2
1.0	2.1594	FM2+A_2

(c) $V/t = 1.2605$, $h_x/|t| = 0.001984$

$10^3 \times H/t$	$10^6 \times \Delta E$ ($\|t\|$)	Phase
1.90	−3.3968	FM1+A_1
1.92	−2.6303	FM1+A_1
1.94	−1.8376	FM1+A_1
1.96	−1.0218	FM1+A_1
1.98	−0.1850	FM1+A_1
2.00	0.6726	FM2+A_2
2.02	1.5486	FM2+A_2
2.04	2.4431	FM2+A_2

(d) $V/t = 1.261$, $h_x/|t| = 0.002501$

$10^3 \times H/t$	$10^6 \times \Delta E$ ($\|t\|$)	Phase
2.40	−3.9711	FM1+A_1
2.48	−0.8706	FM1+A_1
2.50	−0.0422	FM1+A_1
2.52	0.8196	FM2+A_2
2.54	1.6935	FM2+A_2
2.56	2.5858	FM2+A_2
2.58	3.4928	FM2+A_2
2.6	4.4166	FM2+A_2
2.7	9.2533	FM2+A_2

Bibliography

[1] H. K. Onnes. Commun. Phys. Lab. Univ. Leiden. Suppl., **29** (1911).

[2] W. Meissner and R. Ochsenfeld. *Ein neuer Effekt bei Eintritt der Supraleitfähigkeit.* Naturwissenschaften, **21**, 787 (1933). doi:10.1007/BF01504252.

[3] A. M. Forrest. *Meissner and Ochsenfeld revisited.* European Journal of Physics, **4**, 117 (1983).

[4] J. N. Ryabinin and L. W. Shubnikow. *Magnetic Properties and Critical Currents of Supra-conducting Alloys.* Nature, **135**, 581 (1935).

[5] F. London and H. London. *The electromagnetic equations of the supraconductor.* Proceedings of the Royal Society of London A: Mathematical, Physical and Engineering Sciences, **149**, 71 (1935). doi:10.1098/rspa.1935.0048.

[6] W. L. Ginzburg and L. Landau. *On the theory of superconductivity (In Russian).* Zh. Eksp. Teor. Fiz., **20**, 1064 (1950).

[7] J. Bardeen, L. N. Cooper, and J. R. Schrieffer. *Microscopic theory of superconductivity.* Phys. Rev., **106**, 162 (1957). doi:10.1103/PhysRev.106.162.

[8] L. P. Gor'kov. *Microscopic derivation of the Ginzburg-Landau equations in the theory of superconductivity.* J. Exp. Theor. Phys., **9**, 1364 (1959).

[9] P. Kapitza. *Viscosity of liquid Helium below the λ-point.* Nature, **141**, 7 (1938).

[10] J. F. Allen and A. D. Misener. *Flow phenomena in liquid Helium II.* Nature, **142**, 643 (1938).

[11] D. D. Osheroff, R. C. Richardson, and D. M. Lee. *Evidence for a new phase of solid* He^3. Phys. Rev. Lett., **28**, 885 (1972). doi:10.1103/PhysRevLett.28.885.

[12] V. Ambegaokar and N. D. Mermin. *Thermal Anomalies of* He^3*: Pairing in a Magnetic Field.* Phys. Rev. Lett., **30**, 81 (1973). doi:10.1103/PhysRevLett.30.81.

[13] F. Steglich, J. Aarts, C. D. Bredl, W. Lieke, D. Meschede, W. Franz, and H. Schäfer. *Superconductivity in the presence of strong Pauli paramagnetism:* $CeCu_2Si_2$. Phys. Rev. Lett., **43**, 1892 (1979). doi:10.1103/PhysRevLett.43.1892.

[14] J. G. Bednorz and K. A. Müller. *Possible high* T_c *superconductivity in the* Ba–La–Cu–O *system.* Z. Phys. B, **64**, 189 (1986). doi:10.1007/BF01303701.

[15] S. S. Saxena, P. Agarwal, K. Ahilan, F. M. Grosche, R. K. W. Haselwimmer, M. J. Steiner, E. Pugh, I. R. Walker, S. R. Julian, P. Monthoux, G. G. Lonzarich, A. Huxley, I. Sheikin, D. Braithwaite, and J. Flouquet. *Superconductivity on the border of itinerant-electron ferromagnetism in* UGe_2. Nature, **406**, 587 (2000).

[16] D. Aoki, A. Huxley, E. Ressouche, D. Braithwaite, J. Flouquet, J.-P. Brison, E. Lhotel, and C. Paulsen. *Coexistence of superconductivity and ferromagnetism in* URhGe. Nature, **413**, 613 (2001).

[17] N. T. Huy, A. Gasparini, D. E. de Nijs, Y. Huang, J. C. P. Klaasse, T. Gortenmulder, A. de Visser, A. Hamann, T. Görlach, and H. v. Löhneysen. *Superconductivity on the Border of Weak Itinerant Ferromagnetism in* UCoGe. Phys. Rev. Lett., **99**, 067006 (2007). doi:10.1103/PhysRevLett.99.067006.

[18] T. C. Kobayashi, S. Fukushima, H. Hidaka, H. Kotegawa, T. Akazawa, E. Yamamoto, Y. Haga, R. Settai, and Y. Ōnuki. *Pressure-induced superconductivity in ferromagnet* UIr *without inversion symmetry.* Physica B, **378**, 355 (2006). doi:10.1016/j.physb.2006.01.126.

[19] C. Pfleiderer. *Superconducting phases of f-electron compounds.* Rev. Mod. Phys., **81**, 1551 (2009). doi:10.1103/RevModPhys.81.1551.

[20] A. D. Huxley. *Ferromagnetic superconductors.* Physica C, **514**, 368 (2015). doi:10.1016/j.physc.2015.02.026.

[21] K. Machida and T. Ohmi. *Phenomenological theory of ferromagnetic superconductivity.* Phys. Rev. Lett., **86**, 850 (2001). doi:10.1103/PhysRevLett.86.850.

[22] A. J. Leggett. *A theoretical description of the new phases of liquid* ^{3}He. Rev. Mod. Phys., **47**, 331 (1975). doi:10.1103/RevModPhys.47.331.

[23] P. W. Anderson and W. F. Brinkman. *Anisotropic Superfluidity in* ^{3}He*: A Possible Interpretation of Its Stability as a Spin-Fluctuation Effect.* Phys. Rev. Lett., **30**, 1108 (1973). doi:10.1103/PhysRevLett.30.1108.

[24] W. F. Brinkman, J. W. Serene, and P. W. Anderson. *Spin-fluctuation stabilization of anisotropic superfluid states.* Phys. Rev. A, **10**, 2386 (1974). doi:10.1103/PhysRevA.10.2386.

[25] A. Kołodziejczyk, B. V. B. Sarkissian, and B. R. Coles. *Magnetism and superconductivity in a transition metal compound:* Y_4Co_3. J. Phys. F: Met. Phys., **10**, L333 (1980).

[26] B. Wiendlocha, J. Tobola, S. Kaprzyk, and A. Kolodziejczyk. *Electronic structure, magnetism, and spin fluctuations in the superconducting weak ferromagnet* Y_4Co_3. Phys. Rev. B, **83**, 094408 (2011). doi:10.1103/PhysRevB.83.094408.

[27] M. Shimizu, A. Kunihara, and J. Inoue. *Electronic structure and magnetic properties of* Y_9Co_7 *intermetallic compound.* J. Phys. F: Met. Phys., **16**, 1263 (1986).

[28] A. K. Rastogi and B. R. Coles. *The magnetic character of* Y_9Co_7. J. Phys. F: Met. Phys., **15**, 1165 (1985).

[29] C. Pfleiderer, M. Uhlarz, S. M. Hayden, R. Vollmer, H. v. Löhneysen, N. R. Bernhoeft, and G. G. Lonzarich. *Coexistence of superconductivity and ferromagnetism in the d-band metal* $ZrZn_2$. Nature, **412**, 58 (2001).

[30] E. A. Yelland, S. M. Hayden, S. J. C. Yates, C. Pfleiderer, M. Uhlarz, R. Vollmer, H. v. Löhneysen, N. R. Bernhoeft, R. P. Smith, S. S. Saxena, and N. Kimura. *Superconductivity induced by spark erosion in* $ZrZn_2$. Phys. Rev. B, **72**, 214523 (2005). doi:10.1103/PhysRevB.72.214523.

[31] Y. Maeno, H. Hashimoto, K. Yoshida, S. Nishizaki, T. Fujita, J. G. Bednorz, and F. Lichtenberg. *Superconductivity in a layered perovskite without copper.* Nature, **372**, 532 (1994). doi:doi:10.1038/372532a0.

[32] A. P. Mackenzie and Y. Maeno. *The superconductivity of* Sr_2RuO_4 *and the physics of spin-triplet pairing.* Rev. Mod. Phys., **75**, 657 (2003). doi:10.1103/RevModPhys.75.657.

[33] J. F. Annett, B. L. Györffy, and K. I. Wysokiński. *Orbital magnetic moment of a chiral p-wave superconductor.* New J. Phys., **11**, 055063 (2009).

[34] K. I. Wysokiński, J. F. Annett, and B. L. Györffy. *Intrinsic Optical Dichroism in the Chiral Superconducting State of* Sr_2RuO_4. Phys. Rev. Lett., **108**, 077004 (2012). doi:10.1103/PhysRevLett.108.077004.

[35] M. Gradhand, K. I. Wysokiński, J. F. Annett, and B. L. Györffy. *Kerr rotation in the unconventional superconductor* Sr_2RuO_4. Phys. Rev. B, **88**, 094504 (2013). doi:10.1103/PhysRevB.88.094504.

[36] R. Joynt and L. Taillefer. *The superconducting phases of* UPt_3. Rev. Mod. Phys., **74**, 235 (2002). doi:10.1103/RevModPhys.74.235.

[37] A. B. Shick, V. Janiš, V. Drchal, and W. E. Pickett. *Spin and orbital magnetic state of* UGe_2 *under pressure.* Phys. Rev. B, **70**, 134506 (2004). doi:10.1103/PhysRevB.70.134506.

[38] C. Pfleiderer and A. D. Huxley. *Pressure Dependence of the Magnetization in the Ferromagnetic Superconductor* UGe_2. Phys. Rev. Lett., **89**, 147005 (2002). doi:10.1103/PhysRevLett.89.147005.

[39] V. Taufour, D. Aoki, G. Knebel, and J. Flouquet. *Tricritical point and wing structure in the itinerant ferromagnet* UGe_2. Phys. Rev. Lett., **105**, 217201 (2010). doi:10.1103/PhysRevLett.105.217201.

[40] M. M. Wysokiński, M. Abram, and J. Spałek. *Criticalities in the itinerant ferromagnet* UGe_2. Phys. Rev. B, **91**, 081108 (2015). doi:10.1103/PhysRevB.91.081108.

[41] H. Kotegawa, V. Taufour, D. Aoki, G. Knebel, and J. Flouquet. *Evolution toward Quantum Critical End Point in* UGe_2. J. Phys. Soc. Jpn., **80**, 083703 (2011). doi:10.1143/JPSJ.80.083703.

[42] I. Sheikin, A. Huxley, D. Braithwaite, J. P. Brison, S. Watanabe, K. Miyake, and J. Flouquet. *Anisotropy and pressure dependence of the upper critical field of the ferromagnetic superconductor* UGe_2. Phys. Rev. B, **64**, 220503 (2001). doi:10.1103/PhysRevB.64.220503.

[43] F. Lévy, I. Sheikin, B. Grenier, and A. D. Huxley. *Magnetic Field-Induced Superconductivity in the Ferromagnet* URhGe. Science, **309**, 1343 (2005). doi:10.1126/science.1115498.

[44] E. Slooten, T. Naka, A. Gasparini, Y. K. Huang, and A. de Visser. *Enhancement of Superconductivity near the Ferromagnetic Quantum Critical Point in* UCoGe. Phys. Rev. Lett., **103**, 097003 (2009). doi:10.1103/PhysRevLett.103.097003.

[45] R. Troć, Z. Gajek, and A. Pikul. *Dualism of the 5f electrons of the ferromagnetic superconductor* UGe_2 *as seen in magnetic, transport, and specific-heat data*. Phys. Rev. B, **86**, 224403 (2012). doi:10.1103/PhysRevB.86.224403.

[46] T. Hattori, Y. Ihara, Y. Nakai, K. Ishida, Y. Tada, S. Fujimoto, N. Kawakami, E. Osaki, K. Deguchi, N. K. Sato, and I. Satoh. *Superconductivity Induced by Longitudinal Ferromagnetic Fluctuations in* UCoGe. Phys. Rev. Lett., **108**, 066403 (2012). doi:10.1103/PhysRevLett.108.066403.

[47] Y. Tada, S. Fujimoto, N. Kawakami, T. Hattori, Y. Ihara, K. Ishida, K. Deguchi, N. K. Sato, and I. Satoh. *Spin-Triplet Superconductivity Induced by Longitudinal Ferromagnetic Fluctuations in* UCoGe*: Theoretical Aspect*. J. Phys.: Conf. Series, **449**, 012029 (2013). doi:10.1088/1742-6596/449/1/012029.

[48] B. Wu, G. Bastien, M. Taupin, C. Paulsen, L. Howald, D. Aoki, and J.-P. Brison. *Pairing mechanism in the ferromagnetic superconductor* UCoGe. Nat. Commun., **8**, 14480 (2017). doi:10.1038/ncomms14480.

[49] P. W. Anderson. *The resonating valence bond state in* La_2CuO_4 *and superconductivity*. Science, **235**, 1196 (1987). doi:10.1126/science.235.4793.1196.

[50] J. Spałek. *Microscopic model of hybrid pairing: A common appraoch to heavy-fermion and high-*T_c *superconductivity*. Phys. Rev. B, **38**, 208 (1988). doi:10.1103/PhysRevB.38.208.

[51] M. M. Wysokiński, M. Abram, and J. Spałek. *Ferromagnetism in* UGe_2*: A microscopic model*. Phys. Rev. B, **90**, 081114 (2014). doi:10.1103/PhysRevB.90.081114.

[52] M. Abram, M. M. Wysokiński, and J. Spałek. *Tricritical wings in* UGe_2*: A microscopic interpretation*. J. Magn. Magn. Mat., **400**, 27 (2016). doi:10.1016/j.jmmm.2015.07.017.

[53] P. Kubiczek. *Spin-triplet pairing in orbitally degenerate Anderson lattice model* (2016). MSc. Thesis, Jagiellonian University, Kraków, Poland.

[54] J. Jędrak, J. Kaczmarczyk, and J. Spałek. *Statistically-consistent Gutzwiller approach and its equivalence with the mean-field slave-boson method for correlated systems.* arXiv:1008.0021.

[55] J. Jędrak and J. Spałek. *Renormalized mean-field t-J model of high-T_c superconductivity: Comparison to experiment.* Phys. Rev. B, **83**, 104512 (2011). doi:10.1103/PhysRevB.83.104512.

[56] M. Zegrodnik, J. Spałek, and J. Bünemann. *Coexistence of spin-triplet superconductivity with magnetism within a single mechanism for orbitally degenerate correlated electrons: statistically consistent Gutzwiller approximation.* New J. Phys., **15**, 073050 (2013).

[57] M. Zegrodnik, J. Bünemann, and J. Spałek. *Even-parity spin-triplet pairing by purely repulsive interactions for orbitally degenerate correlated fermions.* New J. Phys., **16**, 033001 (2014).

[58] M. Abram, M. Zegrodnik, and J. Spałek. *Antiferromagnetism, charge density wave, and d -wave superconductivity in the extended t-J-U model: Role of intersite Coulomb interaction and a critical overview of renormalized mean field theory.* J. Phys.: Condens. Matter, **29**, 365602 (2017).

[59] O. Howczak and J. Spałek. *Anderson lattice with explicit Kondo coupling revisited: metamagnetism and the field-induced suppression of the heavy fermion state.* J. Phys.: Condens. Matter, **24**, 205602 (2012).

[60] O. Howczak, J. Kaczmarczyk, and J. Spałek. *Pairing by Kondo interaction and magnetic phases in the Anderson-Kondo lattice model: Statistically consistent renormalized mean-field theory.* Phys. Stat. Solidi (b), **250**, 609 (2013). doi:10.1002/pssb.201200774.

[61] M. M. Wysokiński, J. Kaczmarczyk, and J. Spałek. *Correlation-driven d-wave superconductivity in Anderson lattice model: Two gaps.* Phys. Rev. B, **94**, 024517 (2016). doi:10.1103/PhysRevB.94.024517.

[62] J. Spałek and P. Gopalan. *Exchange mediated pairing: Gap anisotropy and narrow-band limit for hybridized electrons.* J. Phys. France, **50**, 2869 (1989).

[63] E. Kądzielawa-Major and J. Spałek. *Anderson-Kondo lattice Hamiltonian from the Anderson-Lattice Model: A modified Schrieffer-Wolff transformation and the effective exchange interactions.* Acta Phys. Pol. A, **126**, 100 (2014).

[64] J. R. Schrieffer and P. A. Wolff. *Relation between the Anderson and Kondo Hamiltonians.* Phys. Rev., **149**, 491 (1966). doi:10.1103/PhysRev.149.491.

[65] S. Paschen and J. Larrea J. *Ordered Phases and Quantum Criticality in Cubic Heavy Fermion Compounds.* J. Phys. Soc. Jpn., **83**, 061004 (2014). doi:10.7566/JPSJ.83.061004.

[66] J. M. Lawrence and S. M. Shapiro. *Magnetic ordering in the presence of fast spin fluctuations: A neutron scattering study of* $Ce\mathrm{In}_3$. Phys. Rev. B, **22**, 4379 (1980). doi:10.1103/PhysRevB.22.4379.

[67] S. Doniach. *The Kondo lattice and weak antiferromagnetism.* Physica B+C, **91**, 231 (1977). doi:https://doi.org/10.1016/0378-4363(77)90190-5.

[68] B. Coqblin, J. Iglesias, N. Perkins, A. S. da R. Simoes, and C. Thomas. *Underscreened Kondo lattice model versus underscreened Anderson lattice model: Application to uranium compounds.* Physica B: Condensed Matter, **404**, 2961 (2009). doi:https://doi.org/10.1016/j.physb.2009.07.136.

[69] P. S. Riseborough, B. Coqblin, and S. G. Magalhães. *The underscreened anderson lattice: A model for uranium compounds.* J. Korean Phys. Soc., **62**, 1431 (2013). doi:10.3938/jkps.62.1431.

[70] A. Huxley, I. Sheikin, E. Ressouche, N. Kernavanois, D. Braithwaite, R. Calemczuk, and J. Flouquet. UGe_2*: A ferromagnetic spin-triplet superconductor.* Phys. Rev. B, **63**, 144519 (2001). doi:10.1103/PhysRevB.63.144519.

[71] N. Kernavanois, B. Grenier, A. Huxley, E. Ressouche, J. P. Sanchez, and J. Flouquet. *Neutron scattering study of the ferromagnetic superconductor* UGe_2. Phys. Rev. B, **64**, 174509 (2001). doi:10.1103/PhysRevB.64.174509.

[72] J. Spałek. *Spin-triplet superconducting pairing due to local Hund's rule and Dirac exchange.* Phys. Rev. B, **63**, 104513 (2001). doi:10.1103/PhysRevB.63.104513.

[73] R. Peierls. *On the theory of diamagnetism of conduction electrons.* Z. Phys., **80**, 763 (1933).

[74] D. R. Hofstadter. *Energy levels and wave functions of Bloch electrons in rational and irrational magnetic fields.* Phys. Rev. B, **14**, 2239 (1976). doi:10.1103/PhysRevB.14.2239.

[75] J. Bünemann, F. Gebhard, and R. Thul. *Landau-Gutzwiller quasiparticles.* Phys. Rev. B, **67**, 075103 (2003). doi:10.1103/PhysRevB.67.075103.

[76] M. C. Gutzwiller. *Effect of correlation on the ferromagnetism of transition metals.* Phys. Rev. Lett., **10**, 159 (1963). doi:10.1103/PhysRevLett.10.159.

[77] M. C. Gutzwiller. *Correlation of electrons in a narrow s band.* Phys. Rev., **137**, A1726 (1965). doi:10.1103/PhysRev.137.A1726.

[78] J. Kaczmarczyk, J. Spałek, T. Schickling, and J. Bünemann. *Superconductivity in the two-dimensional Hubbard model: Gutzwiller wave function solution.* Phys. Rev. B, **88**, 115127 (2013). doi:10.1103/PhysRevB.88.115127.

[79] J. Kaczmarczyk, J. Bünemann, and J. Spałek. *High-temperature superconductivity in the two-dimensional t-J model: Gutzwiller wavefunction solution.* New J. Phys., **16**, 073018 (2014).

[80] J. Kaczmarczyk. *Comparison of two approaches for the treatment of Gutzwiller variational wave functions.* Phil. Mag., **95**, 563 (2015). doi:10.1080/14786435.2014.965235.

[81] Y. Ōnuki, I. Ukon, S. W. Yun, I. Umehara, K. Satoh, T. Fukuhara, H. Sato, S. Takayanagi, M. Shikama, and A. Ochiai. *Magnetic and electrical properties of* U-Ge *intermetallic compounds.* J. Phys. Soc. Jpn., **61**, 293 (1992). doi:10.1143/JPSJ.61.293.

[82] E. Kądzielawa-Major, M. Fidrysiak, P. Kubiczek, and J. Spałek. *Spin-triplet paired phases inside ferromagnet induced by Hund's rule coupling and electronic correlations: Application to* UGe_2. arXiv:1712.08028.

[83] F. Gebhard. *Equivalence of variational and slave-boson mean-field treatments of the periodic Anderson model.* Phys. Rev. B, **44**, 992 (1991). doi:10.1103/PhysRevB.44.992.

[84] A. B. Shick and W. E. Pickett. *Magnetism, spin-orbit coupling, and superconducting pairing in* UGe_2. Phys. Rev. Lett., **86**, 300 (2001). doi:10.1103/PhysRevLett.86.300.

[85] M. Samsel-Czekała, M. Werwiński, A. Szajek, G. Chełkowska, and R. Troć. *Electronic structure of* UGe_2 *at ambient pressure: Comparison with X-ray photoemission spectra.* Intermetallics, **19**, 1411 (2011). doi:10.1016/j.intermet.2011.05.008.

[86] N. Tateiwa, T. C. Kobayashi, K. Amaya, Y. Haga, R. Settai, and Y. Ōnuki. *Heat-capacity anomalies at* T_{sc} *and* T^* *in the ferromagnetic superconductor* UGe_2. Phys. Rev. B, **69**, 180513 (2004). doi:10.1103/PhysRevB.69.180513.

[87] Z. P. Yin, K. Haule, and G. Kotliar. *Kinetic frustration and the nature of the magnetic and paramagnetic states in iron pnictides and iron chalcogenides.* Nature Materials, **10**, 932 (2011).

[88] J. Mravlje, M. Aichhorn, T. Miyake, K. Haule, G. Kotliar, and A. Georges. *Coherence-incoherence crossover and the mass-renormalization puzzles in* Sr_2RuO_4. Phys. Rev. Lett., **106**, 096401 (2011). doi:10.1103/PhysRevLett.106.096401.

[89] T. Kondo, M. Ochi, M. Nakayama, H. Taniguchi, S. Akebi, K. Kuroda, M. Arita, S. Sakai, H. Namatame, M. Taniguchi, Y. Maeno, R. Arita, and S. Shin. *Orbital-dependent band narrowing revealed in an extremely correlated Hund's metal emerging on the topmost layer of* Sr_2RuO_4. Phys. Rev. Lett., **117**, 247001 (2016). doi:10.1103/PhysRevLett.117.247001.

[90] K. A. Chao, J. Spałek, and A. M. Oleś. *Canonical perturbation expansion of the Hubbard model*. Phys. Rev. B, **18**, 3453 (1978). doi:10.1103/PhysRevB.18.3453.

[91] K. A. Chao, J. Spałek, and A. M. Oleś. *The kinetic exchange interaction in doubly degenerate narrow bands*. Phys. Stat. Solidi (b), **84**, 747 (1977). doi:10.1002/pssb.2220840241.

[92] J. Spałek and K. A. Chao. *Kinetic exchange interaction in a doubly degenerate narrow band and its application to* $Fe_{1-x}Co_xS_2$ *and* $Co_{1-x}Ni_xS_2$. J. Phys. C: Solid State Phys., **13**, 5241 (1980).

[93] I. Dzyaloshinsky. *A thermodynamic theory of "weak" ferromagnetism of antiferromagnetics*. J. Phys. Chem. Solids, **4**, 241 (1958). doi:https://doi.org/10.1016/0022-3697(58)90076-3.

[94] T. Moriya. *Anisotropic Superexchange Interaction and Weak Ferromagnetism*. Phys. Rev., **120**, 91 (1960). doi:10.1103/PhysRev.120.91.

[95] R. Žitko. *SNEG – Mathematica package for symbolic calculations with second-quantization-operator expressions*. Computer Physics Communications, **182**, 2259 (2011). doi:https://doi.org/10.1016/j.cpc.2011.05.013.

[96] P. W. Anderson. *Theory of dirty superconductors*. J. Phys. Chem. Solids, **11**, 26 (1959). doi:10.1016/0022-3697(59)90036-8.

[97] A. Ptok and D. Crivelli. *Influence of Finite Size Effects on the Fulde-Ferrell-Larkin-Ovchinnikov State*. Commun. Comput. Phys., **21**, 748–762 (2017). doi:10.4208/cicp.OA-2016-0041.

Spin-triplet paired phases inside ferromagnet induced by Hund's rule coupling and electronic correlations: Application to UGe_2

E. Kądzielawa-Major,[1,*] M. Fidrysiak,[1,†] P. Kubiczek,[2,‡] and J. Spałek[1,§]

[1] *Marian Smoluchowski Institute of Physics, Jagiellonian University, ul. Łojasiewicza 11, 30-348 Kraków, Poland*
[2] *I. Institut für Theoretische Physik, Universität Hamburg, Jungiusstraße 9, D-20355 Hamburg, Germany*

We discuss a mechanism of real-space spin-triplet pairing, alternative to spin fluctuations, and demonstrate its applicability to UGe_2. Both the Hund's rule ferromagnetic exchange and interelectronic correlations contribute to the same extent to the equal-spin pairing, particularly in the regime in which the weak-coupling solution does not provide any. The theoretical results, obtained within the orbitally-degenerate Anderson lattice model, match excellently the observed phase diagram for UGe_2 with the coexistent ferromagnetic (FM1) and superconducting (A_1-type) phase. Additionally, the A_2- and A-type paired phases appear in very narrow regions near the metamagnetic (FM2 $\rightarrow$ FM1) and FM1 $\rightarrow$ paramagnetic first-order phase-transition borders, respectively. The values of magnetic moments in the FM2 and FM1 states are also reproduced correctly.

Introduction.—The discovery of superconductivity (SC) in uranium compounds UGe_2 [1–3], URhGe [4], UCoGe [5], and UIr [6] that appears inside the ferromagnetic (FM) phase, but close to magnetic instabilities, has reinvoked the principal question concerning the mechanism of the spin-triplet pairing. The latter is particularly intriguing, since the spin-triplet SC [7–10] occurs relatively seldom in the correlated systems as compared to its spin-singlet analogue. More importantly, the circumstance that the paired state in both UGe_2 and UIr is absent on the paramagnetic (PM) side of the FM1$\rightarrow$PM discontinuous transition, suggests a specific mechanism providing on the same footing both the magnetic and SC counterparts. Moreover, SC is well established in one particular (FM1) magnetic phase, but not in FM2 or PM phases, where the magnetic moment is either almost saturated or vanishes, respectively. These circumstances pose a stringent test on any pairing mechanism.

The spin-triplet SC mediated by the quantum spin fluctuations has been invoked [11, 12] and tested for UCoGe [13–15] that represents the systems with very low magnetic moments ($m \sim 0.039\,\mu_B$/U [13, 16]) and thus is particularly amenable to the fluctuations in both the weakly-ordered FM and PM regimes. From this perspective, UGe_2 possesses a relatively large magnetic moment in FM1 phase ($m \sim 1\,\mu_B$/U), and in the low-pressure FM2 phase it is even larger ($m \sim 1.5\,\mu_B$/U) [3]. In such a situation a natural idea arises that in this case local correlation effects should become much more pronounced than in UCoGe. Closely related to this is the question of real-space spin-triplet pairing applicability, considered before as relevant to the orbitally-degenerate correlated narrow-band systems [17–25], which in turn is analogous to the spin-singlet pairing proposed for the high-temperature [26–29] and heavy-fermion [30] superconductors.

Here we put forward the idea of the correlation-induced pairing and test it for the case of UGe_2. To implement that program we generalize our approach, applied earlier [31–33] to explain the magnetic properties of UGe_2, and incorporate this specific type of the coexistent SC into that picture. Explicitly, we extend the spin-triplet pairing concepts, originally introduced for the case of multiorbital narrow-band systems [17–23], by including the Hund's rule coupling combined with intraatomic correlations within the orbitally-degenerate Anderson lattice model (ALM), and treat it within the statistically consistent version of the renormalized mean-field theory (SGA [31–33]). In this manner, we demonstrate, in quantitative terms, the applicability of the concept of even-parity, spin-triplet pairing to UGe_2. Furthermore, we provide also a detailed analysis of the two very narrow border regions FM2-FM1 and FM1-PM, in which the A_2-type SC transforms to A_1 and from A_1 to A, respectively, before SC disappears altogether (the notation of the SC phases is analogous to that used for superfluid ^{3}He [34]).

The present mechanism may be regarded as complementary to the reciprocal-space pairing by quantum spin fluctuations which was very successful in explaining the properties of the superfluid ^{3}He [35, 36]. The latter mechanism was also applied to ferromagnets with magnetic moment fluctuations, both on the weakly-FM and PM sides [37, 38]. Specifically, the role of their longitudinal component was emphasized. However, all those considerations have been limited to a single-band situation and therefore, SC is invariably of the p-wave character.

Model and method.—We start with doubly degenerate f states and assume two-dimensional structure of the compound [39, 40]. Within our model, the total number of electrons per formula unit $n^{\rm tot} \equiv n^f + n^c$, with n^f and n^c being the f and conduction (c) electron occupancies, must be exceeding that on $5f$ level for U^{3+} ion [7, 41, 42], i.e., $n > 3$. The best comparison with experiment is here achieved for $n^{\rm tot} \simeq 3.25$. This presumption brings into mind the idea of an orbitally selective localization of one of the three $5f$ electrons under pressure (see below).

Explicitly, we employ a four-orbital ALM defined by the Hamiltonian (with the chemical potential term $-\mu\hat{N}_e$

included)

$$\mathcal{H}-\mu\hat{N}_e = \sum_{ijl\sigma} t_{ij}\hat{c}^{(l)\dagger}_{i\sigma}\hat{c}^{(l)}_{j\sigma} + V\sum_{il\sigma}\left(\hat{f}^{(l)\dagger}_{i\sigma}\hat{c}^{(l)}_{i\sigma} + \text{H.c.}\right) + \\ + \epsilon^f\sum_{il}\hat{n}^{f(l)}_i + U\sum_{il}\hat{n}^{f(l)}_{i\uparrow}\hat{n}^{f(l)}_{i\downarrow} + U'\sum_i \hat{n}^{f(1)}_i\hat{n}^{f(2)}_i - \\ - 2J\sum_i\left(\hat{\mathbf{S}}^{f(1)}_i\cdot\hat{\mathbf{S}}^{f(2)}_i + \frac{1}{4}\hat{n}^{f(1)}_i\hat{n}^{f(2)}_i\right) - \mu\hat{N}_e, \quad (1)$$

involving two f-orbitals (with creation operators $\hat{f}^{(l)\dagger}_{i\sigma}$ with $l = 1, 2$ at lattice site i and spin $\sigma =\uparrow,\downarrow$), hybridized with two species of conduction electrons created by $\hat{c}^{(l)\dagger}_{i\sigma}$ (minimally two c bands are needed, as otherwise one of the f-orbitals decouples and does not participate in the resultant quasiparticle states [43]). Out of general hopping matrix t_{ij} we retain nearest- and next-nearest neighbor hoppings (t, t') and assume local character of f-c hybridization V. Correlations in the f-electron sector are governed by intra-orbital f-f repulsion U, inter-orbital repulsion U', and Hund's coupling J. Here $\hat{n}^{f(l)}_i$, $\hat{\mathbf{S}}^{f(l)}_i$ denote the f-electron number and spin operators on site i, whereas $\hat{N}_e$ is the total particle number. Hereafter, we restrict ourselves to the case of $U' = U - 2J$, $U/|t| = 3.5$, and $t'/|t| = 0.25$.

The SGA approach is based on optimization of the ground state energy within the class of wave functions with partially projected-out double f-orbital occupancies, and can be formulated in terms of effective one-body Hamiltonian

$$\mathcal{H}_{\text{eff}} = \sum_{\mathbf{k},\sigma}\Psi^\dagger_{\mathbf{k}\sigma}\begin{pmatrix} \epsilon_{\mathbf{k}} & 0 & q_\sigma V & 0 \\ 0 & -\epsilon_{\mathbf{k}} & 0 & -q_\sigma V \\ q_\sigma V & 0 & \epsilon^f_\sigma & \Delta^{ff}_{\sigma\sigma} \\ 0 & -q_\sigma V & \Delta^{ff}_{\sigma\sigma} & -\epsilon^f_\sigma \end{pmatrix}\Psi_{\mathbf{k}\sigma} + E_0, \quad (2)$$

derived from the model of Eq. (1) [44]. In Eq. (2) $\Psi^\dagger_{\mathbf{k}\sigma} = \left(\hat{c}^{(1)\dagger}_{\mathbf{k}\sigma}, \hat{c}^{(2)}_{-\mathbf{k}\sigma}, \hat{f}^{(1)\dagger}_{\mathbf{k}\sigma}, \hat{f}^{(2)}_{-\mathbf{k}\sigma}\right)$, $\epsilon_{\mathbf{k}}$ denotes bare c-electron dispersion relation, ϵ^f_σ is an effective f-level, $\Delta^{ff}_{\sigma\sigma} \equiv \mathcal{V}_\sigma\langle\hat{f}^{(1)}_{i\sigma}\hat{f}^{(2)}_{i\sigma}\rangle$ is the f-f equal-spin SC gap parameter, $\mathcal{V}_\sigma \equiv -U'g_{1\sigma} + (J-U')g_{2\sigma}$ denotes effective pairing coupling, and E_0 is a constant. The renormalization factors q_σ, $g_{1\sigma}$, and $g_{2\sigma}$ account for the correlation effects and originate from projection of the trial wave functions (see [44] for explicit expressions).

The basic quantity determined from the diagonalization of $\mathcal{H}_{\text{eff}}$ (see [44]) is the quasiparticle gap $\Delta_{\mathbf{k}}$. For wave vectors lying on the Fermi surface of the normal-state, one obtains

$$\Delta^2_{\mathbf{k}} = \frac{\epsilon^2_{\mathbf{k}}}{(\epsilon_{\mathbf{k}} + \epsilon^f_\sigma)^2}\times(\Delta^{ff}_{\sigma\sigma})^2 + o[(\Delta^{ff}_{\sigma\sigma})^2], \quad (3)$$

so $\Delta_{\mathbf{k}}$ is expressed in terms $\Delta^{ff}_{\sigma\sigma}$ and a weakly $\mathbf{k}$-dependent factor. Therefore, in the remaining discussion we use the latter gap, underlying in this manner the dominant role of f-f pairing.

The quantity particularly relevant to the present discussion, is the equal-spin coupling constant $\mathcal{V}_\sigma$. If positive, this term favors equal-spin triplet SC. We also define the Hartree-Fock (HF/BCS) coupling constant $\mathcal{V}_{\text{HF}} = J - U'$, independently of the spin direction. In the latter approximation the interatomic interaction is attractive when $J - U' = 3J - U > 0$ (this condition defines the BCS limit). One of the principal signatures of correlation importance is that *pairing persists even when the coupling* $\mathcal{V}_{\text{HF}}$ *becomes repulsive* ($\mathcal{V}_{\text{HF}} < 0$) as we show below. The conditions $\mathcal{V}_{\text{HF}} < 0$ and $\mathcal{V}_\sigma > 0$ define the regime of correlation-driven SC.

Results.— The complete phase diagram encompassing both FM and SC states, for selection of Hund's coupling $J/|t| = 1.1$, is shown in Fig. 1. In panel (a) we exhibit the system evolution from the large-moment FM2 phase, through FM1 state with a magnetization plateau at $\sim 0.8\mu_B$ (as compared to $\sim 1\mu_B$ measured for UGe_2 [3]), to the PM phase, as the hybridization magnitude $|V|$ increases. Here changing $|V|$ mimics its pressure variation. Both FM2→FM1 and FM1→PM transitions are of the first order as is observed in UGe_2 below the critical end-point, though the FM2→FM1 transition is of weak-first-order due to proximity to the quantum tricritical point [32] [see panel (d)]. Notably, our model also provides the value of magnetic moment $m \sim 1.6\,\mu_B$ in FM2 phase, close to the experimental $m \approx 1.45\,\mu_B$ [3].

The novel feature, inherent to the degenerate ALM and the principal result of present paper, is the emergence of distinct even-parity spin-triplet SC phases appearing around the magnetic transition points and characterized by non-zero SC gap parameters $\Delta^{ff}_{\sigma\sigma} \equiv \mathcal{V}_\sigma\langle\hat{f}^{(1)}_{i\sigma}\hat{f}^{(2)}_{i\sigma}\rangle_0$, as depicted in Fig. 1(b). The A_1-type SC (i.e., the majority-spin gap $\Delta^{ff}_{\uparrow\uparrow} = 0$ and $\Delta^{ff}_{\downarrow\downarrow} \neq 0$) sets in inside the FM1 phase and transforms to either A_2 phase ($\Delta^{ff}_{\downarrow\downarrow} > \Delta^{ff}_{\uparrow\uparrow} \neq 0$) at FM2-FM1 border or to A state ($\Delta^{ff}_{\uparrow\uparrow} = \Delta^{ff}_{\downarrow\downarrow} \neq 0$) close to the FM1→PM transition point. The latter two states appear in very narrow regions, as illustrated in Fig. 1(e) and (f). The A_2-phase gap is by an order of magnitude smaller than its A_1 counterpart, whereas the A-phase gap is by even four orders of magnitude smaller. Hence, one can safely say that the A_1 phase is so far the only one observable for UGe_2; the A_2 state could be detectable. Note also that the pairing potential $\mathcal{V}_\downarrow$ is maximal near the metamagnetic transition [cf. Fig. 1(c)]. Remarkably, this situation appears without any spin fluctuations involved, which distinguishes the present mechanism from those invoked previously for the U-compounds [12–14]. In the inset of Fig. 1(b), we plot the specific-heat discontinuity (the shaded area) and the related magnetization jumps ob-

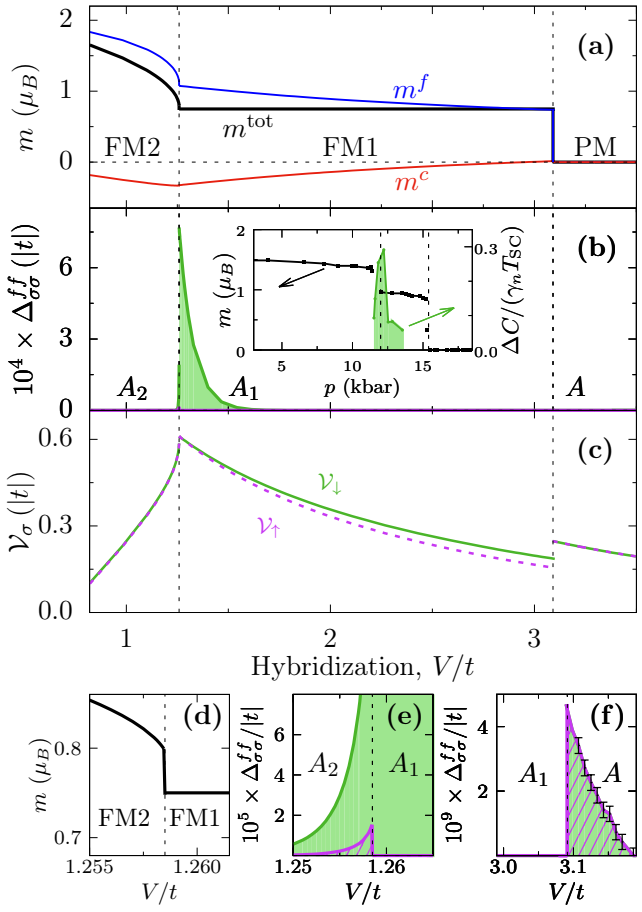

FIG. 1. Calculated zero-temperature phase diagram of UGe_2 for Hund's coupling $J/|t| = 1.1$ versus f-c hybridization V. The remaining parameters read: $t'/|t| = 0.25$, $U/|t| = 3.5$, $\epsilon^f/|t| = -4$, and $n^{\rm tot} = 3.25$. (a) Total magnetic moment $m^{\rm tot}$ per formula unit (black solid line), and the corresponding f and c electron magnetization m^f and m^c (blue and red lines, respectively). m^c represents a residual Kondo compensating cloud. (b) Triplet f-f SC gap component $\Delta^{ff}_{\uparrow\uparrow}$ (purple shading) and $\Delta^{ff}_{\downarrow\downarrow}$ (green shading). Three distinct SC phases A_2, A_1, and A are marked. The A-phase gaps ($\sim 10^{-9}|t|$) are not visible in panel (b). Inset shows experimental magnetization for UGe_2 [3] and the specific-heat jump at the SC transition temperature $T_{\rm SC}$ (normalized by $T_{\rm SC}$ and the linear specific-heat coefficient γ_n) [45]. (c) Effective coupling constant $\mathcal{V}_\sigma$ for spin-up (purple) and spin-down (green) triplet pairing. Note that value of coupling is the largest near the $A_2 \to A_1$ transition. (d) Total magnetic moment near the FM2→FM1 metamagnetic transition. (e)-(f) SC gap components near the FM2→FM1 and FM1→PM transition points, respectively.

served experimentally. The peaks identify the regime of bulk SC; these sharp features are reproduced by our calculation [cd. Fig. 1(b)] and should be contrasted with the first resistivity data [1]. Note also that we obtain small, but clear SC gap discontinuities at both $A_2 \to A_1$ and $A_1 \to A$ transitions (cf. Fig. 1(e) and (f), respectively). We emphasize that all the singularities are physically meaningful and within the numerical accuracy (error bars are shown explicitly for the A phase having the smallest gap magnitude). The question is whether those effects could be observed.

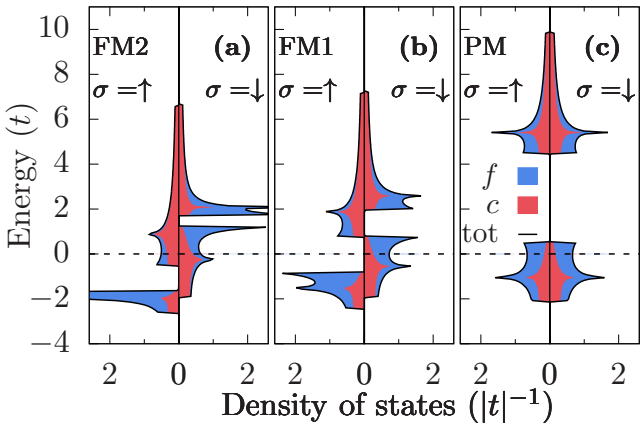

FIG. 2. Spin- and orbital-resolved density of states for $J/|t| = 1.1$ in the (a) FM2 ($V/t = 1.1$), (b) FM1 ($V/t = 1.625$), and (c) PM ($V/t = 3.25$) phases. Orbital contributions are marked in blue and red, whereas the total density of states is plotted by black solid line. Dirac-delta functions have been smeared out by $\epsilon = 10^{-3}|t|$ for numerical purposes.

The nature of FM2 and FM1 phases can be understood by inspection of the corresponding spin- and orbital-resolved densities of states exhibited in Fig. 2. In FM2 state [Fig. 2(a)] f-electrons are close to localization and well below the Fermi energy ϵ_F as they carry out nearly saturated magnetic moments, whereas in FM1 phase [Fig. 2(b)] ϵ_F is placed in the region of spin-down electrons, stabilizing the magnetization plateau (and illustrating the *half-metallic character*), hence only $\Delta^{ff}_{\downarrow\downarrow} \neq 0$. Similar evolution of magnetism has been observed previously for the orbitally non-degenerate model [31–33]. Fig. 2(c) illustrates paramagnetic behavior.

Next, we discuss the fundamental role of the effective pairing potential. Explicitly, in Fig. 3(a) we have plotted renormalized and bare coupling constants as a function of J for $V/t = 1.32$. The dominant component $\mathcal{V}_\downarrow$ remains positive down to $J/|t| \approx 0.76$, whereas the HF/BCS coupling changes sign already for $J/|t| = 3.5/3 \approx 1.17$. Electronic correlations are thus the crucial factor stabilizing the triplet SC close to the FM2-FM1 boundary. Fig. 3(b) shows the dominant gap component for selected values of J. The gap increases very rapidly with the increasing Hund's rule coupling, as detailed in Fig. 3(c), where we plot logarithm of the normalized gap, $\ln(\Delta^{ff}_{\downarrow\downarrow}/\mathcal{V}_\downarrow)$ vs $(\rho_{\epsilon_F}\mathcal{V}_\downarrow)^{-1}$ for fixed hybridization $V/t = 1.32$ that corresponds to the A_1 phase (ρ_{ϵ_F} is the total density of states per f-orbital per spin at ϵ_F). A good linear scaling is observed with the coefficient ≈ -1.08, not to far from the BCS value -1. The binding of f-electrons into local

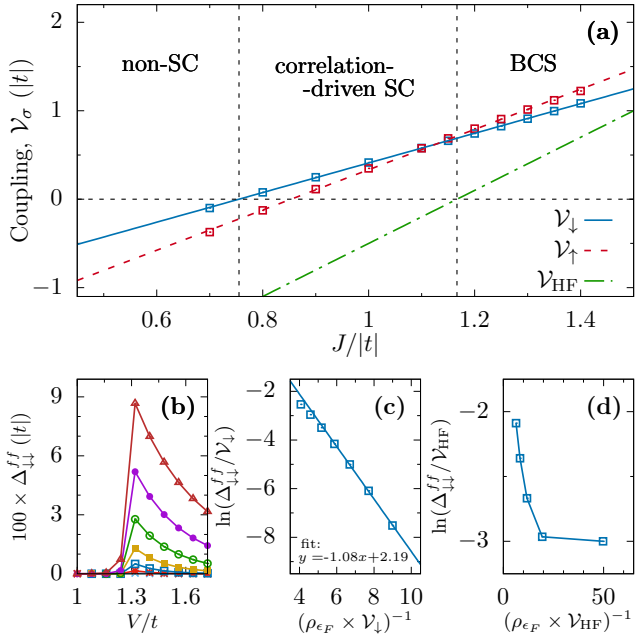

FIG. 3. (a) Dependence of $\mathcal{V}_\sigma$ on the Hund's coupling J for $V/t = 1.32$ (solid blue and dashed red lines). For comparison, the value of the Hartree-Fock (HF/BCS) coupling constant $\mathcal{V}_{\rm HF}$ is also shown by green dash-dotted line. Black dashed vertical lines split the plot into three regions: non-SC, correlation-driven (where SC is not supported at the HF/BCS level, yet is appears due to correlation effects), and BCS regime (where SC phase emerges in the HF/BCS approximation). Note that the value $J/|t| = 1.1$, considered above, falls into the correlation-driven regime. (b) Hybridization-dependence of the SC gap component $\Delta^{ff}_{\downarrow\downarrow}$ for various J near the FM2→FM1 transition. Values of $J/|t|$ (from top to bottom) are 1.4, 1.35, 1.3, 1.25, 1.2, 1.15, and 1.1. (c) Scaling of $\Delta^{ff}_{\downarrow\downarrow}$ with the dimensionless effective coupling $\rho_{\epsilon_F}\mathcal{V}_\downarrow$. Here ρ_{ϵ_F} denotes total density of states per f-orbital per spin, evaluated at the Fermi energy in the normal phase. The gap follows renormalized BCS scaling $\Delta^{ff}_{\downarrow\downarrow} \propto \mathcal{V}_\downarrow \times \exp(-(\rho_{\epsilon_F}\mathcal{V}_\downarrow)^{-1})$. (d) The same as in (c), but with HF/BCS coupling $\mathcal{V}_{\rm HF}$ used instead of $\mathcal{V}_\downarrow$. Breakdown of BCS scaling implies relevance of the correlation-driven coupling renormalization.

triplet pairs is provided partly by the Hund's rule exchange that yields the HF/BCS potential $\mathcal{V}_{\rm HF} = 3J - U$. Fig. 3(d) shows the same as Fig. 3(c), but $\mathcal{V}_{\rm HF}$ has been taken in place of $\mathcal{V}_\sigma$. The breakdown of the scaling implies there a significant effect of local correlations over the Hund's-rule induced pairing.

Discussion.—To underline the quantitative aspect of our analysis of the SC phase we have determined the temperature dependence of the gap in the combined FM1+A_1 state for $J/|t| = 1.1$ and $V/t = 1.3$, i.e., near the gap-maximum point depicted in Fig. 1(b). Selecting the value of $|t| = 0.5\,$eV, we obtain SC critical temperature $T_{\rm SC} \approx 0.92\,$K [44], very close to the experimental value $T_{\rm SC} \sim 0.75\,$K in the highest-quality samples [46].

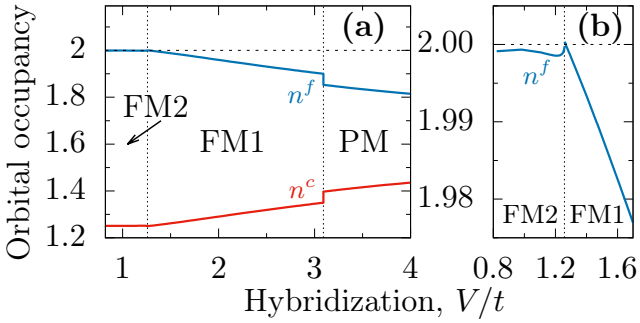

FIG. 4. (a) Occupancies of the f- and c-orbitals as a function of hybridization. (b) Close-up of the FM2→FM1 transition.

Note that for $J \lesssim 1.17|t|$ we do not expect any SC in the HF/BCS approximation. It is gratifying that the value of $J = 1.1|t| = 0.55\,$eV can lead to such a subtle SC temperature scale $T_{\rm SC} < 1\,$K in the situation, where the FM transition temperature T_c is by two orders of magnitude larger or even higher. Equally important is the obtained value of specific-heat jump $\Delta C/(\gamma_n T_{\rm SC}) \simeq 1.44$ (cf. Fig. 2. in [44]), i.e., very close to the BCS value 1.43. Parenthetically, this is not too far from experimental $\Delta C/(\gamma_n - \gamma_0)/T_{\rm SC} \simeq 0.97$ for pressure 1.22 GPa [45] (corresponding closely to our choice of parameters) if we subtract the residual Sommerfeld coefficient γ_0.

The U^{3+} ionic configuration is $5f^3$. Some experimental evidence points to the value close to U^{4+} ($5f^2$) [7, 41]. Here the good values of magnetic moments in both FM2 and FM1 phases are obtained for approximate $5f^2$ configuration and $n^c \approx 1.25$ conduction electrons, as shown in Fig. 4(a). Namely, the results in Fig. 4(b) point clearly to the value $n^f \approx 2$ in FM2 phase and it diminishes almost linearly in FM1 state. Such a behavior explains that the two f-electrons are practically localized in the FM2 phase and therefore, no SC state induced by the Hund's rule and f-f correlations can be expected. On the other hand, the correlations are weaker on the PM side due to substantially larger hybridization and, once again, SC disappears. These results suggest that here the third f-electron may have become selectively itinerant and thus is weakly correlated with the remaining two. It is tempting to ask about its connection with the residual value of γ_0.

In summary, our theoretical phase diagram reproduces the fundamental features observed experimentally in a semiquantitative manner. Within the double-degenerate Anderson lattice model in the statistically consistent renormalized mean-field approximation (SGA), we have analyzed in detail the coexisting FM1, spin-triplet SC phase, having in mind the unique experimental results for UGe_2. Further specific material properties of UGe_2 and related systems can be drawn by incorporating the angular dependence of the hybridization, more realistic multi-orbital structure, as well as the third-dimension.

This work was supported by MAESTRO Grant No. DEC-2012/04/A/ST3/00342 from Narodowe Centrum Nauki (NCN).

* ewa.kadzielawa@doctoral.uj.edu.pl
† maciej.fidrysiak@uj.edu.pl
‡ patryk.kubiczek@physik.uni-hamburg.de
§ jozef.spalek@uj.edu.pl

[1] S. S. Saxena, P. Agarwal, K. Ahilan, F. M. Grosche, R. K. W. Haselwimmer, M. J. Steiner, E. Pugh, I. R. Walker, S. R. Julian, P. Monthoux, G. G. Lonzarich, A. Huxley, I. Sheikin, D. Braithwaite, and J. Flouquet, "Superconductivity on the border of itinerant-electron ferromagnetism in UGe_2," Nature **406**, 587 (2000).

[2] N. Tateiwa, T. C. Kobayashi, K. Hanazono, K. Amaya, Y. Haga, R. Settai, and Y. Onuki, "Pressure-induced superconductivity in a ferromagnet UGe_2," J. Phys.: Condens. Matter **13**, L17 (2001).

[3] C. Pfleiderer and A. D. Huxley, "Pressure dependence of the magnetization in the ferromagnetic superconductor UGe_2," Phys. Rev. Lett. **89**, 147005 (2002).

[4] D. Aoki, A. Huxley, E. Ressouche, D. Braithwaite, J. Flouquet, J.-P. Brison, E. Lhotel, and C. Paulsen, "Coexistence of superconductivity and ferromagnetism in URhGe," Nature **413**, 613 (2001).

[5] N. T. Huy, A. Gasparini, D. E. de Nijs, Y. Huang, J. C. P. Klaasse, T. Gortenmulder, A. de Visser, A. Hamann, T. Görlach, and H. v. Löhneysen, "Superconductivity on the border of weak itinerant ferromagnetism in UCoGe," Phys. Rev. Lett. **99**, 067006 (2007).

[6] T. C. Kobayashi, S. Fukushima, H. Hidaka, H. Kotegawa, T. Akazawa, E. Yamamoto, Y. Haga, R. Settai, and Y. Onuki, "Pressure-induced superconductivity in ferromagnet UIr without inversion symmetry," Physica B **378**, 355 (2006).

[7] C. Pfleiderer, "Superconducting phases of f-electron compounds," Rev. Mod. Phys. **81**, 1551 (2009).

[8] D. Aoki and J. Flouquet, "Ferromagnetism and superconductivity in uranium compounds," J. Phys. Soc. Japan **81**, 011003 (2012).

[9] A. P. Mackenzie and Y. Maeno, "The superconductivity of Sr_2RuO_4 and the physics of spin-triplet pairing," Rev. Mod. Phys. **75**, 657 (2003).

[10] A. D. Huxley, "Ferromagnetic superconductors," Physica C **514**, 368 (2015).

[11] P. Coleman, "Superconductivity: On the verge of magnetism," Nature **406**, 580 (2000).

[12] K. G. Sandeman, G. G. Lonzarich, and A. J. Schofield, "Ferromagnetic superconductivity driven by changing Fermi surface topology," Phys. Rev. Lett. **90**, 167005 (2003).

[13] T. Hattori, Y. Ihara, Y. Nakai, K. Ishida, Y. Tada, S. Fujimoto, N. Kawakami, E. Osaki, K. Deguchi, N. K. Sato, and I. Satoh, "Superconductivity Induced by Longitudinal Ferromagnetic Fluctuations in UCoGe," Phys. Rev. Lett. **108**, 066403 (2012).

[14] Y. Tada, S. Fujimoto, N. Kawakami, T. Hattori, Y. Ihara, K. Ishida, K. Deguchi, N. K. Sato, and I. Satoh, "Spin-Triplet Superconductivity Induced by Longitudinal Ferromagnetic Fluctuations in UCoGe: Theoretical Aspect," J. Phys.: Conf. Series **449**, 012029 (2013).

[15] B. Wu, G. Bastien, M. Taupin, C. Paulsen, L. Howald, D. Aoki, and J.-P. Brison, "Pairing mechanism in the ferromagnetic superconductor UCoGe," Nat. Commun. **8**, 14480 (2017).

[16] N. K. Sato, K. Deguchi, K. Imura, N. Kabeya, N. Tamura, and K. Yamamoto, "Correlation of Ferromagnetism and Superconductivity in UCoGe," AIP Conf. Proc. **1347**, 132–137 (2011).

[17] J. Spałek, "Spin-triplet superconducting pairing due to local Hund's rule and Dirac exchange," Phys. Rev. B **63**, 104513 (2001).

[18] A. Klejnberg and J. Spałek, "Hund's rule coupling as the microscopic origin of the spin-triplet pairing in a correlated and degenerate band system," J. Phys.: Condens. Matter **11**, 6553 (1999).

[19] J. Spałek, P. Wróbel, and W. Wójcik, "Coexistence of Spin-Triplet Superconductivity and Ferromagnetism Induced by the Hund's Rule Exchange," in *Ruthenate and Rutheno-Cuprate Materials*, Lecture Notes in Physics, Berlin Springer Verlag, Vol. 603, edited by C. Noce, A. Vecchione, M. Cuoco, and A. Romano (2002) pp. 60–75.

[20] J. Spałek and M. Zegrodnik, "Spin-triplet paired state induced by Hund's rule coupling and correlations: a fully statistically consistent Gutzwiller approach," J. Phys.: Condens. Matter **25**, 435601 (2013).

[21] M. Zegrodnik, J. Spałek, and J. Bünemann, "Coexistence of spin-triplet superconductivity with magnetism within a single mechanism for orbitally degenerate correlated electrons: statistically consistent Gutzwiller approximation," New J. Phys. **15**, 073050 (2013).

[22] M. Zegrodnik, J. Bünemann, and J. Spałek, "Even-parity spin-triplet pairing by purely repulsive interactions for orbitally degenerate correlated fermions," New J. Phys. **16**, 033001 (2014).

[23] J. E. Han, "Spin-triplet s-wave local pairing induced by Hund's rule coupling," Phys. Rev. B **70**, 054513 (2004).

[24] S. Hoshino and P. Werner, "Superconductivity from emerging magnetic moments," Phys. Rev. Lett. **115**, 247001 (2015).

[25] X. Dai, Z. Fang, Y. Zhou, and F.-C. Zhang, "Even parity, orbital singlet, and spin triplet pairing for superconducting $LaFeAsO_{1-x}F_x$," Phys. Rev. Lett. **101**, 057008 (2008).

[26] P. W. Anderson, P. A. Lee, M. Randeria, T. M. Rice, N. Trivedi, and F. C. Zhang, "The physics behind high-temperature superconducting cuprates: the 'plain vanilla' version of RVB," Journal of Physics: Condensed Matter **16**, R755 (2004).

[27] J. Jędrak and J. Spałek, "Renormalized mean-field t-J model of high-T_c superconductivity: Comparison to experiment," Phys. Rev. B **83**, 104512 (2011).

[28] J. Kaczmarczyk, J. Bünemann, and J. Spałek, "High-temperature superconductivity in the two-dimensional t-J model: Gutzwiller wavefunction solution," New J. Phys. **16**, 073018 (2014).

[29] J. Spałek, M. Zegrodnik, and J. Kaczmarczyk, "Universal properties of high-temperature superconductors from real-space pairing: t-J-U model and its quantitative comparison with experiment," Phys. Rev. B **95**, 024506 (2017).

[30] M. M. Wysokiński, J. Kaczmarczyk, and J. Spałek, "Correlation-driven d-wave supercon-

ductivity in Anderson lattice model: Two gaps," Phys. Rev. B **94**, 024517 (2016).
[31] M. M. Wysokiński, M. Abram, and J. Spałek, "Ferromagnetism in UGe_2: A microscopic model," Phys. Rev. B **90**, 081114 (2014).
[32] M. M. Wysokiński, M. Abram, and J. Spałek, "Criticalities in the itinerant ferromagnet UGe_2," Phys. Rev. B **91**, 081108 (2015).
[33] M. Abram, M. M. Wysokiński, and J. Spałek, "Tricritical wings in UGe_2: A microscopic interpretation," J. Magn. Magn. Mat. **400**, 27 (2016).
[34] J. C. Wheatley, "Experimental properties of superfluid ^{3}He," Rev. Mod. Phys. **47**, 415–470 (1975).
[35] P. W. Anderson and W. F. Brinkman, "Anisotropic superfluidity in ^{3}He: A possible interpretation of its stability as a spin-fluctuation effect," Phys. Rev. Lett. **30**, 1108 (1973).
[36] W. F. Brinkman, J. W. Serene, and P. W. Anderson, "Spin-fluctuation stabilization of anisotropic superfluid states," Phys. Rev. A **10**, 2386 (1974).
[37] D. Fay and J. Appel, "Coexistence of p-state superconductivity and itinerant ferromagnetism," Phys. Rev. B **22**, 3173 (1980).
[38] P. Monthoux and G. G. Lonzarich, "p-wave and d-wave superconductivity in quasi-two-dimensional metals," Phys. Rev. B **59**, 14598 (1999).
[39] A. B. Shick and W. E. Pickett, "Magnetism, Spin-Orbit Coupling, and Superconducting Pairing in UGe_2," Phys. Rev. Lett. **86**, 300 (2001).
[40] A. B. Shick, V. Janiš, V. Drchal, and W. E. Pickett, "Spin and orbital magnetic state of UGe_2 under pressure," Phys. Rev. B **70**, 134506 (2004).
[41] R. Troć, Z. Gajek, and A. Pikul, "Dualism of the $5f$ electrons of the ferromagnetic superconductor UGe_2 as seen in magnetic, transport, and specific-heat data," Phys. Rev. B **86**, 224403 (2012).
[42] M. Samsel-Czekała, M. Werwiński, A. Szajek, G. Chełkowska, and R. Troć, "Electronic structure of UGe_2 at ambient pressure: Comparison with X-ray photoemission spectra," Intermetallics **19**, 1411 (2011).
[43] J. Spałek, D. K. Ray, and M. Acquarone, "A hybridized basis for simple band structures," Sol. Stat. Commun. **56**, 909 (1985).
[44] See Supplemental Material for details.
[45] N. Tateiwa, T. C. Kobayashi, K. Amaya, Y. Haga, R. Settai, and Y. Ōnuki, "Heat-capacity anomalies at T_{sc} and T^* in the ferromagnetic superconductor UGe_2," Phys. Rev. B **69**, 180513 (2004).
[46] A. Harada, S. Kawasaki, H. Mukuda, Y. Kitaoka, Y. Haga, E. Yamamoto, Y. Ōnuki, K. M. Itoh, E. E. Haller, and H. Harima, "Experimental evidence for ferromagnetic spin-pairing superconductivity emerging in UGe_2: A ^{73}Ge-nuclear-quadrupole-resonance study under pressure," Phys. Rev. B **75**, 140502 (2007).
[47] M. C. Gutzwiller, "Effect of correlation on the ferromagnetism of transition metals," Phys. Rev. Lett. **10**, 159–162 (1963).
[48] P. Kubiczek, "Spin-triplet pairing in orbitally degenerate Anderson lattice model," (2016), MSc. Thesis, Jagiellonian University, Kraków, Poland.
[49] J. Bünemann, T. Schickling, and F. Gebhard, "Variational study of Fermi surface deformations in Hubbard models," Europhys. Lett. **98**, 27006 (2012).
[50] M. Fidrysiak, M. Zegrodnik, and J. Spałek, Unpublished.
[51] P.W. Anderson, "Theory of dirty superconductors," J. Phys. Chem. Solids **11**, 26 – 30 (1959).
[52] R. Kishore and S. Lamba, "Specific heat jump in BCS superconductors," Eur. Phys. J. B **8**, 161 (1999).

SUPPLEMENTAL MATERIAL

STATISTICALLY-CONSISTENT GUTZWILLER APPROXIMATION (SGA)

Here we present technical details of the Statistically Consistent Gutzwiller Approximation (SGA), as applied to the four-orbital model discussed in the main text. At zero temperature, this variational technique reduces to the problem of minimizing the energy functional $E_G = \langle\Psi_G|\mathcal{H}|\Psi_G\rangle/\langle\Psi_G|\Psi_G\rangle$ with respect to the trial state $|\Psi_G\rangle = P_G|\Psi_0\rangle$ for fixed electron density. Here $|\Psi_0\rangle$ is (*a priori* unknown) wave-function describing Fermi sea of free quasi-particles, whereas $\hat{P}_G = \prod_{il}\hat{P}^{(l)}_{Gi}$ denotes Gutzwiller correlator [47]. Local correlators $\hat{P}^{(l)}_{Gi} = \sum_\alpha \lambda_\alpha |l\alpha\rangle_{ii}\langle l\alpha|$ adjust weights of many-body configurations $\alpha \in \{\emptyset,\uparrow,\downarrow,\uparrow\downarrow\}$ on each f-orbital (indexed by l) at site i by means of coefficients λ_α multiplying projection operators $|l\alpha\rangle_{ii}\langle l\alpha|$. This is not the most general form of $\hat{P}_G$ [48], but generalization makes the results less transparent and leads only to minor numerical corrections which may be safely disregarded. Evaluation of the expectation values with the correlated wave function is a non-trivial many body problem. The latter can be substantially simplified by setting up a formal expansion about the limit of infinite lattice coordination, which is achieved by imposing a constraint $(\hat{P}^{(l)}_{Gi})^2 \equiv 1 + x\times\Pi_\sigma(\hat{n}^{f(l)}_{i\sigma} - n^{f(l)}_\sigma)$ [49] so that all λ_α are now expressed in terms of single variational parameter x (we have introduced the notation $O \equiv \langle\hat{O}\rangle_0 \equiv \langle\Psi_0|\hat{O}|\Psi_0\rangle$ for general operator $\hat{O}$). This approach has been elaborated in detail earlier for the orbitally-degenerate Hubbard and non-degenerate Anderson model [21, 22, 31, 33].

We now focus on the four-orbital model, discussed in the text, and calculate E_G by means of Wick theorem, allowing for non-zero equal-spin pairing amplitudes $\langle\hat{f}^{(1)}_{i\sigma}\hat{f}^{(2)}_{i\sigma}\rangle_0$, orienting magnetization direction along z axis, and resorting to the Gutzwiller approximation by discarding the contributions irrelevant for infinite lattice coordination. In effect we obtain

$$\begin{aligned}E_G \simeq &\sum_{ijl\sigma} t_{ij}\langle\hat{c}^{(l)\dagger}_{i\sigma}\hat{c}^{(l)}_{j\sigma}\rangle_0 + V\sum_{il\sigma} q_\sigma\left(\langle\hat{f}^{(l)\dagger}_{i\sigma}\hat{c}^{(l)}_{i\sigma}\rangle_0 + \text{C.c.}\right)\\ &+\sum_{i\sigma}\left[U' g_{1\sigma} + (U'-J)g_{2\sigma}\right]|\langle\hat{f}^{(1)}_{i\sigma}\hat{f}^{(2)}_{i\sigma}\rangle_0|^2 +\\ &\sum_i\left[-2JS^{zf(1)}_i S^{zf(2)}_i + (U'-\frac{J}{2})n^{f(1)}_i n^{f(2)}_i\right] +\\ &+\epsilon^f\sum_{il} n^{f(l)}_i + U\sum_{il}\lambda^2_{\uparrow\downarrow} n^{f(l)}_{i\uparrow} n^{f(l)}_{i\downarrow},\end{aligned} \tag{S1}$$

where the renormalization factors are defined as

$$\begin{aligned}q_\sigma =&\lambda_\emptyset\lambda_\sigma + (\lambda_{\uparrow\downarrow}\lambda_{\bar\sigma} - \lambda_\emptyset\lambda_\sigma)\times n^{f(l)}_{\bar\sigma},\\ g_{1\sigma} =&2\times(\lambda^2_{\uparrow\downarrow} - \lambda^2_{\bar\sigma})\times(\lambda^2_\sigma + (\lambda^2_{\uparrow\downarrow} - \lambda^2_\sigma)n^{f(l)}_{\bar\sigma})\times n^{f(l)}_{\bar\sigma},\\ g_{2\sigma} =&(\lambda^2_{\uparrow\downarrow} - \lambda^2_{\bar\sigma})^2\times\left(n^{f(l)}_{\bar\sigma}\right)^2 + (\lambda^2_\sigma + (\lambda^2_{\uparrow\downarrow} - \lambda^2_\sigma)n^{f(l)}_{\bar\sigma})^2.\end{aligned} \tag{S2}$$

The SGA method maps the original many-body problem onto the task of calculating an effective Landau functional $\mathcal{F} = -\beta^{-1}\ln\mathrm{Tr}\exp(-\beta\mathcal{H}_{\text{eff}})$ evaluated with the effective one-body Hamiltonian $\mathcal{H}_{\text{eff}} = E_G(\{P_\gamma, x\}) - \mu N_e + \sum_\gamma\lambda_\gamma(\hat{P}_\gamma - P_\gamma)$, where N_e is total number of electrons in the system, γ runs over bilinears $\hat{P}_\gamma$ composed of creation and annihilation operators, and λ_γ are Lagrange multipliers ensuring that P_γ obtained from optimization of $\mathcal{F}$ and the Bogolubov-de Gennes equations coincide. The values of parameters are determined from the equations $\partial_{P_\gamma}\mathcal{F} = 0$, $\partial_x\mathcal{F} = 0$, and $\partial_{\lambda_\gamma}\mathcal{F} = 0$. Additionally, the value of chemical potential μ is fixed by electron density. Note that the original variational problem is well posed at $T = 0$, whereas the SGA formulation is applicable also for $T > 0$. One can argue (for general coordination number) that for $T \to 0$ optimization of $\mathcal{F}$ with $\mathcal{H}_{\text{eff}}$ yields the variational minimum of E_G within the improved Gutzwiller approximation [28], whereas for $T > 0$ it reflects thermodynamics of projected quasi-particles [50].

Explicit form of the effective Hamiltonian reads

$$\mathcal{H}_{\text{eff}} = \sum_{\mathbf{k},\sigma}\Psi^\dagger_{\mathbf{k}\sigma}\begin{pmatrix}\epsilon_{\mathbf{k}} & 0 & q_\sigma V & 0\\ 0 & -\epsilon_{\mathbf{k}} & 0 & -q_\sigma V\\ q_\sigma V & 0 & \epsilon^f_\sigma & \Delta^{ff}_{\sigma\sigma}\\ 0 & -q_\sigma V & \Delta^{ff}_{\sigma\sigma} & -\epsilon^f_\sigma\end{pmatrix}\Psi_{\mathbf{k}\sigma} + E_0, \tag{S3}$$

where $\Psi^\dagger_{\mathbf{k}\sigma} = \left(\hat{c}^{(1)\dagger}_{\mathbf{k}\sigma}, \hat{c}^{(2)}_{-\mathbf{k}\sigma}, \hat{f}^{(1)\dagger}_{\mathbf{k}\sigma}, \hat{f}^{(2)}_{-\mathbf{k}\sigma}\right)$,

$$\epsilon_{\mathbf{k}} = 2t[\cos(k_x) + \cos(k_y)] + 4t'\cos(k_x)\cos(k_y) - \mu \tag{S4}$$

is the conduction band dispersion,

$$\Delta^{ff}_{\sigma\sigma} = [g_{1\sigma}U' + g_{2\sigma}(U'-J)]\times\langle\hat{f}^{(1)}_{i\sigma}\hat{f}^{(2)}_{i\sigma}\rangle_0 \tag{S5}$$

denotes f-f superconducting gap parameter,

$$\begin{aligned}\epsilon^f_\sigma = \frac{\partial E_G}{\partial n^{f(1)}_{i\sigma}} =& \epsilon^f + U\lambda^2_{\uparrow\downarrow}n^{f(1)}_{i\bar\sigma} + (U'-J)n^{f(2)}_{i\sigma} +\\ &+U' n^{f(2)}_{i\bar\sigma} + \left(\frac{\partial q_{\bar\sigma}}{\partial n^{f(1)}_{i\sigma}}V\sum_l\langle\hat{f}^{(l)\dagger}_{i\bar\sigma}\hat{c}^{(l)}_{i\bar\sigma}\rangle_0 + C.c.\right) +\\ &+\left(\frac{\partial g_{1\bar\sigma}}{\partial n^{f(1)}_{i\sigma}}U' + \frac{\partial g_{2\bar\sigma}}{\partial n^{f(1)}_{i\sigma}}(U'-J)\right)|\langle\hat{f}^{(1)}_{i\bar\sigma}\hat{f}^{(2)}_{i\bar\sigma}\rangle_0|^2 - \mu\end{aligned} \tag{S6}$$

is the renormalized f-orbital energy, and $E_0 \equiv E_G(\{P_\gamma, x\}) - \mu N_e - \sum_\gamma \lambda_\gamma P_\gamma$ is a remainder proportional to unity. Note that the entries of $\mathcal{H}_{\rm eff}$ have been obtained from one condition $\partial_{P_\gamma}\mathcal{F} = 0$ and are given in an explicit form.

The system of equations $\partial_{P_\gamma}\mathcal{F} = 0$, $\partial_x\mathcal{F} = 0$, and $\partial_{\lambda_\gamma}\mathcal{F} = 0$ has been solved by means of GNU Scientific Library. Numerical accuracy for the dimensionless density matrix elements has been chosen in the range 10^{-8}-10^{-9}, depending on the model parameters. We work in thermodynamic limit with number of lattice sites $N \to \infty$ by performing Brillouin-zone integration in all equations. Technically, keeping N finite, but large speeds-up the calculations in a highly parallel setup. However, the calculated superconducting gap parameters range from $\sim 10^{-4}|t|$ down to $\sim 10^{-9}|t|$ which raises the question of the impact of the finite-size effects on the SC state. We can estimate the latter by referring to the Anderson criterion [51] $\Delta^{ff}_{\sigma\sigma} \sim d$, where $d \sim W/N$ is the typical spacing between discrete energy levels ($W \sim$ several $|t|$ denotes bandwidth scale and N is the number of lattice sites). To achieve desired accuracy, one would thus need to consider lattices with $> 10^{10}$ sites.

Since the effective Hamiltonian can be diagonalized analytically with eigenvalues

$$E^{(\lambda)}_{\mathbf{k}\sigma} = \pm\sqrt{q_\sigma^2 V^2 + \frac{1}{2}\left[\left(\Delta^{ff}_{\sigma\sigma}\right)^2 + \left(\epsilon^f_\sigma\right)^2 + \epsilon^2_{\mathbf{k}}\right] \pm \frac{1}{2}\sqrt{\left[\left(\Delta^{ff}_{\sigma\sigma}\right)^2 + \left(\epsilon^f_\sigma\right)^2 - \epsilon^2_{\mathbf{k}}\right]^2 + 4q_\sigma^2 V^2\left[\left(\Delta^{ff}_{\sigma\sigma}\right)^2 + \left(\epsilon_{\mathbf{k}} + \epsilon^f_\sigma\right)^2\right]}}, \tag{S7}$$

one can express the gap $\Delta_{\mathbf{k}}$ in the projected quasiparticle spectrum in terms of the gap parameter $\Delta^{ff}_{\sigma\sigma}$. We get the formula

$$\Delta^2_{\mathbf{k}} = \frac{\epsilon^2_{\mathbf{k}}}{(\epsilon_{\mathbf{k}} + \epsilon^f_\sigma)^2} \times (\Delta^{ff}_{\sigma\sigma})^2 + o[(\Delta^{ff}_{\sigma\sigma})^2], \tag{S8}$$

valid for wave vectors located on the Fermi surface calculated in the normal state. Note that the gap is expressed solely in terms of the f-f pairing amplitude (even though f-c and c-c amplitudes are, in general, non-zero due to hybridization effects) scaled by the $\mathbf{k}$-dependent factor. This justifies using $\Delta^{ff}_{\sigma\sigma}$ as the quantity characterizing the overall SC properties of the system.

DETERMINATION OF THE PHASE DIAGRAM

In Fig. 1(a) we plot the energies of the FM2 + A_2 and FM1 + A_1 phases near the metamagnetic transition for $J/|t| = 1.1$, $U/|t| = 3.5$, $t'/|t| = 0.25$, and $\epsilon^f/|t| = -4$ (the same parameters have been used for plotting Fig. 1. of the main text). The solid lines are quadratic fits to the data in respective phases. The phase-transition point $V_{\rm PT}$ corresponds to the crossing of the lines (marked by the vertical dashed lines) and is displayed in the figure. Note that the lines cross at non-zero angle which is indicative of the first-order transition. Similarly, in Fig. 1(b) the energies near the FM1 + A_1 and PM + A phase boundary are shown. In panels (c)-(d) we plot the difference between extrapolated energies on both sides of the transitions. The latter becomes zero at the transition point.

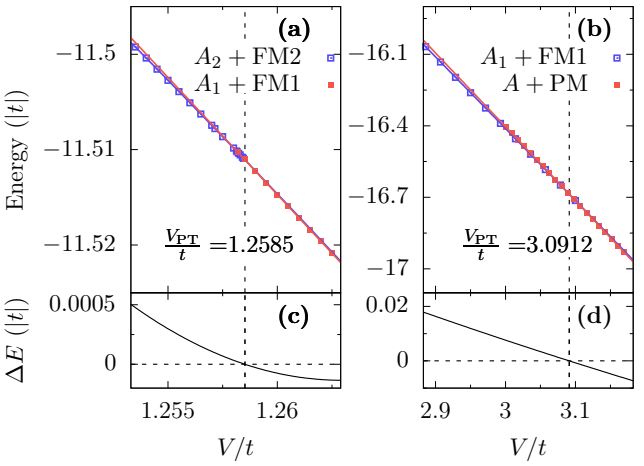

FIG. 1. Crossing of the energies near (a) FM2 + A_2 → FM1 + A_1 and (b) FM1 + A_1 → PM + A transition for $U/|t| = 3.5$. Panels (c)-(d) show the energy differences ΔE between extrapolated energies on both sides of respective phase transitions. The latter become zero at the transition point, denoted as $V_{\rm PT}$, and are displayed in the plot. Model parameters coincide with those used in Fig. 1. of the main text.

Additionally, in Table I we present the analysis of A_1-type SC phase stability for $U/|t| = 3.5$, $V/t = 1.32$, $t'/|t| = 0.25$, $\epsilon^f/|t| = -4$ and a variable Hund's coupling $J/|t| = 1.1 \div 1.4$. Here $E_{\rm FM1}$ is the energy of the FM1 phase with SC suppressed, and $E_{\rm FM1+A_1}$ refers to the FM1 phase coexisting with A_1-type SC. The condensation energy $E_c \equiv E_{\rm FM1} - E_{\rm FM1+A_1}$ is positive for all considered values of hybridization, which illustrates the

TABLE I. Variational ground-state energies for $U/|t| = 3.5$ and $V/t = 1.32$, $t'/|t| = 0.25$, $\epsilon^f/|t| = -4$, $n^{\rm tot} = 3.25$, and selected values of Hund's coupling J. Here $E_{\rm FM1}$ is the energy of the FM1 phase with SC suppressed, and $E_{\rm FM1+A_1}$ refers to the FM1 phase coexisting with the A_1-type SC. The condensation energy $E_c \equiv E_{\rm FM1} - E_{\rm FM1+A_1}$ is also supplied. The numerical accuracy of the energy difference is of the order of 2×10^{-8}.

$J/\|t\|$	$E_{\rm FM1}/\|t\|$	$E_{\rm FM1+A_1}/\|t\|$	$10^4 \times E_c/\|t\|$
1.10	-11.663 459 37	-11.663 459 39	0.0003
1.15	-11.796 917 55	-11.796 917 77	0.0022
1.20	-11.934 039 49	-11.934 041 79	0.0230
1.25	-12.074 935 82	-12.074 951 80	0.1598
1.30	-12.219 724 82	-12.219 802 79	0.7797
1.35	-12.368 534 05	-12.368 822 15	2.8810
1.40	-12.521 501 70	-12.522 354 69	8.5299

stable character of the SC state.

FINITE-TEMPERATURE PROPERTIES

Within the SGA approach, one can also determine the finite-temperature properties of the system. In Fig. 2 we show explicitly the evolution of the gap parameter $\Delta^{ff}_{\downarrow\downarrow}$ and electronic specific heat across the SC transition for $U/|t| = 3.5$, $J/|t| = 1.1$, $V/t = 1.3$, $t'/|t| = 0.25$, and $\epsilon^f = -4$. For this set of parameters the system is close to the FM2→FM1 transition, where SC is most pronounced (cf. Fig. 1 of main text). For the specific choice $|t| = 0.5\,$eV we obtain the SC transition temperature $T_{\rm SC} \simeq 0.92\,$K which is close to the values measured for high-quality UGe_2 samples. On the other hand, we do not get the residual C/T for $T \to 0$ as is observed for UGe_2. This is likely due to more complex electronic structure, not included in the minimal four-orbital model considered here, e.g., by the third $5f$-electron, which provides the selectively delocalized state, as discussed in the text. This conjecture is substantiated by the fact that if we subtract the residual γ_0 from measured Sommerfeld coefficient γ_n then $\Delta C/(\gamma_n - \gamma_0)/T_{\rm SC} \simeq 0.97$ [45], i.e., not too far from the value displayed in Fig. 2(b), which, in turn, is close to the BCS value 1.43 [52].

PHASE DIAGRAM IN THE REGIME OF LARGE HUND'S COUPLING

For the parameters taken in the main text, the A-phase gaps turn out to be of the order $\Delta^{ff}_{\sigma\sigma}/|t| \sim 10^{-9}$, which sets the critical temperature scale at the level of 0.01 mK for $|t| \sim 1\,$eV. This raises a question about observability of the A state. Here we show that the A phase may become substantially enhanced in the regime of strong

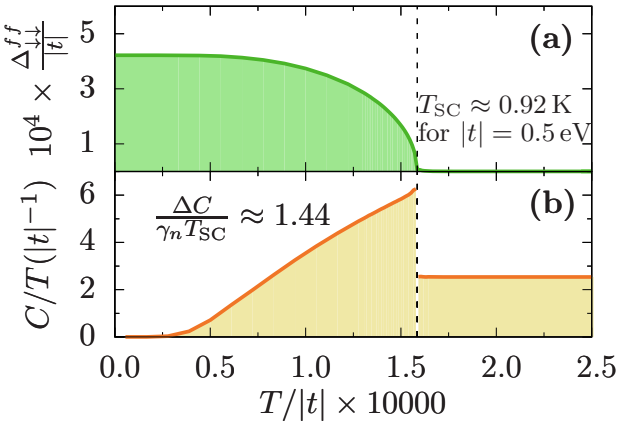

FIG. 2. Temperature-dependence of (a) gap parameter $\Delta^{ff}_{\downarrow\downarrow}$ and (b) electronic specific heat for $U/|t| = 3.5$, $J/|t| = 1.1$, $V/t = 1.3$, $\epsilon^f/|t| = -4$, $t'/|t| = 0.25$, and $n^{\rm tot} = 3.25$.

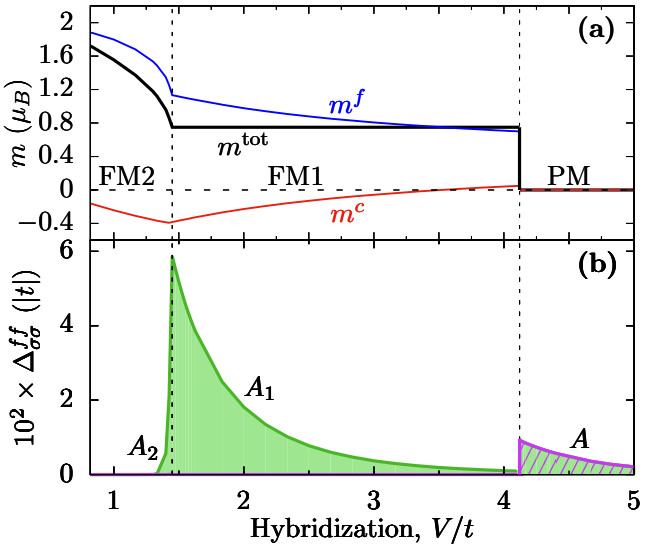

FIG. 3. Phase diagram for $U/|t| = 4$, $J/|t| = 1.6$, $t'/|t| = 0.25$, temperature $T/|t| = 10^{-8}$ and $n^{\rm tot} = 3.25$. (a) Total magnetic moment (black line) and f- and c-electron magnetizations (blue and red lines, respectively). (b) Superconducting gap parameters $\Delta^{ff}_{\downarrow\downarrow}$ (green shading) and $\Delta^{ff}_{\uparrow\uparrow}$ (purple shading).

correlations and large Hund's coupling. In Fig. 3 we show the hybridization-dependence of the magnetization and SC gaps for $U/|t| = 4$, $J/|t| = 1.6$, $t'/|t| = 0.25$, $\epsilon^f/|t| = -4$, and temperature $T/|t| = 10^{-8}$. The general structure of the phase diagram remains unchanged, but the ratio of the gap parameters in the A and A_1 phases is now enhanced by five orders of magnitude relative to the situation considered previously. This suggests that an A-like phase could emerge in systems more strongly correlated than UGe_2. Also, now the A_1 phase is not concentrated in a narrow region around the metamag-

netic transition, but spreads out over entire FM1 part of the phase diagram. This is not consistent with the low-temperature specific-heat data [45] for UGe_2 exhibiting a narrow peak around FM2→FM1 transition. The latter fact justified our choice of smaller $U/|t| = 3.5$ and $J/|t| = 1.1$.

Proceedings of the XVI National Conference on Superconductivity and Strongly Correlated Systems, Zakopane 2013

Anderson–Kondo Lattice Hamiltonian from the Anderson-Lattice Model: A Modified Schrieffer–Wolff Transformation and the Effective Exchange Interactions

E. Kądzielawa-Major* and J. Spałek

Marian Smoluchowski Institute of Physics, Jagiellonian University, W.S. Reymonta 4, 30-059 Kraków, Poland

We derive the Anderson–Kondo lattice model by applying canonical perturbation expansion for the Anderson-lattice model in direct space. The transformation is carried out up to the fourth order by a modified Schrieffer–Wolff transformation: we separate the part of hybridization term responsible for the high-energy processes (involving the largest in-the-system intraatomic Coulomb interaction between f electrons) and replace it with the virtual processes in higher orders. The higher-order processes lead to three separate exchange interactions. The obtained Hamiltonian contains both the Kondo (f–c) and the superexchange (f–f) interactions, as well as a residual hybridization responsible for the heavy-quasiparticle formation. This effective Hamiltonian can be used to analyze the magnetic or the paired states, as well their coexistence in heavy-fermion systems. The magnitudes of both the Kondo exchange and the superexchange integrals are estimated as a function of bare hybridization magnitude.

DOI: 10.12693/APhysPolA.126.A-100

PACS: 71.10.Fd, 71.20.Eh, 71.27.+a, 71.70.Gm

1. Introduction

In this paper we present our main results concerning the canonical perturbation expansion for the Anderson-lattice model in direct space, by transforming out only a part of the f–c hybridization term and replacing it with the virtual processes in higher orders, which in turn yield the effective f–c, f–f, and c–c interactions. The calculations are carried out up to the fourth order, taking into account both two- and three-site processes. These results elaborate and correct the earlier results [1]. We also estimate the magnitude of the derived exchange integrals. The present results provide an effective model for subsequent consideration of magnetism and real-space pairing in heavy-fermion systems [2, 3]. The results represent an application of the modified Schrieffer–Wolff transformation, that leads, among others, to the itineracy of originally localized f electrons.

2. Model

The basic feature of Anderson-lattice model is the hybridization term V_{im} representing the quantum-mechanical mixing between the two types of electrons: the atomic (f) and the conduction (c) states. We assume that $|V_{im}| \ll U$, where U is the magnitude of the f–f Coulomb interaction in the same atomic f-state. Other Coulomb interactions (in the conduction band and between bands) are disregarded. Additionally, we put $\epsilon_f \sim V_{im}$, which means that the atomic level is located below, but not too far from the Fermi surface. Therefore, one can calculate nontrivial corrections in small parameter V_{im}/U to the electronic f and c states if the strong Coulomb interaction $\sim U$ and the hybridization $\sim V_{im}$ are included.

The starting Anderson-lattice Hamiltonian in the site (real-space) language reads

$$\mathcal{H} = \sum_{\substack{mn\sigma \\ m\neq n}} (t_{mn} - \mu\delta_{mn})\, \hat{c}^{\dagger}_{m\sigma}\hat{c}_{n\sigma} + \epsilon_f \sum_{i\sigma} \hat{N}_{i\sigma} + U\sum_{i} \hat{N}_{i\uparrow}\hat{N}_{i\downarrow} + \sum_{im\sigma}\left(V_{im}\hat{f}^{\dagger}_{i\sigma}\hat{c}_{m\sigma} + V^{*}_{im}\hat{c}^{\dagger}_{m\sigma}\hat{f}_{i\sigma}\right), \quad (1)$$

where $\hat{c}^{\dagger}_{m\sigma}$, $\hat{c}_{m\sigma}$ are creation and annihilation operators of electrons in c-state in real-space representation (m is the site number and σ the spin), $\hat{f}^{\dagger}_{i\sigma}$, $\hat{f}_{i\sigma}$ are creation and annihilation operators of f-electrons on i-th site with spin σ, $\hat{N}_{i\sigma} \equiv \hat{f}^{\dagger}_{i\sigma}\hat{f}_{i\sigma}$ is the number of f-electrons on site i, t_{mn} is hopping integral for c-electrons, ϵ_f is the bare energy of the originally localized $4f$ electrons, V_{im} is hybridization matrix element and U is intraatomic Coulomb interaction (the high-energy scale in the system).

The starting point in the derivation of the effective Hamiltonian via a canonical perturbation expansion (introduced for Anderson-lattice model in [1]) is a division of the hybridization term into two parts. Namely, we divide the term into two, reflecting the low- and the high-energy processes, i.e., those which do not and do involve energy U, respectively, as depicted schematically in Fig. 1. In formal language, it amounts to separating the hybridization term in the following manner:

*corresponding author; e-mail: ewa.kadzielawa@uj.edu.pl

$$\hat{f}^{\dagger}_{i\sigma}\hat{c}_{m\sigma} \equiv \left(1-\hat{N}_{i\bar{\sigma}}\right)\hat{f}^{\dagger}_{i\sigma}\hat{c}_{m\sigma} + \hat{N}_{i\bar{\sigma}}\hat{f}^{\dagger}_{i\sigma}\hat{c}_{m\sigma}. \tag{2}$$

Next, by treating as a perturbation only the part connected with high-energy processes, i.e., $\sim (\hat{N}_{i\bar{\sigma}}\hat{f}^{\dagger}_{i\sigma}\hat{c}_{m\sigma} +$ H.c.), we calculate explicitly the effective Hamiltonian using the canonical perturbation expansion up to the fourth order. The low-energy part remains unchanged and represents a residual hybridization, which will introduce, among others, the itineracy of the starting (bare) localized f states. In general, the canonical perturbation expansion method allows for differentiation between the two terms in (1), which are of the same order ($\sim V_{im}$). The differentiation constitutes the main difference between the present transformation and that introduced originally by Schrieffer and Wolff [4]. It will lead to far reaching consequences, e.g., the itineracy of originally atomic (f) electrons.

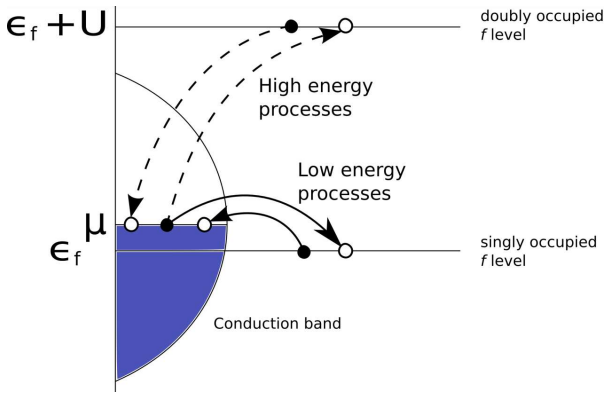

Fig. 1. Low- and high-energy interband hopping processes in direct space induced by the hybridization between f and c states. Only the high-energy f–c mixing processes (involving energy U) are transformed out and replaced by exchange processes in the second and the fourth orders. Low-energy processes remain unchanged in effective Hamiltonian as residual hybridization. In effect, such transformation differs from the standard Schrieffer–Wolff transformation, where both terms are transformed out.

It should be noted that in the present approach the number of f electrons $\sum_i N_i$ is not conserved, neither before nor after the transformation. Instead, only the total number of electrons in the system, $n_i^{(\mathrm{e})} = N_i + n_i$ is fixed, where $n_i \equiv \sum_\sigma c^{\dagger}_{i\sigma}c_{i\sigma}$. This last circumstance allows for an itineracy of strongly correlated f electrons; it allows to represent one of the principal differences with the Schrieffer–Wolff approach.

3. Canonical perturbation expansion: a brief summary

To develop the canonical perturbation expansion (CPE) we proceed as follows [1]. Due to the fact that important are the double occupancies of f electrons on the same site, we project them out from Hamiltonian with the help of operators P_l:

$$\sum_l P_l = 1 \qquad \text{and} \qquad P_l P_{l'} = \delta_{ll'} P_l. \tag{3}$$

Operators P_l project the states onto subspace with $(l-1)$ double occupancies in the system of f sites. We redefine initial Anderson-lattice model using projection operators P_l in the following manner:

$$\mathcal{H}_0 \equiv P_1\mathcal{H}P_1 + P_2\mathcal{H}P_2, \tag{4}$$

$$\mathcal{H}_1 \equiv P_1\mathcal{H}P_2 + P_2\mathcal{H}P_1. \tag{5}$$

In this representation, $\mathcal{H}_1$ describes the processes changing by one number of double occupancies

$$P_2\mathcal{H}P_1 = (P_1\mathcal{H}P_2)^{\dagger} \equiv \sum_{im\sigma} V_{im}\hat{N}_{i\bar{\sigma}}\hat{f}^{\dagger}_{i\sigma}\hat{c}_{m\sigma}. \tag{6}$$

In reality, only the effective Hamiltonian projected onto P_1 subspace will matter; the role of the higher-energy subspaces will show up through virtual processes only.

Now, we introduce the canonical transformation of (1) using the transformation generator $\mathcal{S}$ of the form

$$\tilde{\mathcal{H}}(\varepsilon) = \mathrm{e}^{-\mathrm{i}\varepsilon\mathcal{S}}(\mathcal{H}_0 + \varepsilon\mathcal{H}_1)\mathrm{e}^{+\mathrm{i}\varepsilon\mathcal{S}}, \tag{7}$$

where ε is a parameter, which groups the terms of the same order of expansion in V_{im} (at the end we put $\varepsilon = 1$). Expanding the exponential functions into a Taylor series and eliminating the linear term $\sim \varepsilon$ by setting the physical condition

$$\mathcal{H}_1 = \mathrm{i}[\mathcal{S}, \mathcal{H}_0], \tag{8}$$

we obtain up to the fourth order

$$\tilde{\mathcal{H}}(\varepsilon) = \mathcal{H}_0 - \frac{\mathrm{i}}{2}\varepsilon^2[\mathcal{S},\mathcal{H}_1] - \frac{1}{3}\varepsilon^3[\mathcal{S},[\mathcal{S},\mathcal{H}_1]] + \frac{\mathrm{i}}{8}\varepsilon^4[\mathcal{S},[\mathcal{S},[\mathcal{S},\mathcal{H}_1]]] + \mathcal{O}(\varepsilon^5). \tag{9}$$

With the use of the definition of projection operators we can find form of $P_l\mathcal{S}P_{l+1}$ from condition (8), by putting $P_l\mathcal{S}^{(0)}P_{l+1} = 0$ and iterating the solution [1]. Finally, we obtain

$$P_l\mathcal{S}^{(n\to\infty)}P_{l+1} = -\mathrm{i}\,(P_l\mathcal{H}_1P_{l+1})\,(P_{l+1}\mathcal{H}_0P_{l+1} - P_l\mathcal{H}_0P_l)^{-1}. \tag{10}$$

Let us note that $P_l\mathcal{S}P_l \sim P_l$, thus we can always choose $\mathcal{S}$ in such a way that $P_l\mathcal{S}P_l = 0$, because if we project (8) with operator P_l on both sides we obtain that $P_l\mathcal{S}P_l$ commutes with $\mathcal{H}_0$.

In the atomic limit, the difference $P_{l+1}\mathcal{H}_0P_{l+1} - P_l\mathcal{H}_0P_l$ can be replaced by mean value of energy difference between subspaces with l and $(l-1)$ double occupancies. By making this approximation, we neglect renormalization of the low-energy hybridization processes by the higher order contributions (i.e., neglect the terms $\sim V_{im}$ in the denominator of (10)). In effect, we have

$$P_{l+1}\mathcal{H}_0P_{l+1} - P_l\mathcal{H}_0P_l \approx \langle P_{l+1}\mathcal{H}_0P_{l+1}\rangle - \langle P_l\mathcal{H}_0P_l\rangle = U + \epsilon_f - \mu \equiv U + \epsilon_f. \tag{11}$$

Finally, by projecting out the expansion introduced by expression (9) on the subspace without double occupan-

cies, the effective Hamiltonian can be obtained in the form

$$P_1\tilde{\mathcal{H}}P_1 \approx P_1\mathcal{H}_0P_1 - \frac{1}{U+\epsilon_f}P_1\mathcal{H}_1P_2\mathcal{H}_1P_1 + \frac{1}{(U+\epsilon_f)^3}\Big(P_1\mathcal{H}_1P_2\mathcal{H}_1P_1\mathcal{H}_1P_2\mathcal{H}_1P_1 - \frac{1}{2}P_1\mathcal{H}_1P_2\mathcal{H}_1P_3\mathcal{H}_1P_2\mathcal{H}_1P_1\Big), \quad (12)$$

where we have put $\varepsilon = 1$. Let us note that the third-order term is always zero, because we have chosen that $P_l\mathcal{S}P_l = 0$.

The term $P_1\mathcal{H}_1P_2\mathcal{H}_1P_1$ describes virtual process in the second order in which in intermediate state a single double occupancy occurs. In the fourth order two different types of processes appear: those with passing through the subspace (P_1) without double occupancies and those with passing through that subspace with up to two double occupancies (P_3).

In what follows we restrict ourselves to the most interesting part, that is to the Hamiltonian projected onto the subspace without double occupancies (12). This part will be discussed in detail, because it is helpful in determining the ground state for different magnetic and superconducting phases of heavy fermions with nominal $4f^1$ starting configuration (Ce^{3+} ions).

4. Results: Kondo (f–c) and superexchange (f–f) integrals

An explicit form of the effective Hamiltonian can be found, if we carry out a careful analysis of all possible processes, which can show up in the second and the fourth orders of the expansion. After collecting the all possible diagrams containing two- and three-site processes (examples are shown in Fig. 2), we evaluate them

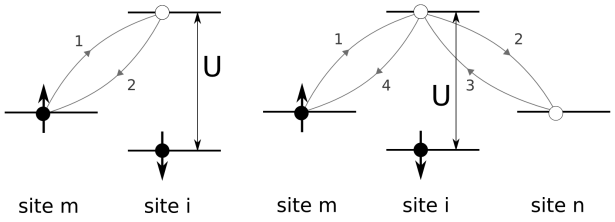

Fig. 2. Examples of processes in the second (left) and the fourth (right) orders of the CPE expansion.

using definitions (4)–(6). In effect, the complete effective Hamiltonian (12) with projected out double occupancies ($\hat{\mathcal{H}}_{\rm eff} \simeq P_1\tilde{\mathcal{H}}P_1$) has the following form:

$$\hat{\mathcal{H}}_{\rm eff} \simeq \sum_{m\neq n,\sigma}(t_{mn}-\mu\delta_{mn})\,\hat{c}^\dagger_{m\sigma}\hat{c}_{n\sigma} + \epsilon_f\sum_{i,\sigma}\hat{\nu}_{i\sigma} + \sum_{i,m,\sigma}\Big(V_{im}\Big(1-\hat{N}_{i\bar{\sigma}}\Big)\hat{f}^\dagger_{i\sigma}\hat{c}_{m\sigma} + \text{H.c.}\Big) + \sum_{i,m}J^{(\rm K)}_{im}\left(\hat{\boldsymbol{S}}_i\cdot\hat{\boldsymbol{s}}_m - \frac{\hat{n}_m\hat{\nu}_i}{4}\right) + \sum_{i\neq j,\sigma}J^{(\rm H)}_{ij}\left(\hat{\boldsymbol{S}}_i\cdot\hat{\boldsymbol{S}}_j - \frac{\hat{\nu}_i\hat{\nu}_j}{4}\right) + 2\mathrm{i}\sum_{\langle mi\rangle\langle mj\rangle}J^{(\rm H)}_{ij}\left(1+\frac{n_f}{n_{\rm c}}\right)\hat{\boldsymbol{s}}_m\cdot\Big(\hat{\boldsymbol{S}}_j\times\hat{\boldsymbol{S}}_i\Big), \quad (13)$$

where the projected particle-number operators are $\nu_{i\sigma} \equiv \Big(1-\hat{N}_{i\bar{\sigma}}\Big)\hat{N}_{i\sigma}$, and $\nu_i \equiv \sum_\sigma \nu_{i\sigma}$; $\hat{\boldsymbol{S}}_i$ and $\hat{\boldsymbol{s}}_m$ are the local spin operators in the fermion representation for f and c electrons, respectively; $n_{\rm c} \equiv \langle n_m\rangle$ and $n_f \equiv \langle\nu_i\rangle$ are average occupancies. The first three terms represent the projected starting Hamiltonian with residual (projected) hybridization only. The next three represent, respectively: the Kondo interaction, the superexchange part and the interaction of Dzialoshinskii–Moriya-type, the last appearing only if the c-electrons are present. The noncollinearity of the magnetic ordering of c electrons ($\sim \hat{\boldsymbol{S}}_i\cdot(\hat{\boldsymbol{s}}_n\times\hat{\boldsymbol{s}}_m)$), as well as the superexchange interaction between them, were neglected in effective Hamiltonian (13) since the c bandwidth $W_{\rm c} = 2z|t_{\langle mn\rangle}|$ is by far the largest energy in the c-electron subsystem.

The corresponding exchange integrals have the following forms:

$$J^{(\rm K)}_{im} \equiv 2\frac{|V_{im}|^2}{U+\epsilon_f} - 4\frac{|V_{im}|^4}{(U+\epsilon_f)^3} - 4\sum_{n(i)}\frac{|V_{im}|^2|V_{in}|^2}{(U+\epsilon_f)^3}\left(1-\frac{n_c}{2}\right) - 2\sum_{n(i)}\frac{|V_{im}|^2|V_{in}|^2}{(U+\epsilon_f)^3}n_c - 2\sum_{j(m)}\frac{|V_{im}|^2|V_{jm}|^2}{(U+\epsilon_f)^3}n_f, \quad (14)$$

$$J^{(\rm H)}_{ij} \equiv \sum_{m(i)}\frac{|V_{jm}|^2|V_{im}|^2}{(U+\epsilon_f)^3}n_c. \quad (15)$$

The first of them represents the effective Kondo exchange integral calculated here to the fourth order; the second, the exchange integral for both the Heisenberg part and the novel three-spin interactions. Note that in order to estimate the corresponding exchange integrals, the average occupancies n_c and n_f have been taken for the actual occupancies. Obviously, $n_{\rm e} = n_c + n_f$. Now, we can estimate numerically the values of (14) and (15), as discussed next.

5. Estimates of exchange integrals

The numerical estimates of the exchange integrals appearing in (14) and (15) are shown in Figs. 3 and 4 for the two values of Coulomb interaction U: $\epsilon_f + U = 3$ eV and $\epsilon_f + U = 5$ eV, respectively. We have also assumed that hybridization has nonzero value only for nearest neighbours $V_{\langle im\rangle} = V$, where the number of nearest neighbors $z = 4$ and the hybridization magnitude $|V| = 0.3\div0.5$ eV. Typically for Ce systems the number of electrons per site is $n_c = 1$ and $n_f = 1$. Let us note that to estimate $J^{(\rm H)}_{ij}$ we assume that sites i and j are next nearest neighbors, such that summation in (15) allows only those m, which are nearest neighbors with both i and j.

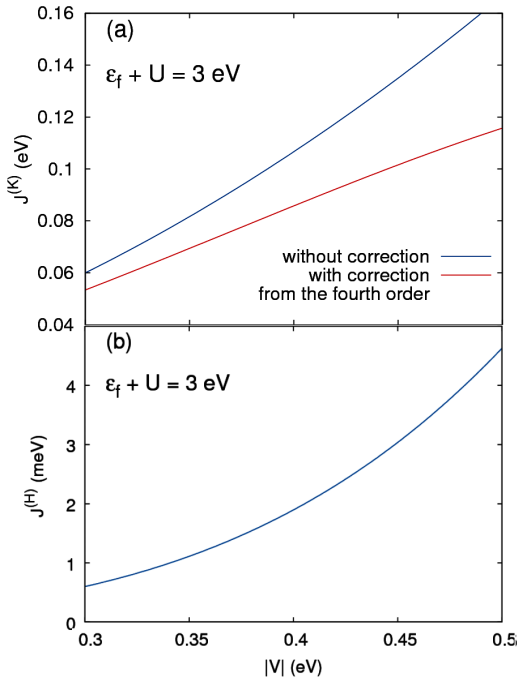

Fig. 3. Exemplary values of the Kondo exchange integral $J^{(\mathrm{K})}$ with and without correction from the fourth order (a) and that for the superexchange integral $J^{(\mathrm{H})}$ (b); both as a function of bare hybridization magnitude $|V|$, for $\epsilon_f + U = 3$ eV.

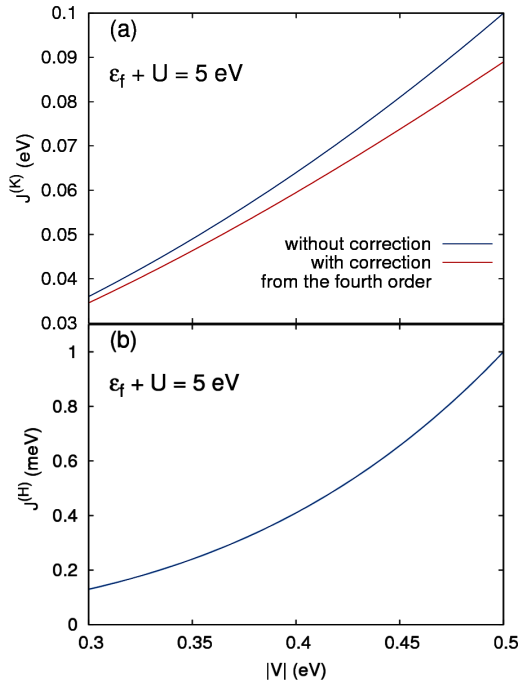

Fig. 4. Values of the Kondo exchange $J^{(\mathrm{K})}$ with and without correction coming from the fourth order (a) and of superexchange $J^{(\mathrm{H})}$ integral (b); both integrals as a function of bare hybridization magnitude $|V|$, and for $\epsilon_f + U = 5$ eV.

Let us note that $J^{(\mathrm{K})}$ in Fig. 3a is always antiferromagnetic; the fourth order effects reduce the second-order value by $\approx 30\%$ for the smaller U-value. Likewise, the f–f exchange $J^{(\mathrm{H})}$ is also always antiferromagnetic and more than an order of magnitude smaller, as it should be, since it contains solely the fourth-order processes. For the larger value of U the integral $J^{(\mathrm{H})}$ and the correction from the fourth order in $J^{(\mathrm{K})}$ are smaller. Let us note also that the present approach contains short range interaction between asymptotically itinerant fermions ($V_{im} \neq 0$).

6. Concluding remarks

The value of the Kondo exchange and the superexchange integrals have been evaluated as a function of hybridization magnitude. In the metallic state there appears a 3-spin interaction (the last term in (13)), which may introduce a noncollinearity of the spins in the magnetic heavy-fermion state. A detailed analysis of the results will be published separately.

Acknowledgments

The work was supported in part by the project TEAM awarded to our group by the Foundation for Polish Science (FNP) for the years 2011–2014, as well as by the grant MAESTRO from the National Science Centre (NCN), No. DEC-2012/04/A/ST3/00342.

References

[1] J. Spałek, P. Gopalan, *J. Phys. (France)* **50**, 2869 (1989).

[2] O. Howczak, J. Spałek, *J. Phys. Condens. Matter* **24**, 205602 (2012).

[3] O. Howczak, J. Kaczmarczyk, J. Spałek, *Phys. Status Solidi B* **250**, 609 (2013).

[4] J.R. Schrieffer, P.A. Wolff, *Phys. Rev.* **149**, 491 (1966).